Modelling of Mechanical Interaction in Piezoelectric Actuated Resonant System

THÈSE N° 7124 (2016)

PRÉSENTÉE LE 2 SEPTEMBRE 2016
À LA FACULTÉ DES SCIENCES ET TECHNIQUES DE L'INGÉNIEUR
LABORATOIRE D'ACTIONNEURS INTÉGRÉS
PROGRAMME DOCTORAL EN ROBOTIQUE, CONTRÔLE ET SYSTÈMES INTELLIGENTS

ÉCOLE POLYTECHNIQUE FÉDÉRALE DE LAUSANNE

POUR L'OBTENTION DU GRADE DE DOCTEUR ÈS SCIENCES

PAR

Dan SHI

acceptée sur proposition du jury:

Prof. J. A. Schiffmann, président du jury
Prof. Y. Perriard, Dr Y. R. C. Civet, directeurs de thèse
Prof. J. Shen, rapporteur
Prof. B. Lemaire-Semail, rapporteuse
Prof. M.-O. Hongler, rapporteur

EPFL

ÉCOLE POLYTECHNIQUE
FÉDÉRALE DE LAUSANNE

Suisse
2016

不积跬步，无以至千里；不积小流，无以成江海。

— 荀子《劝学篇》

Step after step, the ladder is ascended.

Acknowledgements

Abstract

Automatic assembly system has been continuously drawing attention since the beginning of the 20th century. Parts feeding system is one of the important subsystems. The parts feeding system is used for delivering bulk parts into separated individual parts. Flexible parts feeder gains attention because of the flexibility and the short changeover. However, due to the random vibration of the tooling plate in this parts feeder, the efficiency is low, especially for complicated geometry parts.

Studies in this thesis are developments based on an industrial project to solve the problem of random vibration. The proposed approach is to make use of the standing waves created by the piezoelectric actuators on the tooling plate. Therefore, the investigation focus mainly on two aspects: resonance analysis and the mechanical interaction.

With regard to resonance analysis, we firstly investigate the piezoelectric actuator's dimensions and the influence on the plate amplitude. We discover that bigger the piezoelectric actuator is, larger the vibrating amplitude is. We also find that for a piezoelectric actuator with a given surface, piezoelectric actuator's shape can be modified to increase the amplitude. The larger edge of the piezoelectric actuator should be orientated consistency with the bending direction. The limit of the dimension and shape modification is that the larger edge of the piezoelectric actuator should be smaller than the half wavelength of the resonant mode. Secondly, we study the plate geometry influence on the relative nodal lines position between modes. The length-to-width ratio changes the nodal line positions. We propose a parameter, which relates the relative distance between the nodal positions of two successive modes and the wavelength of the second mode, as the first step for plate optimization.

With regard to the mechanical interaction, we firstly study the part's vertical displacement under a resonant vibrating plate. Numerical simulations, validated by experiments of the part's vertical displacement show that we can obtain a certain vertical displacement by either a high vibrating frequency with low amplitude or a lower frequency with higher amplitude. We also study the horizontal movement from anti-nodes to nodes. The established model considers the amplitude variation from anti-node to node. Part's vertical displacement is limited to small value to avoid parts' random movement. This leads to a slow horizontal movement.

We apply the aforementioned researches to three applications. Firstly, for parts separation, two desirable standing waves are used to separate the parts. The two modes should satisfy this condition: the anti-nodes of the first mode are the nodes of the second mode and the nodes of the first mode are the anti-nodes of the second mode. The predicable positions (nodes) on the plate could be used to reduce the random vibration in the existing parts feeder. Secondly,

Résumé

Les systèmes d'assemblage automatique sont des sujets d'études depuis le début du 20ème siècle. Un des composants important de ces derniers est l'élément d'alimentation en pièces. Sa fonction principale est d'ordonner les pièces stockées 'en vrac' afin qu'elles puissent être saisies une par une par le système de préhension et ceci pour les manipuler par la suite dans le but de leur assemblage final. Les systèmes d'alimentation flexibles deviennent intéressants de par leur versatilité. Cependant, en raison de la vibration stochastique des pièces, leur rendement est faible, surtout pour des pièces de géométrie complexe.

Les travaux développés dans cette thèse sont basés sur un projet industriel dont le but est de résoudre le problème de vibration aléatoire. La solution envisagée est d'utiliser des ondes stationnaires créées par les actionneurs piézoélectriques sur un plateau. Les recherches se concentreront principalement sur deux aspects : le phénomène de résonance mécanique et l'interaction mécanique entre une plaque vibrante et une pièce unitaire.

Pour la partie concernant la résonance, nous examinerons tout d'abord l'influence des dimensions de l'actionneur piézoélectrique sur l'amplitude de vibration d'une plaque mécanique. Nous verrons que plus la surface de l'actionneur est grande, plus l'amplitude de vibration est importante. Dans le cas d'une surface de l'actionneur donnée, la forme de celui-ci peut être modifiée pour en augmenter l'amplitude. Le plus grand coté de l'actionneur piézoélectrique doit aussi être orienté dans la même direction que la flexion. La taille de l'actionneur piézo-électrique ne doit cependant pas être plus grande que la demi-longueur d'onde du mode de résonance. Dans un second temps, nous étudierons l'influence de la géométrie de la plaque sur la position des lignes nodales relatives entre les modes. Le rapport longueur sur largeur modifie en effet ces positions. Nous proposerons un paramètre qui se rapporte à la distance relative entre les positions nodales de deux modes successifs et de la longueur d'onde du deuxième mode. Ceci permettra de caractériser le comportement d'une plaque donnée et pourra être utile pour une future étape d'optimisation de la plaque-outil.

En ce qui concerne l'interaction mécanique, nous étudierons tout d'abord le déplacement vertical de la pièce créé par une plaque mise en résonance. Des simulations numériques, validées par des expériences, montreront que nous pouvons obtenir un certain déplacement vertical soit en combinant une fréquence de vibration élevée avec une faible amplitude ou alors une fréquence plus basse mais avec une amplitude plus élevée. Nous étudierons également le mouvement horizontal d'une pièce allant du ventre vers le nœud de vibration. Le modèle établi tiendra compte de la variation d'amplitude entre les ventres et les nœuds. Le déplacement vertical de la pièce sera limité pour éviter tout mouvement stochastique des

pièces qui engendrerait un mouvement horizontal relativement lent.

Ces différents points de recherche seront illustrés au travers de trois applications. Tout d'abord, deux ondes stationnaires seront combinées pour séparer les pièces. Ces deux modes doivent satisfaire la condition suivante : les ventres du premier mode sont les nœuds du second mode, et les nœuds du premier mode sont les ventres du second mode. Les positions prédéterminées (nœuds) sur la plaque seront utilisées pour connaître la position des pièces sans avoir recours à un système de vision. D'autre part, une série de modes sera déterminée et utilisée pour transporter les pièces d'un point à un autre. Les modes pertinents seront obtenus en réglant le rapport longueur sur largeur de la plaque. Un prototype viendra valider la partie concernant le transport de pièces. Enfin, des modes particuliers, qu'on appelle « dégénérés », seront utilisés pour créer une onde quasi-progressive. Des simulations et des expériences viendront confirmer cette dernière étude.

Mots clefs :Assemblage automatique, Système d'alimentation, Onde stationnaire, Résonance, Actionneur piézoélectrique, Système « bouncing ball », Interaction mécanique, Onde quasi-progressive

Contents

Contents

1 Introduction

1.1 Background and motivation

For a wide variety of manufacturing industries, assembly accounts for more than 50% of the manufacturing cost [7]. With the trend of decreasing product life cycles and to be flexible for a wide variety of parts types, products are more and more manufactured in flexible (automated) assembly system (FAS). A generic FAS consists of three basic parts: a flexible **parts feeder**, one or more flexible **assembly stations** and a programmable **manipulator** (Fig. 1.1). The manipulator will pick the parts from certain known positions, place them on the assembly station and perform the assembly task. The parts feeder should deliver parts in bulk, separate them individually and present them into a certain orientation for the pick-up. The design of the part feeders is responsible for up to 30 % of the cost and 50 % of the work failure of an assembly single station [32]. Therefore, the parts feeder design is critical for the flexible assembly system.
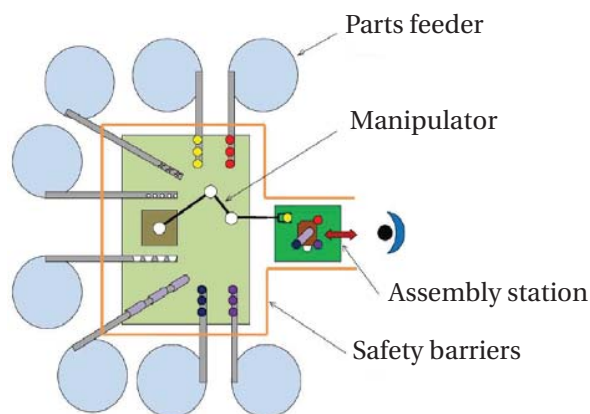
Figure 1.1: Layout of the generic flexible assembly system [53]

The parts feeder can be divided into two groups: *traditional part feeding system* (vibratory bowl feeder as a typical example) and *flexible part feeding system* ("flexible" means adapted to a wide variety of part shapes). The vibratory bowl feeder (Fig. 1.2) is the most widely used and the most versatile in mass production for simple parts due to the low cost and high productivity. In this feeder, there is one track passing around the inside wall of the bowl, the effect of the bowl vibration causes the parts to climb up the track toward the outlet at the top of the bowl. The design of the track (wiper blade, slotted track, pressure break ...) works as a filter that admits the parts having a desirable orientation and rejects other parts for recycling [7]. However, this parts feeder has limited flexibility. When the parts geometry changes, this track must be redesigned, this involves experimental trials. This process is time consuming and thus makes the changeover long. Moreover, if the parts have a complicated shape and many possible natural resting aspects, only one of these orientations will arrive at the outlet of the vibratory bowl feeder. The feed rate can be thus very low. When the batch size is reduced, the vibratory bowl feeder does not become cost efficient any more.

1. Parts
2. Storage hoppers
3. Hopper driver
4. Feeder controls
5. Bowl
6. Vibrating base unit
7. Level controler
8. Track
9. Linear power track
10. Part sensor
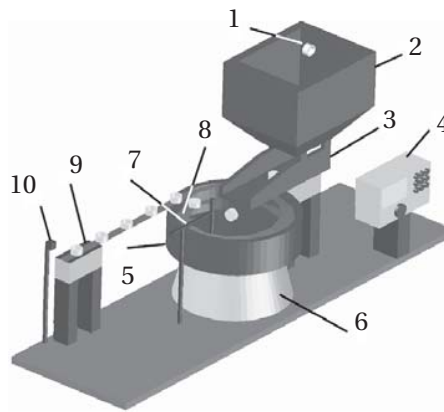
Figure 1.2: Parts feeding system using vibratory bowl feeder [65]

The flexible parts feeding system is more suitable for small-batch and medium-batch manufacturing because of the short changeover. There are typical two variants of parts separation for this parts feeding system - part separation with conveyors [12, 13, 32] (an example is shown in Fig. 1.3) or tooling plate part separation [8, 21] (an example is shown Fig. 1.4). It typically includes five components: (1) a buffer conveyor, (2) a vibrating plate (which is called tooling plate) or a vision conveyor and a return conveyor, (3) the vibrating actuators or drive for conveyors, (4) a vision system, and (5) a robot. The difference is the way to separate parts. With regard to the flexible parts feeder using vision conveyors for separation, the buffer conveyor feeds bulk parts towards the conveyors for separation. The vision conveyor moves parts under the vision system, and the robot picks up the available parts. Parts that are not picked up fall onto the return conveyor. The control should optimize the conveyors' speed to avoid parts starvation (where non parts are visible to the camera on the vision conveyor) and parts

saturation (where too many parts prevent part pose detection or grasping) [32]. With regard to the flexible parts feeder with tooling plate, the buffer conveyor feeds parts onto the tooling plate. The vibrating actuators vibrate the tooling plate to separate the parts and make the parts isolated [51]. Then, the vision system finds parts in any orientation as long as the parts are separated from each other. The vision system detects the separated parts and communicates with the robot so that this latter grasps the available parts. Afterwards, the actuators vibrate the tooling plate and repeat the previous operation until the number of parts left on the tooling plate is smaller than the predefined value. Then the buffer conveyor feeds new parts on the tooling plate. With the help of the vision system and the robot, the flexible feeding system is able to deal with various parts without track redesign. When the part geometry changes, the flexible system only needs to change the vibrating condition by reprogramming rather than hardware changes and therefore allows minimal hardware change cost.
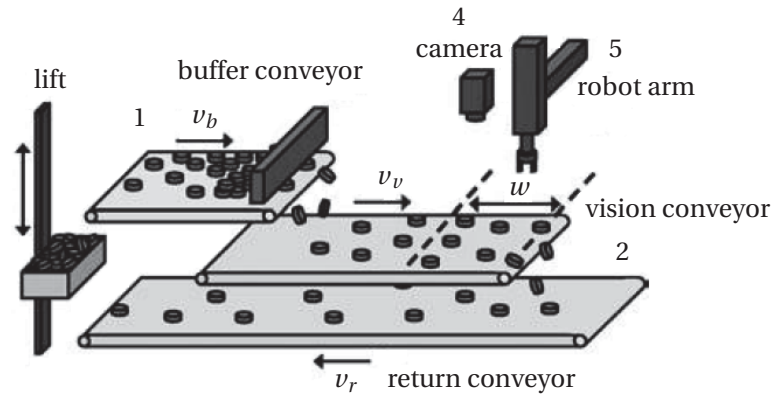
Figure 1.3: Flexible parts feeding system with conveyor for part separation [32]
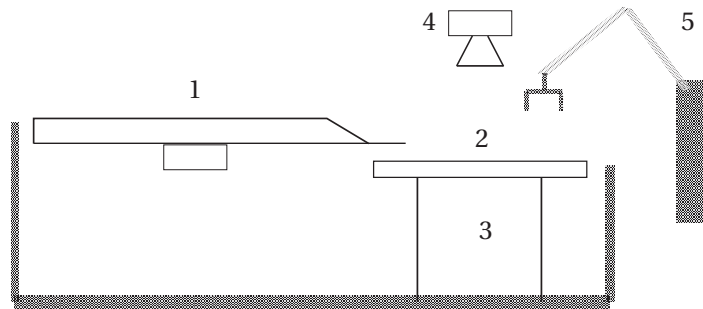
Figure 1.4: Flexible parts feeding system with tooling plate for part separation [51]

The flexible parts feeder with separation conveyors generally takes more space than the one with the tooling plate. Considering the industrial project in cooperation, in this thesis, we concern the parts feeder with the tooling plate. To improve the efficiency of this flexible parts feeding system, various studies have been done on the robot [33, 57], the vision system

[36], the parts pose [46, 37], the vibrating conveyor [67, 49] and the vibrating actuators [51]. Normally, the vision system needs parts well separated from each other on the vibrating plate to be able to recognize the parts. Therefore, it becomes the key point for the system efficiency that the vibrating plate could separate the parts well.

There are studies on the vibrating actuators in order to change the parts position and avoid overlap. For example, Perroud et al. [51] has presented a system which use three vibrating actuator in x, y and z direction to create plate vibration in these three directions or any combination of these three directions, specifically for parts smaller than 3 mm^2. Thanks to the five degrees of freedom of the vibrating plate created by the three vibrator actuators, their system allows effective separation and orientation for small parts where the capillarity and electrostatics force are no longer negligible compared to gravity. Vorstenbosch et al. [66] have put forward the approach to use saw-tooth input signal to obtain different acceleration between parts downward and upward process in order to separate and re-orientate the small parts between 0.5 - 5.0 mm.

(a) Parts feeder   (b) three vibrators
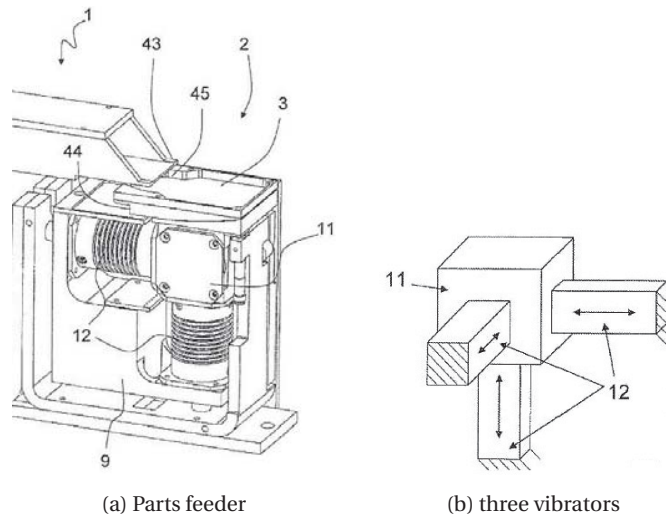
Figure 1.5: Parts feeder with three independent vibrators[51]

The tooling plate is used to change the part state to desirable position. At least, they should provide sufficient acceleration to separate the parts. Majority of the existing tooling plate works under low frequencies, typical 50 - 80 Hz. This frequency generally creates rigid-body vibration on the tooling plate. This rigid-body vibration provides random and uncontrollable orientation of the parts. Therefore, the parts, especially complicated parts, may vibrate many times on the plate before being picked up. This makes the efficiency of the entire parts feeder quite low.

In summary, the flexible feeding system becomes more and more widely used for small-batch and media-batch production. However, this system has a main problem: **random vibration**, which leads to low efficiency. To reduce this randomness, a novel approach is proposed.

Standing waves created by piezoelectric actuators on the tooling plate will be used. In order to address this problem, it is necessary to understand the parts behaviour under existing system condition. Besides, we will investigate the relevant subjects (piezoelectric actuators, standing waves and part-plate interaction) and then apply them to realize the proposed approach.

1.2 Objective and scope of the research

Based on the background introduction and the addressed problem, the objectives and the scope of the researches are presented below.

- *Increase amplitude with piezoelectric actuators*
  The piezoelectric actuators are chosen as the exciter for the standing waves thanks to its compactness, wide frequency bandwidth. It is essential to study how the piezoelectric actuator influences the amplitude and how to obtain desirable amplitude.

- *Obtain desirable resonant modes of a plate*
  With regards to the features of a resonant plate, there are two important aspects: the mode shape and the natural frequencies. The mode shape relates with the anti-nodes and nodes positions. We will study the mode shape variants with the plate geometry changes. The natural frequencies of a plate are discrete and are associated with the mode shapes. Moreover, they play an important role for the interaction between the plate and a part. Therefore, it is important to keep this point in mind for the research.

- *Investigate parts-plate interaction*
  When a part interacts with a vibrating plate, the part behaviour is affected by the vibrating frequency, vibrating amplitude and the material of both the part and the plate. The part behaviours include whether it will stick to the plate or jump on the plate and the travelling distance in different directions. We will study the vertical displacement of a part under different vibrating frequencies and amplitudes. This study could help to control vibrating frequency and vibrating amplitude for close or entangled parts separation. Besides, we will also study the horizontal movement. This study could help vibrating frequency and amplitude control for parts transportation.

- *Validate the feasibility of the proposed approach*
  The proposed approach is to create standing waves on the tooling plate and obtain definite positions in order to reduce the parts vibration randomness. We want to use the researches in our thesis to validate the feasibility of this proposed approach.

This is a total novel approach for the parts feeder. Further industrial considerations (such as cost, efficiency, parts of different shapes, system optimization) are out of the scope of our researches.

1.3   Outline of the thesis

In chapter 2, concepts and existing researches that are relevant to the proposed solution will be summarized. Firstly, the working principles and features of piezoelectric actuators will be introduced. Examples of researches using piezoelectric actuators will be elaborated. Secondly, the boundary condition as an important factor will be discussed. Existing studies using standing waves for parts orientation or other wave manipulations will be addressed. Thirdly, parts behaviour studies will be summarized and a brief illustration for parts behaviour in full range of vibrating condition (combination of vibrating frequency and amplitude) will be introduced.

In chapter 3, we will concentrate on **resonance analysis**. First, the basic theories on resonance will be presented. Then FEM simulation and experiments on modal analysis and harmonic responses will be performed to provide the basis. According to these validated FEM models, we will study the plate geometry influence on the mode shapes. Because the vibrating amplitude is important for part-plate interaction, researches about piezoelectric actuator influence on resonant amplitude will be carried out.

In chapter 4, first, the numerical model for **mechanical interaction between a part and a vibrating plate** will be established in commercial software (Solidworks). The bouncing ball system will be used for the model validation by comparing analytical and numerical simulations. Afterwards, this model will be used to investigate the vertical displacement of a ball and a cylinder under different vibrating frequency and amplitude. Moreover, the model will be used to study the horizontal movement.

In chapter 5, we will present three **applications** based on researches developed in this thesis. Firstly, we will use a pair of modes alternatively to separate parts. Experiments will be carried out to validate whether it is feasible to obtain the desired pair modes and necessary vibrating amplitude. Secondly, we will make use of a series of standing waves in the right sequence to transport parts. A prototype will be manufactured and experiments will be performed to validate the feasibility of parts transportation. Thirdly, degenerated modes in a square plate will be used to create quasi-travelling waves.

In chapter 6, we will conclude the work done in this thesis. We will summarize the academic contribution and industrial applications. At the end, we will put forward the outlook.

2 Literature Review

Our studies are based on an industrial project about parts feeder in automatic assembly. A new approach which uses piezoelectric actuated resonant plate is brought forward. This approach is different from the traditional approaches for this problem. We will give a brief summary about the research topics that will be used in our system. The related concepts and existing pertinent researches are elaborated.

2.1 Piezoelectric actuator

First, we will give the working principles and features of piezoelectric actuators. Then we will review some existing researches dealing with piezoelectric actuators on the relevant topics.

2.1.1 Working principles and features

Working principle and constitution equations

Piezoelectricity was first demonstrated by the brothers Pierre and Jacques Curie in 1880. Piezoelectricity includes direct piezoelectric effect (by applying stress on a solid piezoelectric material, it will exhibit electric charge or voltage) and reverse piezoelectric effect (by imposing electric voltage to a solid piezoelectric material, it will have strain and deformation) [61].

These effects are associated with non-centrosymmetric structure of crystal. For example, a typical non-centrosymmetric crystal (such as perovskite structure in Fig. 2.1) has a net non-zero charge in each unit cell of crystal. A mechanical stress on the crystal further shifts the position of the titanium ion, changing thus the polarization strength of the crystal. This is the direct piezoelectric effect. When the crystal is subjected to an electric field, it results in a relative shift in the position of the titanium ion, leading to the distortion of the unit. This is the source of the inverse piezoelectric effect.

Piezoelectricity can occur in natural material, such as quartz or be given to engineered materials, such as lead zirconate titanate (PZT), by the poling process. Equations 2.1 and 2.2

represent the relationship for inverse piezoelectric effect and direct piezoelectric effect, respectively. Symbols, description and unit are listed in Table 2.1. Details for the matrices of a poled PZT piezoelectric ceramic are in Eq. (2.3), Eq. (2.4) and Eq. (2.5).
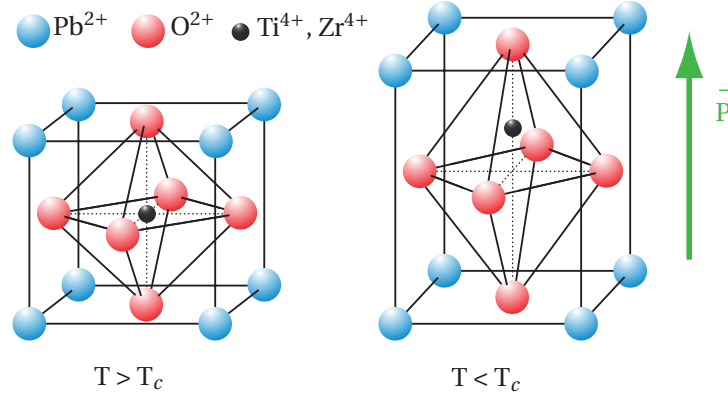
Figure 2.1: Perovskite structure of PZT [52]

$$\{S\} = \left[s^E \right] \{T\} + [d] \{E\} \tag{2.1}$$

$$\{D\} = \left[d^t \right] \{T\} + \left[\epsilon^T \right] \{E\} \tag{2.2}$$

Table 2.1: Piezoelectricity parameters [45]

Symbol	Description	Element unit
$\{S\}$	strain vector	$-$
$\{D\}$	electric displacement vector	$C \cdot m^{-2}$
$\{T\}$	stress vector	$N \cdot m^{-2}$
$\{E\}$	electric field vector	$V \cdot m^{-1}$
$\left[s^E \right]$	elastic compliance matrix at constant electric filed	$m^2 \cdot N^{-1}$
$[d]$	piezoelectric charge coefficient matrix	$C \cdot N^{-1}$ or $m \cdot V^{-1}$
$\left[d^t \right]$	piezoelectric charge coefficient matrix (transposed)	$C \cdot N^{-1}$ or $m \cdot V^{-1}$
$\left[\epsilon^T \right]$	dielectric permittivity matrix at constant stress	$F \cdot m^{-1}$

$$\left[s^E \right] = \begin{bmatrix} s_{11}^E & s_{12}^E & s_{13}^E & 0 & 0 & 0 \\ s_{21}^E & s_{22}^E & s_{23}^E & 0 & 0 & 0 \\ s_{31}^E & s_{32}^E & s_{33}^E & 0 & 0 & 0 \\ 0 & 0 & 0 & s_{44}^E & 0 & 0 \\ 0 & 0 & 0 & 0 & s_{55}^E & 0 \\ 0 & 0 & 0 & 0 & 0 & s_{66}^E \end{bmatrix} \tag{2.3}$$

$$[d] = \begin{bmatrix} 0 & 0 & d_{31} \\ 0 & 0 & d_{32} \\ 0 & 0 & d_{33} \\ 0 & d_{24} & 0 \\ d_{15} & 0 & 0 \\ 0 & 0 & 0 \end{bmatrix} \tag{2.4}$$

$$[\epsilon] = \begin{bmatrix} \epsilon_{11} & 0 & 0 \\ 0 & \epsilon_{22} & 0 \\ 0 & 0 & \epsilon_{33} \end{bmatrix} \tag{2.5}$$

The piezoelectric charge constant d_{ij} is the ratio of achievable mechanical stress to electric field applied (For actuator application). The elastic compliance coefficient s_{ij} is the ratio of the relative deformation S to the mechanical stress T. Eq. (2.1) and Eq. (2.2) indicate that the mechanical and electrical energy are mutually dependent in piezoelectric material. These equations are used both for an analytical approach or finite element method (FEM).

Multilayer piezoelectric actuators

One of the piezoelectric actuator problems is that they need high drive voltage (few thousands of volts). In order to achieve a low driving voltage (lower than 300 V), Kenji Uchino put forward the multilayer structure in 1978 for piezoelectric actuators [62, 63].

As shown in Fig. 2.2, a multilayer actuator is composed of several thin layers of piezoelectric material, alternating with internal electrodes. Internal electrodes are successively positive and negative. All positive internal electrodes are connected by one external electrode to one side of the component; negative internal electrodes are connected to the other side of the component.
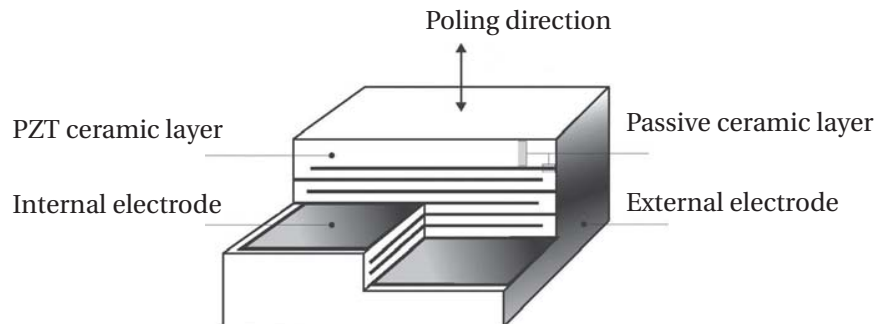
Figure 2.2: Structure of a multilayer actuator [47]

The strain induced in a ceramic is proportional to the applied electric field strength (Eq. (2.1)). By using a thinner layer of piezoelectric ceramic, the distance between internal electrodes is reduced, thus the applied electric field strength is increased. For example, the piezoelectric actuator later used in our system has 25 internal layers of 67 μm. This multilayer actuator structure makes it feasible to use piezoelectric actuator drive voltage under 200 V. In the other hand, the multilayer structure can also be considered as a bulky piezoelectric actuator that is supplied by an equivalent voltage. For example, during experiments, the actuator has 25 internal layers and is driven by a voltage of 200 V. In FE method, the piezoelectric actuator has only one layer and is supplied by an equivalent voltage of 5000 V. The equivalent method allows reducing the mesh element and nodes quantity in simulation in the subsequent FE analysis (3.2.2).

Current and power dissipation

Piezoelectric actuator can be driven under three methods: DC drive for static operation; AC drive for dynamic operation; Pulse drive for switch operation. For resonance or vibration, the piezoelectric actuator will be supplied by an AC drive. Eq. (2.6) describes the relationship between sinusoidal peak current I_p, operating peak-peak voltage U_{pp} and operating frequency f. This will help to determine the minimum specifications of a piezoelectric actuator drive.

$$I_p = \pi f C_{piezo} U_{pp} \tag{2.6}$$

where, C_{piezo} is the piezoelectric actuator capacitance.

Under AC drive, the power dissipated by a piezoelectric actuator can be estimated by Eq. (2.7). $tan(\delta)$ is the energy dissipation factor provided by the supplier. The energy dissipation increases linearly with the capacitance. This energy dissipation is transformed to heat in the piezoelectric actuator and thus limits the piezoelectric actuator working frequency. According to Eq. (2.6), if the piezoelectric actuator capacitance is smaller, the drive current can be smaller. Thus, the energy dissipated in the piezoelectric actuator would be reduced.

$$P = \frac{\pi}{4} f C_{piezo} \tan(\delta) U_{pp}^2 \tag{2.7}$$

2.1.2 Relevant researches on piezoelectric actuator

Piezoelectric actuators have already been applied to bowl parts feeder. Choi et al. [15] have used piezoelectric actuators on the bowl parts feeder in order to design more effective bowl parts feeder compared to the traditional electromagnetic actuator. This indeed provides accurate and adjustable feeding speed thanks to the quick response time, wide frequency bandwidth and accurate control capability of the piezoelectric actuators. Yagi et al. [68] have used piezoelectric actuators for bowl parts feeder. Here the piezoelectric actuators work as actuator and sensors at the same time. They detected the "non-vibration current component" I_{b0} and "total current" to calculate the "vibration current" (Fig. 2.3). This vibration current

is linear with the amplitude of the parts feeder. Therefore, they can accurately control the vibrating amplitude by controlling the vibration current of the piezoelectric actuator without the traditional photoelectric sensor. However, the system still uses bowl feeders. This cannot avoid the drawbacks of redesigning the track of the bowl when the geometry of parts to be dealt with is changed.
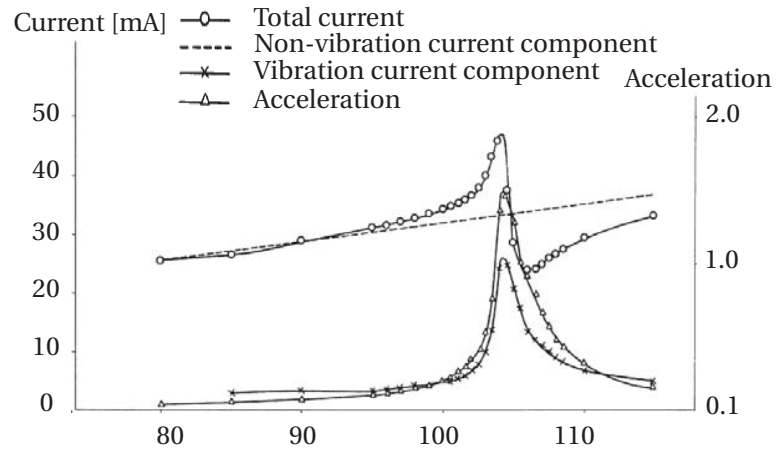
Figure 2.3: Piezoelectric actuator current characteristics using for vibration control [68]

Except in typical parts feeders, piezoelectric actuators have also been investigated for applications related with particle separation. Ooe et al. [48] have proposed to use piezoelectric actuators to create standing waves in the a capillary (dimension: out diameter 800 μm, inner diameter 760 μm, length 80 mm) in order to separate the blood cells from the whole blood (shown in Fig. 2.4). Similarly, we might apply this standing wave separation principle to our system and the piezoelectric actuators could be the exciter because they are compact and have wider frequency bandwidth compared to traditional electromagnetic vibrators.
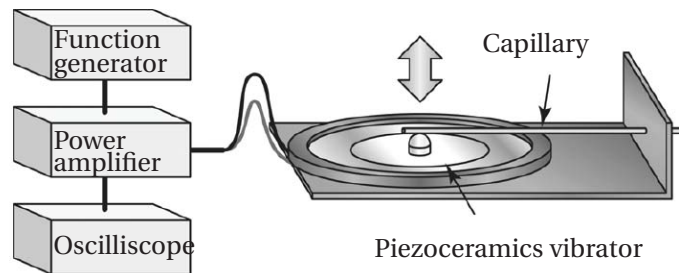
Figure 2.4: Blood cell separation using standing waves created by piezoceramics vibrator [48]

Piezoelectric actuators have also been used to create travelling waves in micropump for moving a liquid [27]. Hernandez et al. have proposed the structure in Fig. 2.5 to create

travelling waves in the flexible metal blade (4 in Fig. 2.5) and in the channel that rests on this latter in order to pump the liquid through the channel from its inlet to its outlet. The advantage of this invention is that they are able to create travelling using only two linear piezoelectric transducers (2 and 3 in Fig. 2.5) with a Langevin structure. Moreover, thanks to the piezoelectric transducer, there is no magnetic field in the system.
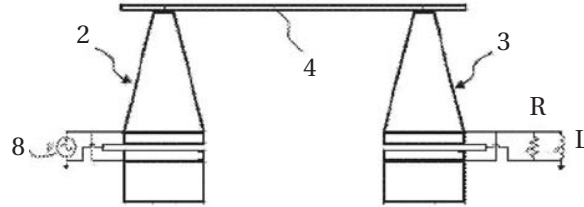
Figure 2.5: Ultrasonic travelling wave micropump for moving a liquid [27]

In the other hand, piezoelectric actuators have already been used for the excitation control. Several studies have focused on how to reduce the vibration using piezoelectric actuators [22, 64]. Z. Kusculuoglu et al. [34] have presented piezoelectric actuator with an electrical resistive-inductive shunt circuit to absorb the vibration at resonance. Dimitriadis et al. [17] have investigated the geometry of the actuators in order to suppress certain modes of vibration. They have presented that if the piezoelectric actuator covers the whole wave-length, the corresponding mode is suppressed.

There are studies which investigate the piezoelectric actuator position and dimension effects on the displacement. Casset et al. [10, 11] have studied the design of a thin-film piezoelectric actuator for haptic applications and obtained around 1 μm vibration for a silicon rectangular plate. They have investigated the piezoelectric film length, width, and position influences. The piezoelectric actuators have a thickness of 2 μm (illustrated in Fig. 2.6). Their studies use an array of piezoelectric actuators for a resonant mode. Moreover, the exciting voltage is low (lower than 10 V), and the resonant system is small silicon substrate (60 mm × 40 mm × 725 μm).
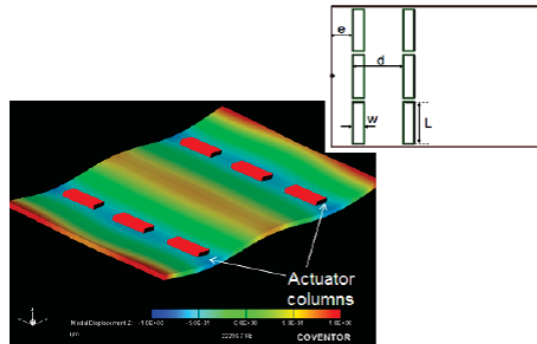
Figure 2.6: Piezoelectric thin-film optimization [10]

Barboni et al. [5] have studied the length and the position influence on a beam (Fig. 2.7a). To obtain maximum displacement of the beam, the actuator with a given length must be located on the beam with the actuator's two edges corresponding to the points of equal curvature (Fig. 2.7c). On the other hand, when the position a of the actuator is fixed, the length h should satisfy the condition that the opposite edges of the actuator must be at the positions with opposite curvatures (Fig. 2.7b). When the beam is clamped at one end, the position of zero deflection is not always the position of zero curvature (Fig. 2.7b and Fig. 2.7c). Therefore, the optimal position of the actuator is not the center of the deflection (For example, the optimal position in Fig. 2.7c is a = 0.711, and the center of the deflection is a = 0.680). However, when the boundary conditions of the two ends of the beam are the same, the center position of the deflection is the center position of the curvature. Therefore, the optimal position of a simply supported is also the center of the deflection (Fig. 2.7d). This study investigates the actuator optimization in 1D but does not refer to 2D actuators.

(a) two-bonded PZT and beam structure	(b) Optimal length h for fixed position a
(c) Optimal position a for fixed length h	(d) Two ends simply supported
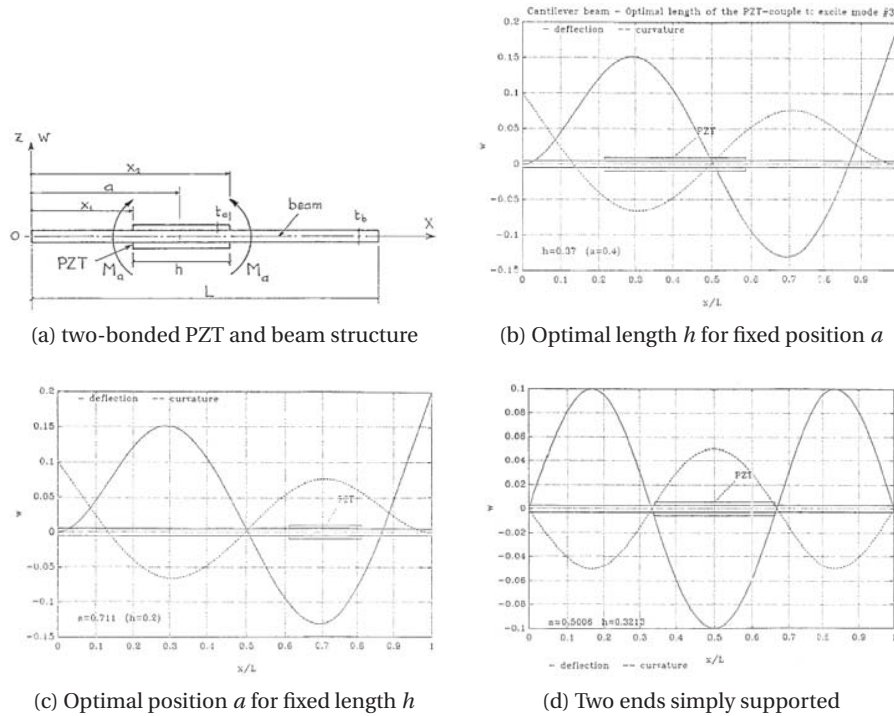
Figure 2.7: Piezoelectric actuator position and length optimization [5]

2.2 Resonant modes - standing waves

2.2.1 Boundary condition

One important point preliminary to the modal analysis is how to consider the boundary condition. Normally, the structure is tested in a "free" condition or "fixed" condition [19].

"Free" means that the test structure is not attached to any surrounding environment. There will be no reaction and constraints for the structure. However, in practice, it is not feasible to provide a truly free support; the structure must be held in certain way. But it is generally feasible to provide a system which is closely approximated to the free condition: suspension system [9] or foam-support system [50] (Fig. 2.8). The suspension system is carried out by suspending the test-structure in the air with very soft elastic strings which are placed as close as possible to the nodal points of mode in question [9]. Depending on the studied Eigenmode, one needs to change the suspension points so that the modes are influenced as little as possible. The suspension system is suitable when the modes have been already determined and there are not so many modes to study. The foam-support system is implemented by putting the structure on very soft foam. "Fixed" means that selected points or surface of the test structure are fixed to the ground. In practice, it is much more difficult to implement this "fixed" condition, because it is very difficult to provide a base or foundation which is sufficiently rigid for the test structure. Besides, in theory, the "free" boundary condition structure has more degrees of freedom than "fixed" boundary condition structure. Therefore, it includes more modes [19].

(a) Elastic suspension system [9]   (b) Foam-support system [50]
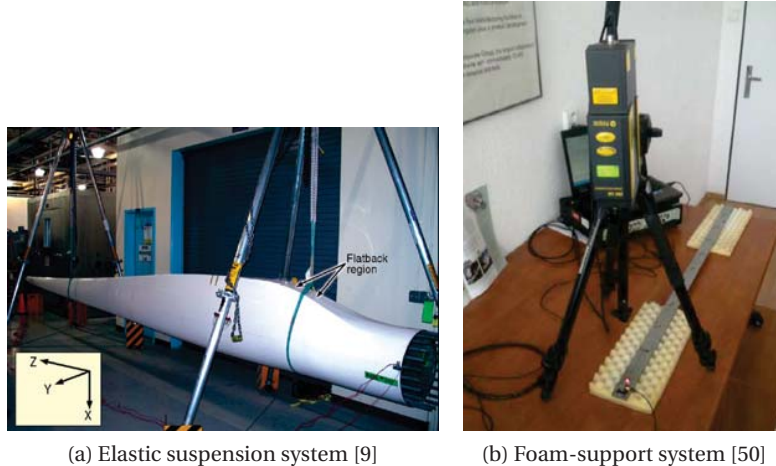
Figure 2.8: Free boundary condition experiment implements

2.2.2   Relevant researches

Böhringer et al. [6] have used standing waves to align planar parts. Depending on the mode shapes and node positions of the plate, the planar parts can be controlled to specific position sensor-less (as shown in Fig. 2.9b). Vibrating exciter in their study are the traditional electro-magnetic ones. The low working frequency limits the numbers of nodal lines. Moreover, the traditional exciter is bulky.

Another typical application is that combining two standing waves in the ring-type structure to

(a) Schematic of experimental setup   (b) Parts alignment
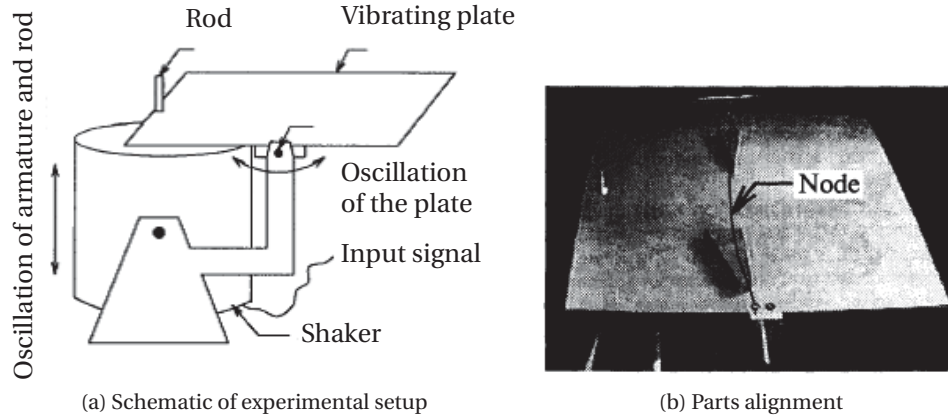
Figure 2.9: Standing wave for parts alignment [6]

create travelling wave for piezoelectric ultrasonic motors [31, 18]. In the ring-type structure, there are two standing waves (called degenerated modes), which have the same resonant frequencies but different spatial pattern. However, there are studies which discuss the standing waves in non-ring-type structures. Setter et al. [55] have tuned the standing waves on a rectangular plate to obtain different vibration pattern from a single plate. They use 32 voice-coil actuators and more than 500 sensed locations to tune the force distribution by iteration in order to obtain the arbitrary vibration patterns. Fig. 2.10 depicts the representation of the structure (Fig. 2.10a) and the same structure after tuning process (Fig. 2.10b). The working frequency of the plate is smaller than 100 Hz. In this study, one plate can create different wave patterns. However, the system was complicated and bulky as well.
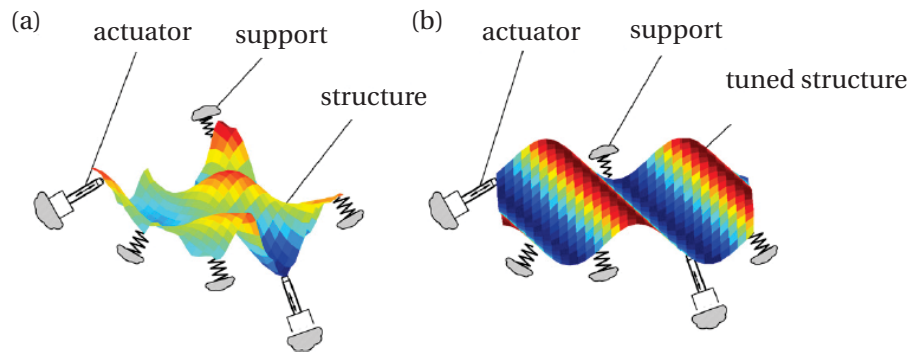
Figure 2.10: (a) Vibrating structure before tuning (b) a travelling wave of the same structure after tuning [55]

Manceau et al. [42, 43] have made use of piezoelectric actuators to create quasi-travelling waves in rectangular and square structure which are not ring type structure (Fig. 2.11). However, the system is quite small, $20 \times 30 \times 1 \ mm^3$ for the resonant structure.
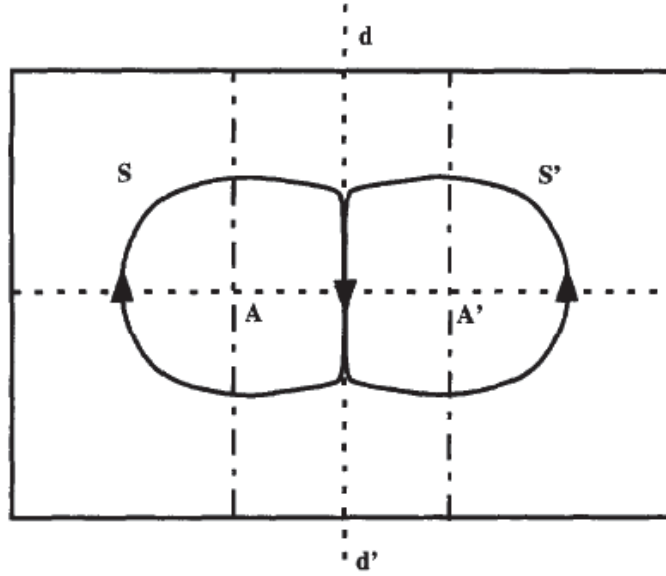
Figure 2.11: Quasi-travelling waves created by standing wave in rectangular plate. The quasi-travelling wave propagates along the curve S and S', the dash-dot (-··-) lines and dashed lines (--) are the nodal lines for the two modes, respectively [42].

2.3 Parts' behaviour under vibration

With regards to the parts in automatic industry, previous researches include parts natural stable pose [24] and parts vibration behaviour under the vibrating plate [16, 25]. A lot of researches are based on the well-known bouncing ball system [28]. The basic system consists of a ball and a horizontal plate which vibrates in the vertical direction (Fig. 2.12) [41]. According to the applications, the variants of this research include: (1) the horizontal plate vibrate in a direction that has specific angle with the horizontal level [67]; (2) the vibrating plate has a small angle with the horizontal level and the vibration direction is along a direction which has an angle with the plate surface [39]; (3) the vibrating plate has a small angle with the horizontal level with elliptical vibration [29, 3]. Depending on the vibration conditions, the parts behaviour changes. Parts behaviour in case of standing waves has never been studied and it will be interesting to investigate it.

When one studies the bouncing ball subject, the key tool is the dimensionless parameter k defined by Eq. (2.8), which is determined by the plate vibrating frequency and vibrating amplitude. The ball may stick to the plate, jump periodically or chaotically [60, 29]. When $k < 1$, ball is in the sticking region, that means because of the small acceleration, ball always sticks to the plate and moves together with this latter [30, 29] - there is "no bouncing". Increasing k, the ball will have periodic and chaotic vibrations as illustrated in Fig. 2.13. When $1 < k < k_{1,1}$, ball is in the region where the acceleration is big enough and the ball starts jumping, but still sticks to the plate for some time, with $k_{1,1}$ expressed in (2.9). e is the restitution coefficient
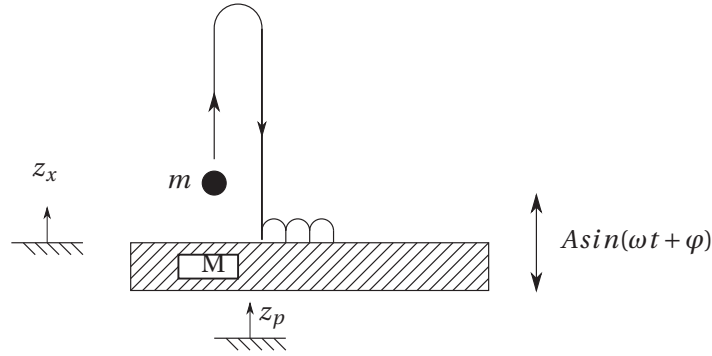
Figure 2.12: Schematic of a bouncing ball system [41], where z_p is the plate displacement, A is the vibrating amplitude, ω is the angular frequency, φ is the initial phase of the vibration, z_r is the relative distance between the part and the plate in the normal direction to the plate surface, m is the ball mass and the black dot represents the ball.

(Eq. (2.12)). When $k > k_{1,1}$, ball is in the jumping region. In this region, the ball can vibrate periodically or chaotically. "pattern-m, r = n" means that during one period of the ball, the ball has "m" kinds of pattern and for each pattern, the plate has "n" periods (Fig. 2.13). With this definition, when $k_{1,1} < k < k_{2,1}$, ball has vibration "pattern-one, r = 1". $k_{2,1}$ is expressed in Eq. (2.10). When $k_{2,1} < k < k_{3,1}$, ball has "pattern-two, r = 1". $k_{3,1}$ can be calculated with Eq. (2.11). When k increases, a new state "pattern η, r = 1" occurs and so on, until $k_{\infty,1}$ where the chaotic region is reached [59]. When k keeps increasing, the ball will have vibration of "pattern-one, r = 2", "pattern-two, r = 2", ... and chaotic (Fig. 2.13).

$$k = \frac{A\omega^2}{g} \tag{2.8}$$

$$k_{1,r} = \pi r \left(\frac{1-e}{1+e}\right) \tag{2.9}$$

$$k_{2,r} = \sqrt{4\frac{\left(1+e^2\right)^2}{(1+e)^4} + \pi^2 r^2 \left(\frac{1-e}{1+e}\right)^2} \tag{2.10}$$

$$\delta_F = \frac{k_{\eta+1,r} - k_{\eta,r}}{k_{\eta+2,r} - k_{\eta+1,r}} = 4.6992... \qquad \eta = 3,4,5... \tag{2.11}$$

We give one example of the variety of k in Table 2.2. According to this table, we can calculate the range k for periodic vibration (r = 1) and the range k for the chaotic vibration (vibration changes from r = 1 to r = 2), the values are respectively, 0.60 (between 1.57 and 2.17) and 0.97 (between 2.17 and 3.14). The range of periodic vibration is much narrower than that of chaotic. This means that even with good control, the ball will reach the chaotic vibration easily. Moreover, the external vibration disturbance in the environment and the load variety (number of parts) interface bowl's vibration and thus lead to chaotic vibration.
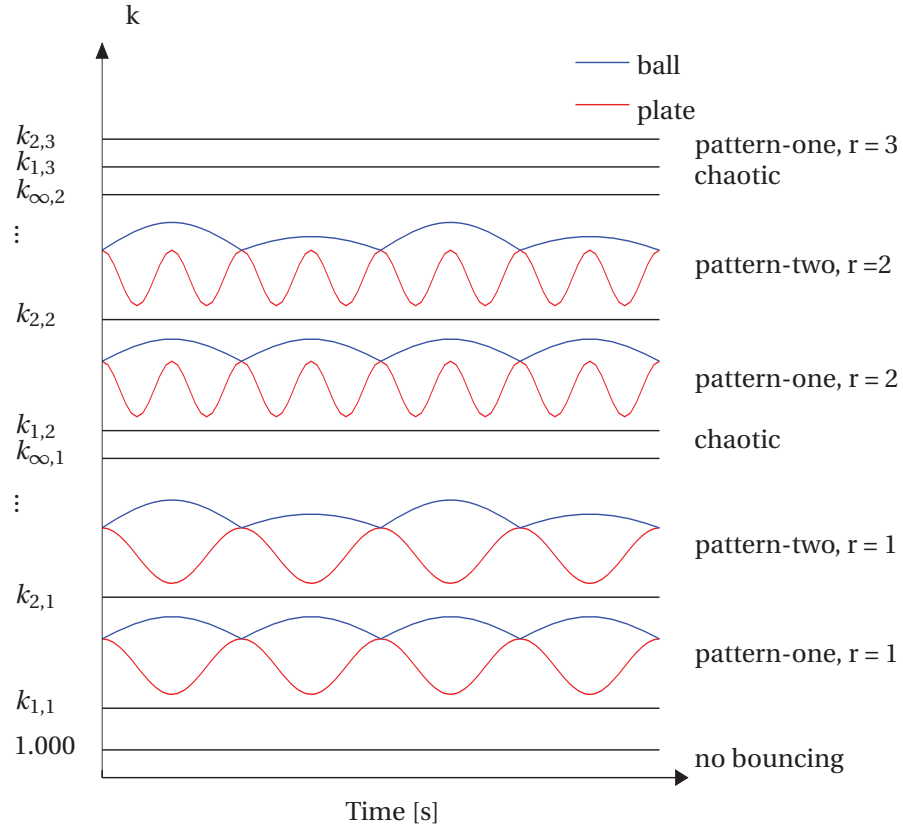
Figure 2.13: Bouncing ball behaviour under vibrating plate [29]

Table 2.2: k examples (e = 0.333)

r	$k_{1,r}$	$k_{2,r}$	$k_{3,r}$	$k_{4,r}$	$k_{5,r}$	$k_{6,r}$	...
1	1.57	2.01	2.13	2.16	2.17	2.17	...
2	3.14	3.38	3.44	3.45	3.45	3.45	...
3	4.72	4.88	4.92	4.92	4.92	4.92	...

Coefficient of restitution

There are two ways to study the impact: coefficient of restitution and impact force (calculated with assumed penetration and contact stiffness [58]). Coefficient of restitution is normally used in the research of bouncing ball system. It describes how the kinetic energy varies after a collision between two parts. Eq. (2.12) gives the relationship between the coefficient of restitution and the velocities before and after impact. This coefficient depends on the two materials of the structures involved in the impact. Generally, the collisions are inelastic meaning the kinetic energy is not conserved but dissipated during the impact. In an inelastic

collision, the coefficient of restitution is between 0 and 1.

$$e = \frac{v_{f,b} - v_{f,a}}{v_{i,a} - v_{i,b}} \qquad (2.12)$$

where $v_{f,a}$ is the final velocity of object A after impact. $v_{f,b}$ is the final velocity of object B after impact. $v_{i,a}$ is the initial velocity of object A before impact. $v_{i,b}$ is the initial velocity of object B before impact.

Actually, the coefficient of restitution is not a constant. It varies with the masses, the impact velocity of the two bodies and the shape of the impact parts [35]. However, we use a constant value to simplify the model as long as the research subject's error is acceptable.

2.4   Summary and conclusions

In this chapter, we have summarized the relevant subjects related with the proposed solution. Firstly, we have presented the working principles and features of piezoelectric actuators. Some examples of existing researches using piezoelectric actuators were discussed. Afterwards, researches using resonant modes for parts manipulator or wave control were addressed. At the end, parts behaviour studies were summarized and the pertinent subject (bouncing ball system) was introduced. Reviews on existing studies helped us to understand the parts feeder system and gave a clue to our researches.

3 Piezoelectric actuated plate resonance analysis

In this chapter, firstly, we will first give the theories about equation of motion and damping and information about the piezoelectric actuator. Then we will use experimental results to validate the simulation in FE modal analysis and harmonic response. Afterwards, we will study the piezoelectric actuator's influence on the plate amplitude in terms of piezoelectric dimension, shape and orientation, and thickness. At the end, we will study the plate geometry influence on the mode shapes, specifically, the relative nodal line positions between two successive modes.

3.1 Conventions and methods

Equation of motion

Equation of motion is the first step in structure vibration analysis. It can be expressed as [1]:

$$[M]\{\ddot{u}\} + [C]\{\dot{u}\} + [K]\{u\} = \{F\} \tag{3.1}$$

where
$\{u\}$ = displacement vector
$\{\dot{u}\}$ = velocity vector
$\{\ddot{u}\}$ = acceleration vector
$[M]$ = mass matrix
$[C]$ = damping matrix
$[K]$ = stiffness matrix
$\{F\}$ = applied load vector

The displacements, velocities and accelerations are unknowns which vary with time. Mass, damping, stiffness and applied load are known constants and known function which varies with time. This equation can be used for modal and harmonic response. For modal analysis, the applied load $\{F\}$ is zero (we assume that the mass and stiffness are constant with time). Normally, we do not consider damping (except for damped modal analysis) for modal analysis.

The modal analysis is used to determine the natural frequencies and corresponding mode shapes. For harmonic response analysis, all the loads $\{F\}$ vary at the same frequency (we assume that the structure has constant mass and stiffness; the damping may be constant or frequency-dependent). The harmonic response analysis is used to determine the displacement response under harmonic loads. In this thesis, we will use FEM (Finite Element Method, implemented in ANSYS), which solves the equation of motion numerically , to perform modal analysis and study the harmonic response for a structure.

Damping

Damping has an influence on the vibrating amplitude of a resonant system. The damping are generally divided into two types: material damping and system damping. The material damping represents the energy loss at a molecular level. The system damping represents the energy dissipated in the structure. It includes the energy dissipation of the structure internal joints and interfaces between the structure and supports. When certain components in the entire structure have much higher damping than others, such as a cast iron or rubber components in a steel weldment assembly, material damping coefficient needs to be considered as input separately. If the whole structure has components whose damping are quite close to each other, an overall system damping coefficient is determined to be applicable for the entire structure, material damping is not necessary [2]. The target structure in our study is made of aluminium and its damping can be represented by the overall system damping coefficient. Damping ratio is a dimensionless measure for the system damping coefficient. It is the ratio between actual damping coefficient "c" and critical damping c_c.

$$\zeta_r = \frac{c}{c_c} \tag{3.2}$$

$$\omega_r = \omega_0 \sqrt{1 - \zeta_r^2} \tag{3.3}$$

For SDoF system (single-degree-of-freedom system), critical damping can be calculated by $c_c = 2m\omega_r$. ω_r is the damped natural frequency for r_{th} mode [20], "m" is the mass of the system.

Most mechanical structures' damping ratio are usually well below 10% [2]. This induces a difference between ω_r and ω_0 of about 0.5% (according to Eq. (3.3)). Therefore, for a modal analysis, damping is generally not taken into account. With regard to the harmonic response, the damping affects the vibrating amplitude. It is quite difficult to obtain damping without measurements. Damping ratio can be measured using logarithmic decrement method [23] in time domain or the half-power method [20] in frequency domain. Logarithmic decrement method can be calculated by the data from the free vibration decay caused by a spike input such as an impact with a hammer. The ideal impact is a perfect impulse, which has an infinitely small duration, causing a constant amplitude in all the frequency domain. However, in reality, a hammer strike cannot last for an infinitely small duration, but has a known contact time. This duration influences the frequency component. A large contact time causes a small range

of frequency bandwidth. For the logarithmic decrement method, the impact duration should be well controlled to obtain the desired frequency bandwidth. Half-power method is suitable for lightly damped system with well-separated modes and good frequency resolution. In the following, half-power method is applied to ensure that all the modes in question are studied. Eq. (3.4) gives the equation which allows calculating the damping ratio using the half-power method which is also illustrated in Fig. 3.1.
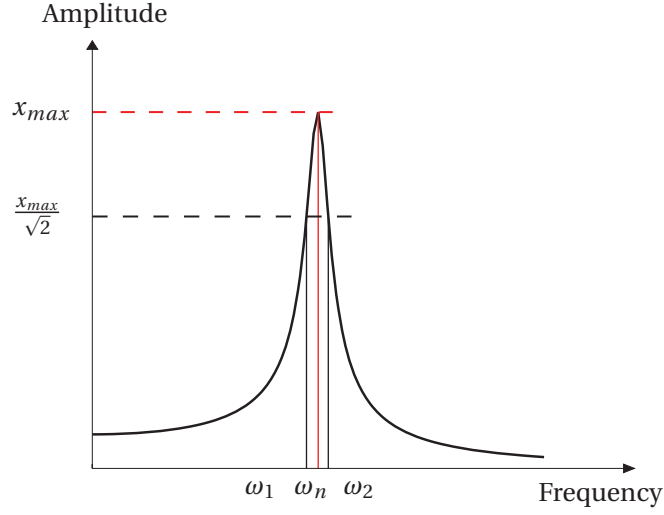
Figure 3.1: Half-power method for damping measurement [20]

$$\zeta = \frac{\omega_2 - \omega_1}{2\omega_d} \tag{3.4}$$

Free boundary condition

Based on the discussion in subsection 2.2.1, considering that we want to study several modes and also the simplicity of implementation, free boundary condition is chosen in our system. In all the experiments, it will be performed with foam - support system. The foam (shown in Fig. 3.2) is used in the experiment as support and is assumed to be considered as free boundary condition (this will be validated in subsection 3.2.2). It is a low density, flexible polyurethane foam. The surface is convoluted with egg crate. The uniform egg crate shape will provide evenly distributed support force.

Piezoelectric actuator

In our system, we choose commercial piezoelectric actuator [47], which is familiar to our laboratory, as the first step of our research. The shape of the existing piezoelectric actuator is square prism. The piezoelectric actuator is polarized in the direction perpendicular to the square surface of the square prism (with size of $10 \times 10 \times 2 \ mm^3$ and $5 \times 5 \times 2 \ mm^3$).
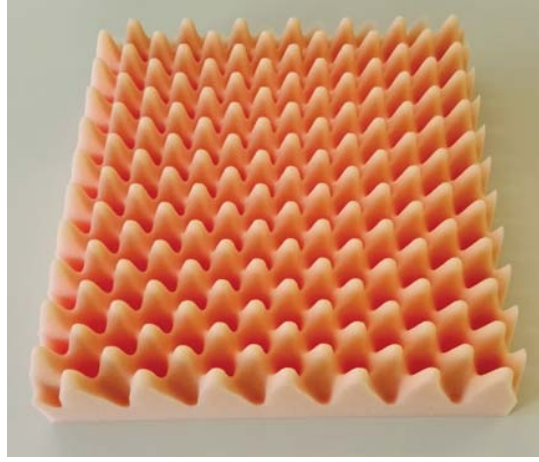
Figure 3.2: Free boundary condition equivalent foam

The piezoelectric actuators have displacement in the direction of their thickness as the solid red arrow shown in Fig. 3.3. The corresponding piezoelectric charge coefficient is $d_{33} = 290 \times 10^{-12} \ C \cdot N^{-1}$. Due to the Poisson ratio, there are also displacement in the directions of the piezoelectric actuator's surface as shown by the dashed black arrows in Fig. 3.3. The equivalent piezoelectric charge coefficient is $d_{31} = 130 \times 10^{-12} \ C \cdot N^{-1}$. The piezoelectric actuator can be mounted to the resonant structure by gluing its bottom or top surface on the structure.
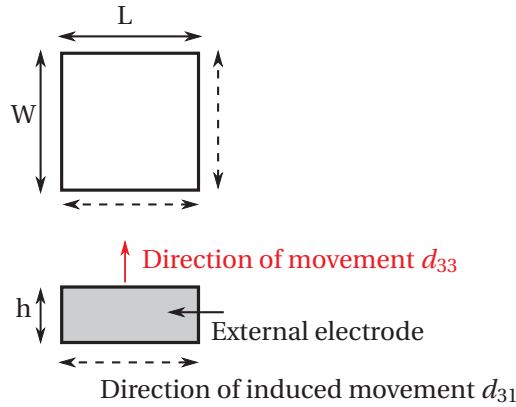
Figure 3.3: Piezoelectric actuator in use [47]

According to the study of Barboni et al. [5], for a piezoelectric actuator with given dimension, the plate can obtain maximum deflection when the two opposite edges of the piezoelectric actuator are located to the points of equal curvature. In our system, for free boundary conditions, when the two opposite edges of the piezoelectric actuator are located to the points with equal curvature, it is exactly at the maximum deflection. This means that the piezoelectric should be located to the anti-nodes. Considering the surface bonding with plate, we agree

on the **piezoelectric actuator's position choice**: If the anti-nodes of the plate's mode shapes are on the edges or the corners of the plate, we do not consider them as valid positions for piezoelectric actuators.

Since negative electric field can induce loss of polarization, DC offset is superposed on the harmonic excitation to avoid it. In our system, all input voltage for piezoelectric actuator in experiments will be always a sinusoidal wave of U_{pp} with a DC offset of $\frac{U_{pp}}{2}$. For example, a typical input voltage is a sinusoidal wave of 100 V_{pp} with 50 V DC offset.

3.2   Modal analysis and harmonic response

Modal analysis is used to determine the natural frequencies and corresponding mode shapes. It is the starting point for structure engineering analysis. Harmonic response is used to study the plate amplitude with piezoelectric actuators under different kinds of voltage and frequency excitations. In this section, we will use both FE simulations and experimental verifications interactively to carry out the study.

Fig. 3.4 illustrates the four modules, which include two FE models and two experiments. Module A is the finite element (FE) modal analysis. We use numerical FE model to firstly predict the natural frequencies of a specific structure. Module B is the modal analysis experiments which include the measurement of natural frequencies and mode shape demonstration, separately. The correlation between these natural frequencies and their corresponding mode shapes is identified by mode shape demonstration, especially useful for modes whose natural frequencies are quite close with each other. This module is used to validate the modal analysis in module A. The validated FE model in module A can be used for modal analysis of other structures.
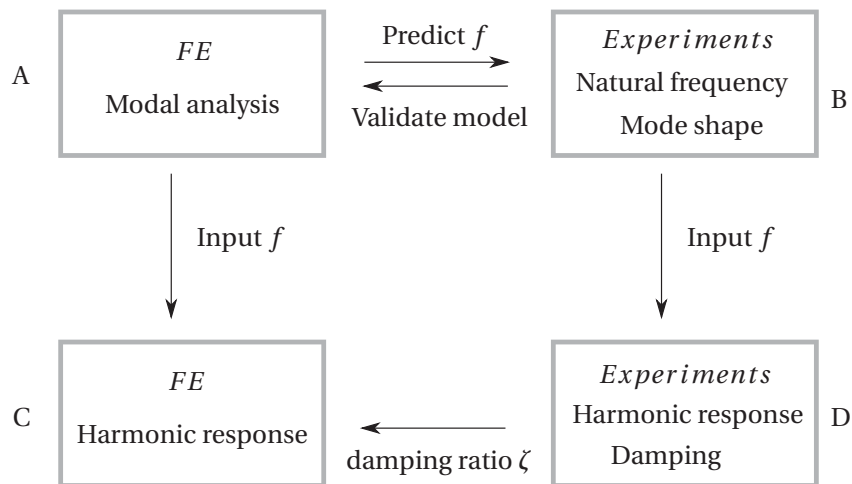
Figure 3.4: Structural analysis flow chart

Module C is the FE model for harmonic response analysis. This simulation needs the damping ratio from experiments of module D. To well implement harmonic response experiments, it is necessary to obtain accurate natural frequencies from module B. The experimental amplitude of the plate will be used to verify the FE harmonic response in module C. And the validated FE harmonic response can be used to study the harmonic response under different voltages. Moreover, it can be used to investigate how to improve the harmonic response, such as increase the vibrating amplitude.

Geometry and material

The structure for modal analysis and harmonic response is a simple square aluminium plate ($180 \times 180 \times 3 \ mm^3$). We have chosen this structure for three reasons. Firstly, the plate size is similar to the industrial tooling plate on which the thesis work is based. Secondly, the simple plate is used to reduce the difference between FE model and experimental prototype which derives from the manufacturing process. Thirdly, the square plate is chosen because it provides special mode pairs that will be discussed in chapter 5.

The aluminium alloy used for the structure has the following properties:

- Density $\rho = 2{,}770 \ kg \cdot m^{-3}$
- Young's modulus $E = 7.10 \times 10^{10}$ Pa
- Poisson's ratio $v = 0.33$

3.2.1   Modal analysis

FE simulation

To study the structure system and choose the desirable modes, numerical method - FE (finite element) method, is applied. Actually, for simple structure, analytical method can also solve the problems [38]. However, the solution needs to be classified according to which kinds of modes they are. When the modes have symmetry about coordinate axes and both diagonals, the solution will be different from the solution of modes that have symmetry about the coordinate axes and antisymmetric about diagonals. Thus it will be difficult to use analytical method to study a lot of modes of the structure. So we have chosen to use FE method. We can thus obtain several natural frequencies and mode shapes at one time. The FE model is implemented in ANSYS workbench [4]. Eq. (3.1) becomes Eq. (3.5), and is the basis of simulation for modal analysis.

$$[M]\{\ddot{u}\} + [K]\{u\} = 0 \tag{3.5}$$

Mode representation
Fig. 3.5 gives two mode shapes illustration for the square plate with free boundaries. The

values of the deformation have no physical significance. It is the "shape" of the vibration modes that are meaningful. The local maximum and local minimum values correspond to the anti-nodes and nodes, respectively. In the modes shown in Fig. 3.5a and Fig. 3.5b, the nodal lines (dark blue lines) are parallel to direction x and y. This kind of modes exist also in rectangular plate. We name this mode as mode (2, 2) (Mode (m, n) means "m" and "n"are designated numbers attached to the mode shapes, where "m" is the number of half-wavelength across the x direction and "n" is the number of half-wavelength across the y direction). We observed that there are one anti-node in the center and eight anti-nodes on the edges or at the corners of the plates. To excite this mode, according to the convention on the piezoelectric actuator's position choice, the piezoelectric actuator should be mounted in the center of the plate. Fig. 3.5c and Fig. 3.5d show an example of special mode in the square plate. This kind of modes has nodal lines that are parallel to or pass through the diagonals of the plate. The right position of the excitation is also the center of the plate. In the following of this thesis, we will use only 2D illustration.
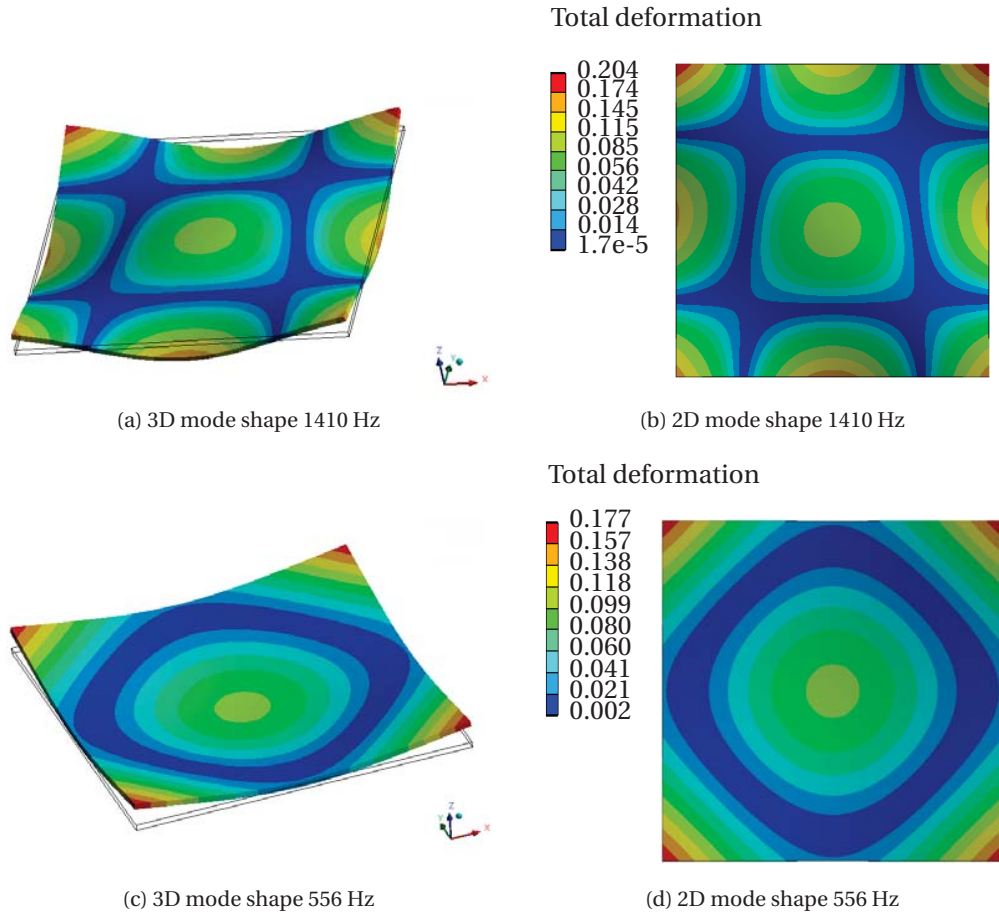
Total deformation

| (a) 3D mode shape 1410 Hz | (b) 2D mode shape 1410 Hz |

Total deformation

| (c) 3D mode shape 556 Hz | (d) 2D mode shape 556 Hz |

Figure 3.5: Mode shape illustration

Different mode shapes

A mechanical structure with free boundaries has many natural frequencies and corresponding mode shapes. To help to choose the desirable modes and possible corresponding exciter position, Fig. 3.6 presents the FE simulation results in terms of mode shapes and resonant frequencies. The dark blues are the nodal positions. The red squares indicate the valid positions for piezoelectric actuators.

In Fig. 3.6a, the anti-node positions are in the four corners of the plate. According to the agreement on the piezoelectric actuator's position choice, there is no valid position for piezoelectric actuator. Therefore, this kind of mode is considered as inappropriate modes in this thesis. Fig. 3.6b shows a typical mode whose nodal lines are parallel to x and y directions but without the same number of half-wavelength across these two directions.

Fig. 3.6c and Fig. 3.6d show two other mode shapes. For each mode shape, their nodal lines are only parallel to either x direction or y direction. The two modes have exactly the same natural frequencies but different mode shapes (modes which are called degenerated modes). Although these two mode shapes have the same natural frequency, we can excite each modes with different piezoelectric actuators. For example, the mode shown in Fig. 3.6c can be excited with piezoelectric actuators at positions A_1 or A_2 without interference from the mode shown in Fig. 3.6d, because positions A_1 or A_2 are nodal positions in the mode shown in Fig. 3.6d. In the same manner, the mode shown in Fig. 3.6d can be excited with piezoelectric actuators at positions B_1 or B_2.

Fig. 3.6e and Fig. 3.6f present two additional mode shapes. There are respectively four and five positions that can be used to mount the piezoelectric actuators. These two modes are the specific modes in square plate, whose nodal lines are parallel to or pass through the diagonals of the plate (Fig. 3.6f and Fig. 3.6e). Additionally, there is one interesting feature about the relative position between these two mode shapes. The anti-nodes in Fig. 3.6e are close to nodes in Fig. 3.6f. Moreover, the nodes in Fig. 3.6e are close to anti-nodes in Fig. 3.6f. This special feature will be used for parts separation in automatic assembly part feeder (Details are in section 5.2).

We have also observed some phenomenons: Firstly, one piezoelectric can be used to excite different mode shapes. For example, a piezoelectric actuator mounted in the center underneath the plate can excite the modes in Fig. 3.5b, Fig. 3.5d and Fig. 3.6f with resonant frequencies of 1410 Hz, 556 Hz and 2765 Hz, respectively. Secondly, for modes which have close natural frequencies, appropriate position for piezoelectric actuator can excite expected modes without interference from other modes. For example, with regard to modes in Fig. 3.5b, Fig. 3.6c and Fig. 3.6d, they have very close natural frequencies. We can obtain these three modes by exciting piezoelectric actuators at the positions in the center, A_1 or A_2, and B_1 or B_2, respectively, without interferences from the other two modes. Because the excited position of piezoelectric actuator for one mode is the anti-nodes for the other two modes.

(a) 302 Hz
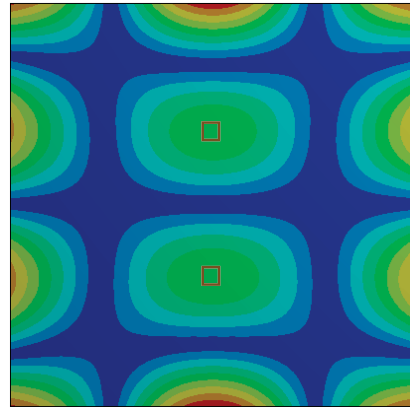
(b) 2338 Hz
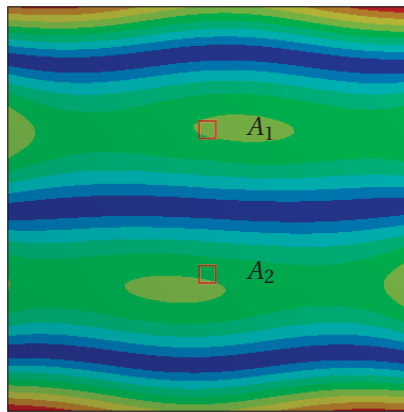
(c) 1386 Hz
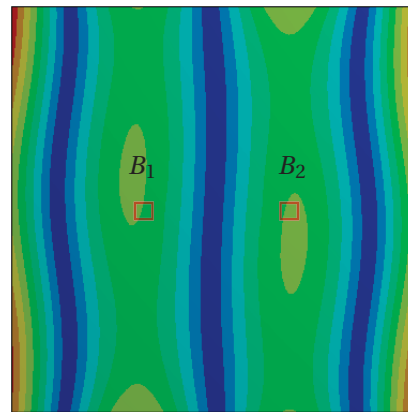
(d) 1386 Hz
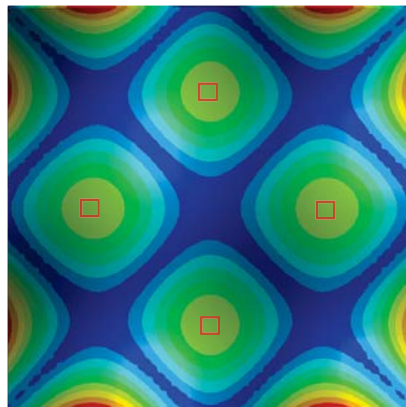
(e) 2629 Hz
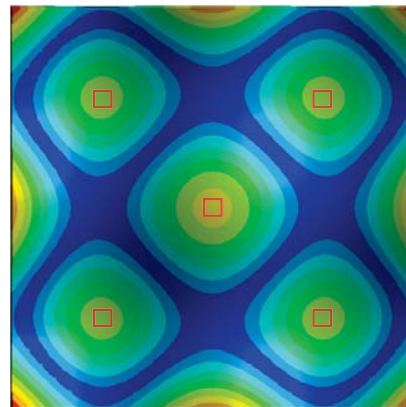
(f) 2765 Hz

Figure 3.6: Different mode shapes

Experiments for modal analysis

To verify the FE model simulation, experiments for modal analysis have been performed. These experiments include finding the **natural frequencies or resonant frequencies** and visualizing the corresponding **mode shapes**.

The entire experimental set-up has four parts. The first part is the plate itself - the resonant structure; the second part is the exciter; the third part is the measurement equipment or method; and the last part is the analyser to perform the analysis for the data. The structure support is foam and is supposed to be equivalent to free boundary condition. The exciter is one or several piezoelectric actuator(s) and is (are) glued underneath the aluminium plate. Thus, the piezoelectric actuator will induce stress between itself and the plate and work as a surface contact exciter. The typical measurement of the structure response will be the displacement or the velocity. Doppler laser vibrometer is used to detect the velocity of specific point. It has the advantage that there is no interfering with the structure thanks to the non-contact measurement.

Natural frequencies

The typical way to obtain the structure natural frequencies is to use FRF (frequency response function) method. The frequency response function is the ratio between the output response and the input response, typically the ratio between the output displacement and the input force. This method can provide not only the natural frequencies but also the mode shapes in the case of complete measurements. This method involves displacement measurements and force measurements. The force measurements are usually complicated.

For our specific application, a method to detect specific natural frequencies in an easy way - is to measure the equivalent capacitance-resistance series connection spectrum of the plate and piezoelectric actuator system and obtain the resonant frequencies according to the **resistance spectrum**. The piezoelectric actuator itself can be equivalent to a series connection of a capacitor and a resistance. The resistance stands for the heat energy dissipated in the actuators. When the piezoelectric actuator is mounted with a plate and works at plate resonance, the resistance stands for the heat energy and the energy that is dissipated in the structure because of damping in order to keep the standing waves. The dissipated heat energy is quite small compared to the energy that is transferred to the structure. Therefore, in the measured resistance spectrum, the frequencies at which the resistances are maxima in the local frequency range can be considered as the resonant frequencies. Liu et al. [40] uses the similar method to study the energy transfer of a simply supported structure. In this thesis, we will use this method to obtain the resonant frequencies (very close to natural frequencies when the damping is small). Impedance analyser Agilent 4294A is used to measure the capacitance-resistance spectrum of the system. The impedance analyser works with an oscillation level of 500 mV. The frequency increment step is 1 Hz. The system is the above mentioned square aluminium plate with a piezoelectric actuator glued underneath the plate in the center. With regard to

this piezoelectric actuator and plate configuration, we study the modes that can be excited at a frequency lower than 8,000 Hz. Fig. 3.7 shows the resistance spectrum of the study system. There are six local maxima. Their values (marked with "f_d maxima-R") are listed in Table 3.1.
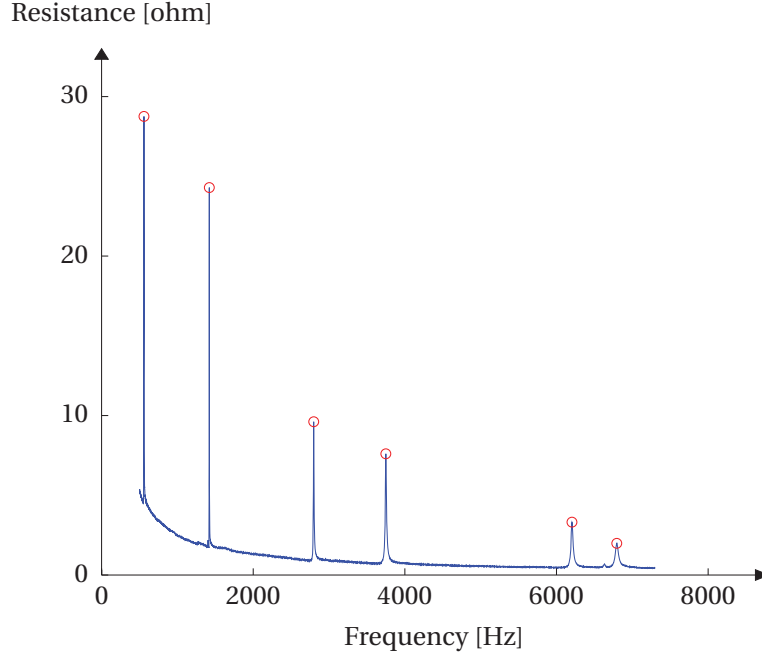
Figure 3.7: Resistance spectrum of a piezo-plate system

We will verify this method by comparing the resonant frequencies obtained from this method with resonant frequencies obtained from typical displacement based method. The displacement is measured with a Doppler Laser Vibrometer (Polytec compact laser vibrometer CLV 1000). The input voltage for the piezoelectric actuator is a sinusoidal wave of 100 V_{pp} with 50 V DC offset. For each mode, there is a maximum. We will also measure the amplitude in each resonant frequency's vicinity at least larger than the frequency bandwidth ($\Delta \omega = \omega_2$ - ω_1) in order to obtain the damping ratio ζ (Details refer to the following part **Damping ratio measurement**). For each mode, the frequency increment is 1 Hz or 2 Hz (The minimum frequency increment step 1 Hz is limited by the piezoelectric actuator's drive, 2 Hz frequency increment is applied when the plate amplitude vary slightly with frequency changes. We do not measure the amplitude that is too far from the resonant modes). Fig. 3.8 shows the amplitude spectrum in the full range below than 8000 Hz. Corresponding resonant frequencies are listed in Table 3.1, marked with "f_d reference".

We see that all "f_d maxima-R" are bigger than "f_d reference". However, the absolute value of "f_d maxima-R" is close to "f_d reference" with an error of less than 0.20%. The absolute error of the resonant frequencies between the two methods are marked "f_d error". According to the damping ratio measurement with displacement based method, half frequency bandwidth for each mode is calculated. All the "f_d error" are smaller than the half frequency bandwidth $\frac{\Delta \omega}{2}$.

31
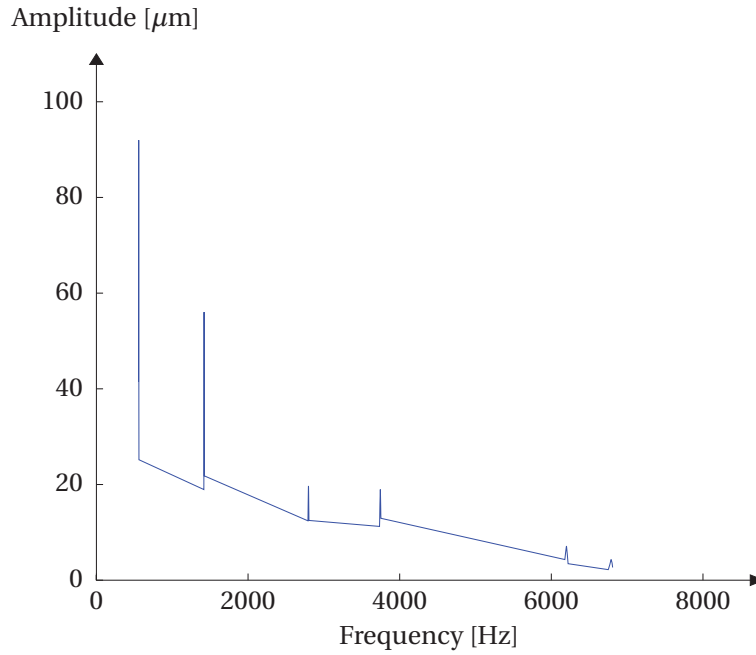
Figure 3.8: Displacement spectrum of piezo-plate system

Table 3.1: Comparison of resonant frequencies

f_d reference [Hz]	f_d maxima-R Hz	error %	f_d error [Hz]	damping ratio ζ	$\frac{\Delta\omega}{2}$ [Hz]
558	559	0.18	1.0	0.0018	1.0
1420	1421	0.07	1.0	0.0009	1.3
2797	2798	0.04	1.0	0.0020	5.6
3745	3749	0.11	4.0	0.0016	6.0
6199	6204	0.11	5.0	0.0024	14.9
6788	6795	0.10	7.0	0.0027	18.3

Even if there is error, at frequencies measured with from **resistance spectrum** method, the plate can still provide at least $\frac{1}{\sqrt{2}}$ of the maximum amplitude. We will use this method in our system to obtain the resonant frequencies quickly.

Damping ratio experiments

Vibrating amplitude is influenced by the damping ratio. Since it is difficult to obtain damping without experiment measurements, half-power method describe in section 3.1 is used to obtain the damping ratio. Fig. 3.9 shows an example of the plate amplitude changing with frequency, from where we can extract the damping ratio. Damping ratio of some resonant modes are listed in Table 3.1. All the damping ratios are small. These small values validate that the damping ratio can indeed be ignored in modal analysis.
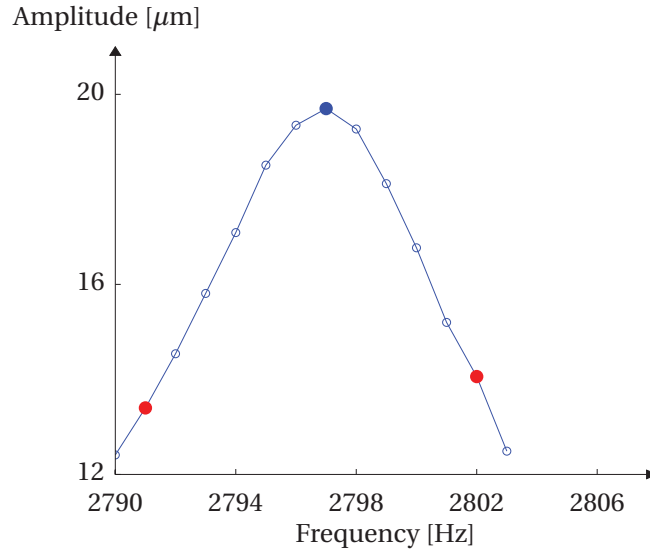
Figure 3.9: Experimental plate displacement for damping ratio extraction

Mode shape demonstration

It is important to visualize the mode shape. It helps to establish the correlation between resonant frequencies and mode shapes, especially for modes whose resonant frequencies are close to each other and may interfere with each other. A way to visualize the mode shape is the technique called "Chladni figure" [14]. The method is to use small particles, such as sand, to demonstrate the nodal lines of specific modes on a plate or a membrane structure. In our case, sugar is used as the small particles.

The center of the plate on the top surface is defined as the origin of the coordinate system. To obtain the modes in Fig. 3.6e and Fig. 3.6f, two piezoelectric actuators are glued underneath the plate at the positions (0 mm, -52.50 mm, -3 mm) and (0 mm, 0 mm, -3 mm). Fig. 3.10 represents these two modes, where the sugar lines indicated the nodal lines. The red squares mark the piezoelectric actuator in the backside of the plate. This "Chladni figure" based mode shape demonstration has coherence with FE simulation.

All the three piezoelectric actuators are glued onto this plate to find more mode shapes. Their positions are (0 mm, 0 mm, -3 mm) for piezoelectric actuator 1, (0 mm, 33.75 mm, -3 mm) for piezoelectric actuator 2, and (0 mm, -52.50 mm, -3 mm) for piezoelectric actuator 3. All the modes are verified in terms of resonant frequencies and corresponding mode shapes. Table 3.2 gives the natural frequencies comparison between FE model and maximum-resistance measurement. These are all modes that can be excited by the three piezoelectric actuators, whose resonant frequencies are lower than 9000 Hz. There are still inappropriate modes, which are similar to mode in Fig. 3.6a. Moreover, there are modes that can not be created with the actual three piezoelectric actuators, such as mode in Fig. 3.6d.

Firstly, the experimental results show that they are all obtained in practice. This means the

<div align="center">(a) 2650 Hz   (b) 2798 Hz</div>

Figure 3.10: Various mode demonstration

Table 3.2: FE model resonant frequencies verification

f_d maxima-R Hz	f_d FE model Hz	error %	Actuated piezo
559	553	-1.07	1
1405	1382	-1.64	2
1421	1410	-0.77	1
2360	2338	-0.93	2
2650	2629	-0.79	3
2798	2765	-1.18	1
3749	3723	-0.69	1
4532	4453	-1.74	2
4801	4766	-0.73	3
5460	5384	-1.39	3
6204	6163	-0.66	1
6637	6569	-1.02	2
6795	6707	-1.30	1
7538	7453	-1.13	2
7694	7622	-0.94	1
8085	7990	-1.18	3
8742	8662	-0.92	2

foam in the experiments is soft enough to be considered as free boundary condition. Secondly, the error between "f_d maxima-R" and "f_d FE model" is less than 2.00%. This difference may be associated to the material or the manufacture process or the foam used for free boundaries. This error is acceptable for justifying that the FE model will be used as numerical model for

similar structure modal analysis.

3.2.2 Harmonic response

Most FE analyses are based on displacement. Analyses on structure stress, strain, and reaction force can be derived from displacements [2]. The displacement will be used to validate the FE harmonic analysis.

FE harmonic response

In FE harmonic response, we need firstly, the natural frequencies from FE modal analysis. Secondly, damping is also an input. We will use the damping ratio obtained from experiments for each FE harmonic response. The piezoelectric actuator parameter used in the system are listed in Table 3.3 (Details see NCE 46 in appendix A.4). These are the parameter provided by the supplier ([47]). They need to be transformed to Ansys form (Details are in appendix A.2). The equivalent voltage to a sinusoidal wave of 100 V_{pp} is applied to the piezoelectric actuator.

Table 3.3: Piezoelectric material parameters [47]

name	symbol	value	unit
density	ρ	7,700	kg $\cdot m^{-3}$
elastic compliances	s_{11}^E	1.30E-11	$m^2 \cdot N^{-1}$
elastic compliances	s_{12}^E	-4.35E-12	$m^2 \cdot N^{-1}$
elastic compliances	s_{13}^E	-7.05E-12	$m^2 \cdot N^{-1}$
elastic compliances	s_{33}^E	1.96E-11	$m^2 \cdot N^{-1}$
elastic compliances	s_{44}^E	3.32E-11	$m^2 \cdot N^{-1}$
elastic compliances	s_{55}^E	3.32E-11	$m^2 \cdot N^{-1}$
elastic compliances	s_{66}^E	3.47E-11	$m^2 \cdot N^{-1}$
piezoelectric charge constant	d_{31}	-1.28E-10	$C \cdot N^{-1}$
piezoelectric charge constant	d_{33}	3.28E-10	$C \cdot N^{-1}$
piezoelectric charge constant	d_{15}	3.27E-10	$C \cdot N^{-1}$
relative dielectric constant	ϵ_{11}	1,190	
relative dielectric constant	ϵ_{33}	1,330	

The vibrating z direction amplitude at the plate surface center is shown in Fig. 3.11 for the Eigenfrequency of 2766 Hz. The maximum amplitude is 20.62 μm. The experimental measured value is 19.70 μm as shown in Fig. 3.9, giving an error of 4.67 %. This error may be induced by manufacturing tolerance or boundary conditions.

Fig. 3.12 illustrates the z direction deformation distribution of the plate under resonant frequency response. The response has the same shape as the mode shape shown in Fig. 3.6f. This means the plate is correctly excited for this resonant mode. Different from modal analysis, here the deformation values have physical senses. It represents the real amplitude.
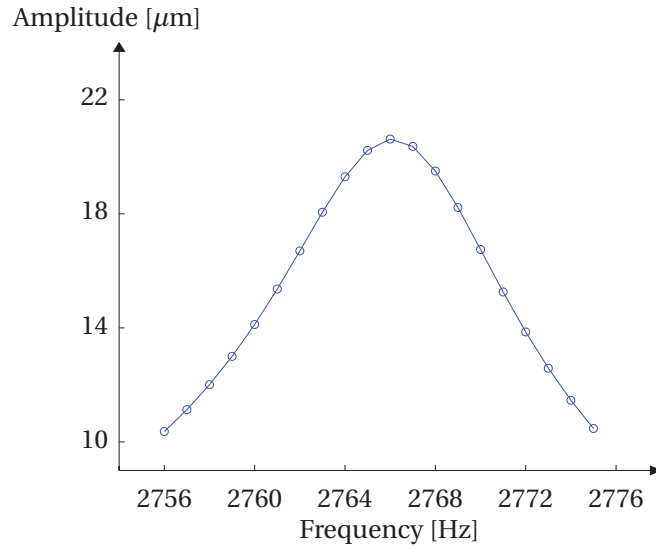
Figure 3.11: Harmonic response simulation result in the vicinity of 2765 Hz

Directional deformation (Z axis)
Unit: μm
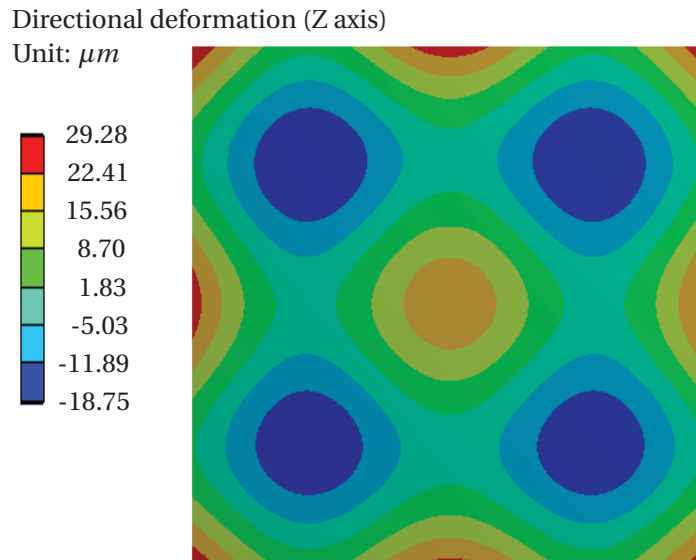
Figure 3.12: Harmonic response under resonant frequency 2765 Hz

Harmonic response experiments

The piezoelectric actuator is driven with a sinusoidal signal of 100 V_{pp} with 50 V DC offset. For each resonant mode, the frequency range includes the resonant frequencies and frequencies that allow to extract the damping ratio. Table 3.4 gives comparison of the harmonic response. The damping ratio ζ is measured by experiments for each mode. "Sim f_d" is the simulation resonant frequency. "Sim max. A" is the simulation maximum vibrating amplitude. "Exp f_d" is the experimental resonant frequency. "Exp max. A" is the experimental maximum vibrating amplitude. The maximum difference is 10.21 %. We can say that the FEM model for

harmonic analysis is verified according to the coherence between simulation and experimental displacements. This coherence also validates that even if the foam can not provide ideal boundaries, it is soft enough to provide acceptable equivalent free boundaries.

Table 3.4: Harmonic response amplitude comparison

ζ	Exp Current A	Sim f_d Hz	Sim max. A μm	Exp f_d Hz	Exp max. A μm	max. A dif %
0.0018	0.06	553	90.45	558	91.98	-1.66
0.0009	0.16	1400	55.43	1420	56.04	-1.09
0.0017	0.29	2629	21.16	2646	20.30	4.24
0.0020	0.32	2765	20.62	2797	19.70	4.67
0.0017	0.44	3723	26.37	3740	24.31	8.47
0.0024	0.70	6163	6.85	6199	7.06	-2.97
0.0024	0.75	6569	3.97	6627	4.08	-2.70
0.0027	0.75	6707	4.75	6788	4.31	10.21

3.2.3 Summary

With the modal analysis we have done, we have obtained the natural frequencies and corresponding mode shapes. This information is useful for the harmonic response. The FE harmonic response is validated with experiments. In the following, we will use the validated FE modal analysis and harmonic response to do our researches.

3.3 Piezoelectric actuator's dimension and shape influence on plate's amplitude

The resonant frequency and the amplitude are the two important features of the structure. The resonant frequency depends on the plate size, the shape and the material. The vibrating amplitude changes depending on the resonant modes. In this section, we will investigate the piezoelectric actuator surface area, shape and orientation influence on plate amplitude for different modes.

3.3.1 Piezoelectric actuator's surface area effect

Simulations

First, we have studied the Eigenmode shown in Fig. 3.13c. The mode has the same number of half-wave length in both x, y directions. The piezoelectric actuator is square and is bonded underneath the plate in the center. We have analysed the plate displacement on the top surface in the center (red point).

(a) Mode 1

(b) Mode 2

(c) Mode 3

(d) Mode 4
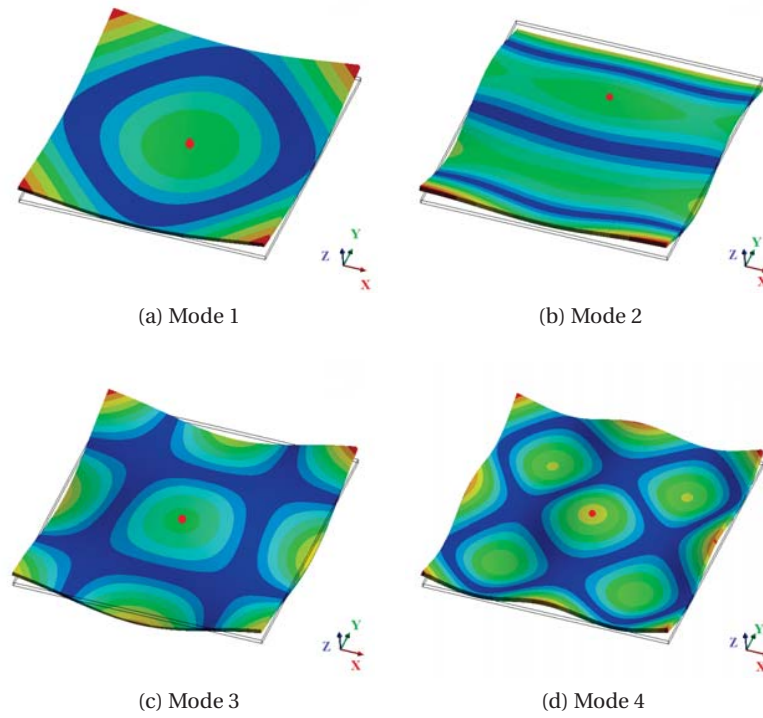
Figure 3.13: Four Eigenmodes of the square plate

Fig. 3.14 presents the plate displacement in z direction with piezoelectric actuator length increment. We can see that, for this mode, when the piezoelectric actuator length increases, the plate displacement raises. The relationship between the plate displacement and piezoelectric actuator length is close to quadratic. This indicates that the plate displacement is linked to the piezoelectric actuator surface area.
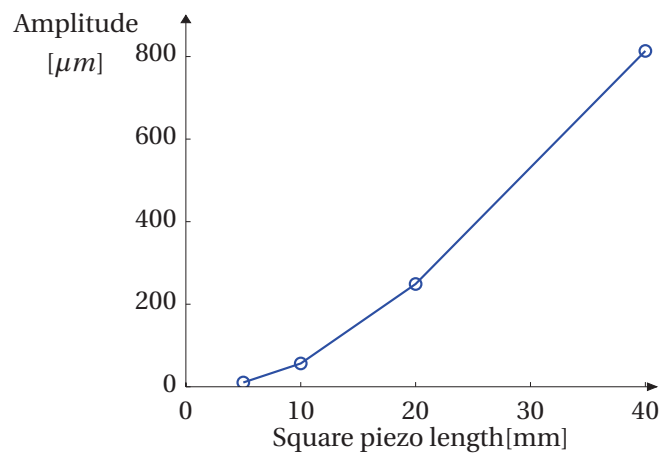
Figure 3.14: Vibrating amplitude according to piezo edge length

We have analysed the plate displacement for different modes with two kinds of actuator to study the surface influence on other modes. Table 3.5 lists the numerical response for the four modes which are illustrated in Fig. 3.13. They are divided into two groups. The first group (mode 1, 3 and 4) presents symmetric resonant modes. Whereas the second one (mode 2) has only bending along Y direction. The piezoelectric actuator is underneath the red point. Piezo 's' means that the piezoelectric actuator surface is $5.0 \times 5.0 \ mm^2$. Piezo 'L' means the piezoelectric actuator surface is $10.0 \times 10.0 \ mm^2$. 'A' is the plate displacement on the top surface at the position of the piezoelectric actuator.

Table 3.5: Plate displacement with two different piezo actuators

Mode No.	Piezo	f_r [Hz]	A [μm]	Ratio A_L/A_s
1	s	555	17.09	
1	L	553	90.90	5.32
2	s	1384	7.06	
2	L	1383	40.21	5.70
3	s	1414.5	10.82	
3	L	1410.0	56.80	5.48
4	s	2782	3.79	
4	L	2767	20.65	5.45

The amplitudes with 'L' piezoelectric actuator are much larger than that with 's' one. The ratio between the two displacements is around 5. Fig. 3.15 and Fig. 3.16 give the frequency response for the mode 1 and mode 2.
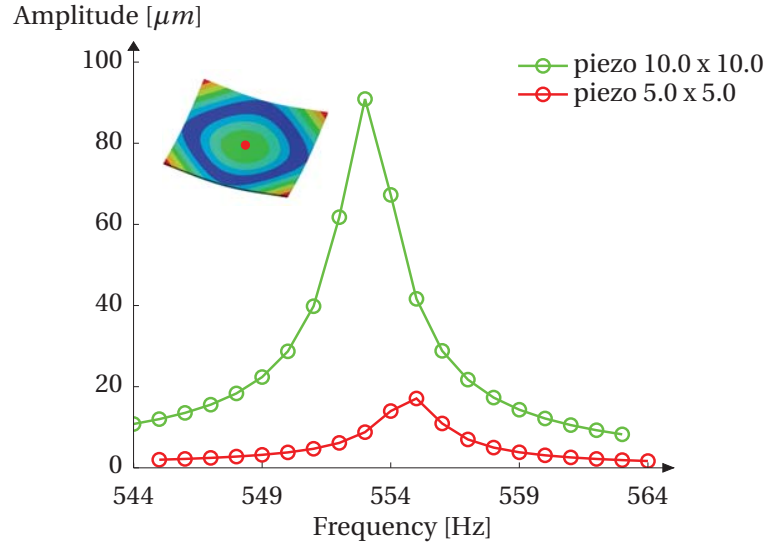
Figure 3.15: Plate displacement for mode 1

According to the above analysis, if we increase the piezoelectric actuator area, we can obtain

higher plate displacement. However, piezoelectric actuator is equivalent to a capacitance. When the piezoelectric actuator area increases, the piezoelectric actuator capacitance will be bigger. According to Eq. (2.6) and Eq. (2.7) [52], piezoelectric actuator drive current will be higher and energy dissipation in piezoelectric actuator will increase. This energy is transformed to heat in the piezoelectric actuator and thus limits the piezoelectric actuator working frequency. Thus, for some cases, we cannot increase the piezoelectric actuator surface any more.
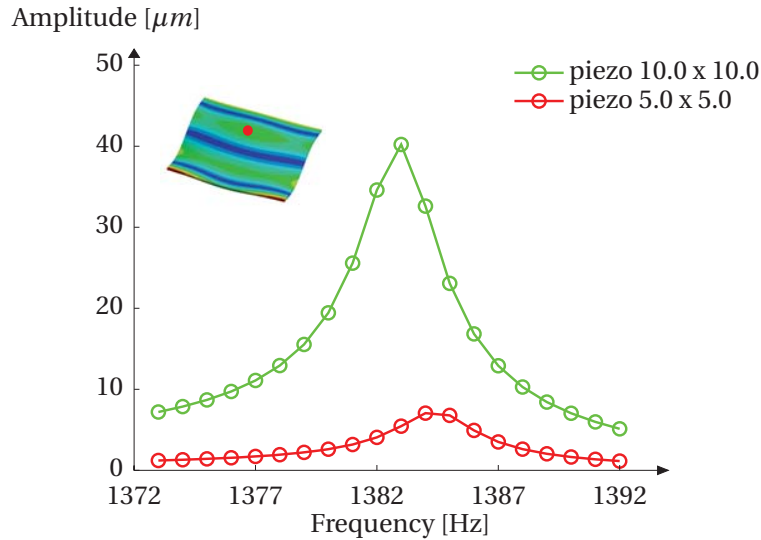
Figure 3.16: Plate displacement for mode 2

Experiments

Experiments on two identical plates with two kinds of piezoelectric actuators have been carried out to validate the simulation analysis. The two kinds of piezoelectric actuators are: $10 \times 10 \times 2 \ mm^3$ and $5 \times 5 \times 2 \ mm^3$. The plate sketch is in Fig. 3.17. Plate main body has a size of $160(L) \times 120 \ (W) \times 3 \ (h) \ mm^3$. Experimental setup is shown in Fig. 3.18. The plate displacement measurement is carried out with a Doppler Laser Vibrometer (DLV).

In experiments, both piezoelectric actuators are powered by a sinusoidal wave of $100 \ V_{pp}$ with 50 V DC offset. In simulation, both piezoelectric actuators are supplied by an equivalent voltage. The response displacement and corresponding mode for plates with both piezoelectric actuators in simulation and experiments are shown in Fig. 3.19. The damping ratio is obtained by half-power method [20]. It is used as input in the simulation. The mode shape using for plate displacement study with both piezoelectric actuator is shown in Fig. 3.19.

From this figure, we can observe obviously that the plate with larger piezoelectric actuator has much bigger displacement than the other one. Numerical values are listed in Table 3.6. The difference between simulation and experiments for resonant frequency is less than 2.0 %. For
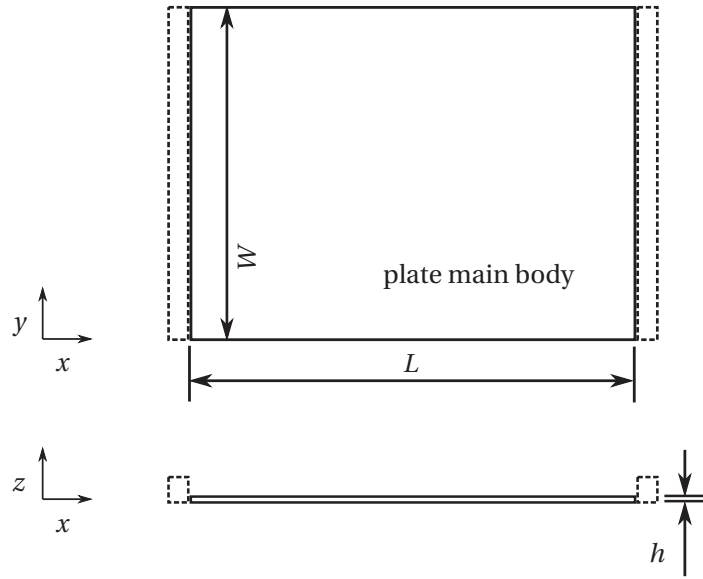
Figure 3.17: Plate sketch
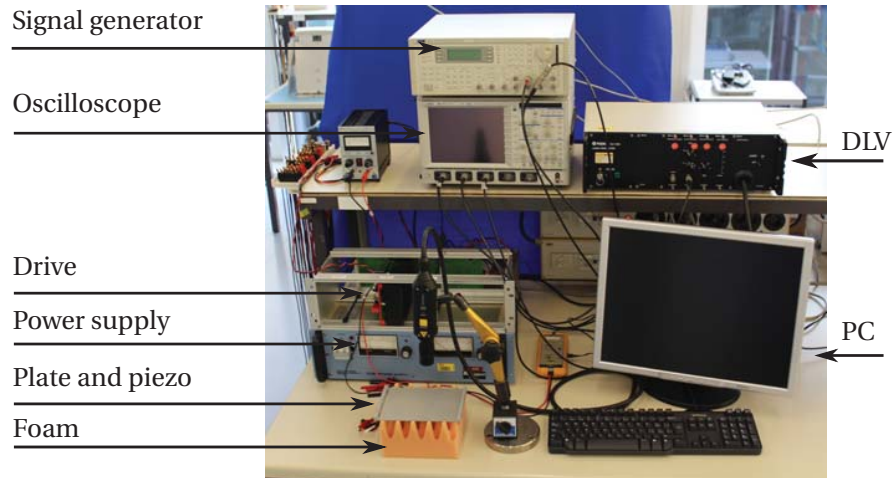
Figure 3.18: Experimental setup

the plate displacement, the maximum difference is 25.34% (experimental results are used as reference for the difference). This could be explained by connection between the main body of the plate and the bars of the plate (dashed parts shown in Fig. 3.17). Indeed, the difference is less than 10% considering simple structure such as a square plate.
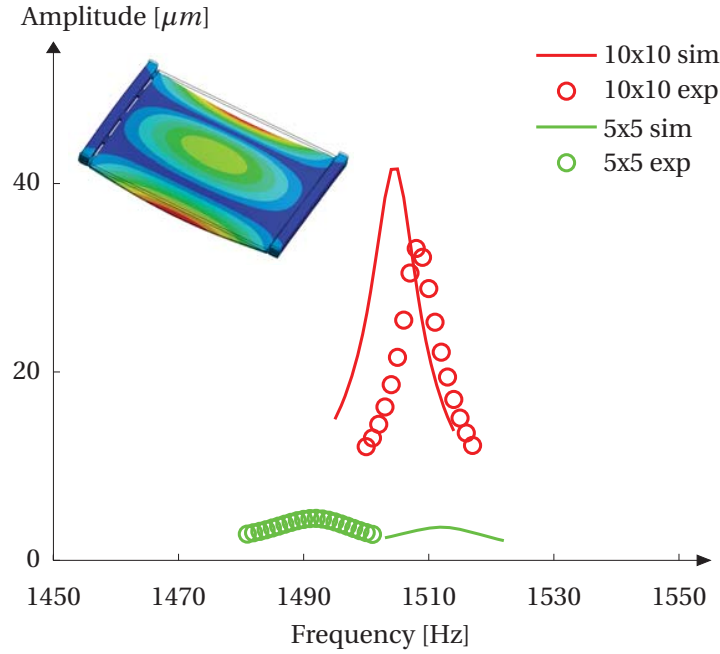
Figure 3.19: Experiment validation

Table 3.6: Comparison between simulations and experiments

item	piezo 10x10x2	piezo 5x5x2
damping ratio	0.0023	0.0052
Sim f_r [Hz]	1504	1512
Exp f_r [Hz]	1508	1492
Sim A [μm]	41.50	3.53
Exp A [μm]	33.11	4.45
f_r dif [%]	-0.27	1.34
A dif [%]	25.34	-20.75

3.3.2 Piezoelectric actuator's shape and orientation effect
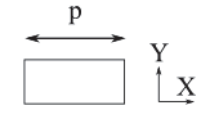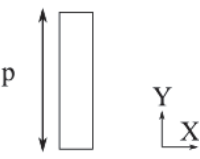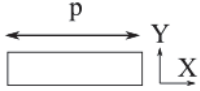
As discussed above, the piezoelectric actuator area could be limited due to the capacitance. Thus, we have studied the plate displacement according to the shape and orientation of the piezoelectric actuator for a fixed area of 100 mm^2 considering the mode 2 and the mode 3.

Table 3.7 gives the plate displacement (mode 3) in the center 'P_1' ($x = 0.00$ mm, $y = 0.00$ mm). Even if the areas are the same, the plate displacements are different. From the table, we notice that the piezoelectric actuators which are bonded in different orientations, but with the same shape, create almost the same plate displacements. For example, case 2 and case 3 have almost the same amplitude response even if their piezoelectric actuator orientations are different. We

define 'p' the dimension of the longer edge of the piezoelectric actuator in case of mode where there are the same numbers of half wave in both x and y directions. Mode 3 is applicable to this case. For configurations with piezoelectric actuators "15.0 × 6.7" and "6.7 × 15.0", the dimension of the longer edge of piezoelectric actuators is p = 15.0 mm. We also observe that bigger 'p' is, higher the plate displacement is at 'P_1'.

Table 3.7: Plate displacement for mode 3

case No.	piezo shape	p [mm]	piezo area [mm × mm]	f_r [Hz]	A [μm]
1		10.0	10.0 × 10.0	1410	56.47
2		15.0	6.7 × 15.0	1411	60.50
3		15.0	15.0 × 6.7	1411	60.85
4		20.0	5.0 × 20.0	1411.5	73.44
5		20.0	20.0 × 5.0	1411.5	73.44

To study the plate displacement distribution, we have investigated the plate displacement along the line 'L_x' ($y = 0$ mm). Fig. 3.20 presents the plate displacement for the three configurations. The amplitude presented in Table 3.7 is the point 'P_1' ($x = 0.00$ mm, $y = 0.00$ mm). According to this figure, we observed that when 'P_1' has bigger displacement, all the points along the line 'L_x' have bigger displacement. Thus, we can deduce that the whole surface of the plate has higher displacement.

We have also studied the displacement when the resonant mode has not the same half-wavelength number for x and y direction (for example, mode 2). Mode 2 has only bending along y direction. Table 3.8 lists the displacement with different piezoelectric actuator shapes and orientations. Because there is only bending along y direction, 'p' is the dimension of the piezoelectric actuator's edge which is parallel to y direction. First we observe that the piezoelectric actuators with the same shape but different orientations do not create the same displacement. Besides, the plate displacement has positive correlation with parameter 'p'.
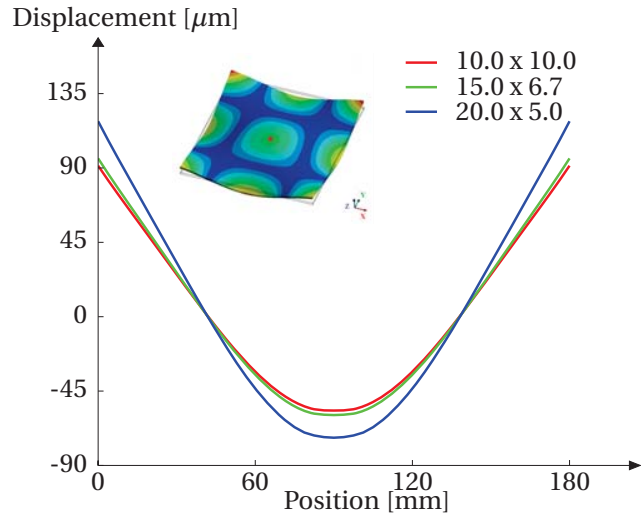
Figure 3.20: Plate displacement (mode 3) along the line 'L_x'

Table 3.8: Plate displacement for mode 2

case No.	piezo shape	p [mm]	piezo area [mm × mm]	f_r [Hz]	A [μm]
1		5.0	20.0 × 5.0	1380	30.73
2		6.7	15.0 × 6.7	1381	33.23
3		10.0	10.0 × 10.0	1383	40.21
4		15.0	6.7 × 15.0	1386	54.09
5		20.0	5.0 × 20.0	1388	65.42

Fig. 3.21 presents the plate displacement distribution along the line 'L'_y ($x = 0.00$ mm) for mode 2. The amplitude presented in Table 3.8 is the point 'P_2' ($x = 0.00$ mm, $y = 33.75$ mm). When this point 'P_2' has larger displacement, all the points along the line 'L'_y' have bigger displacement.

Fig. 3.22 illustrates the plate amplitude according to the parameter 'p'. Both modes have the same trend. The plate displacement is bigger when the piezoelectric actuator length along the bending mode direction is longer.
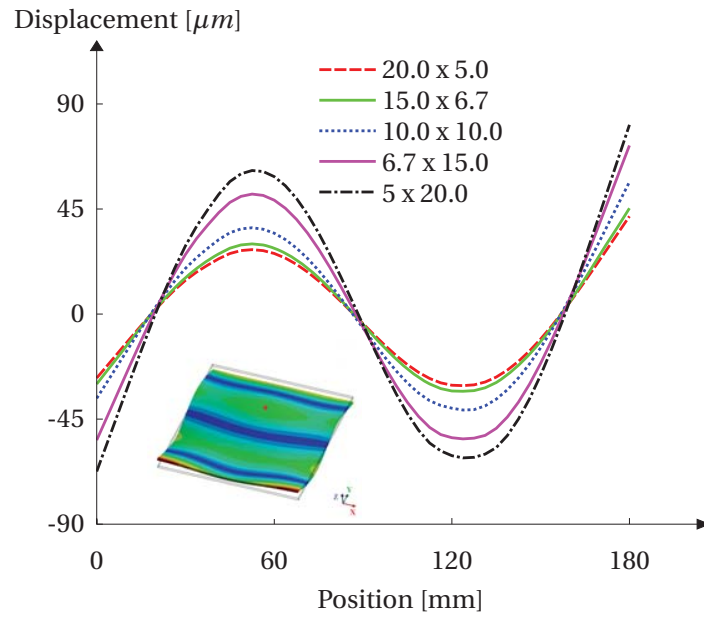
Figure 3.21: Plate displacement (mode 2) along Y direction
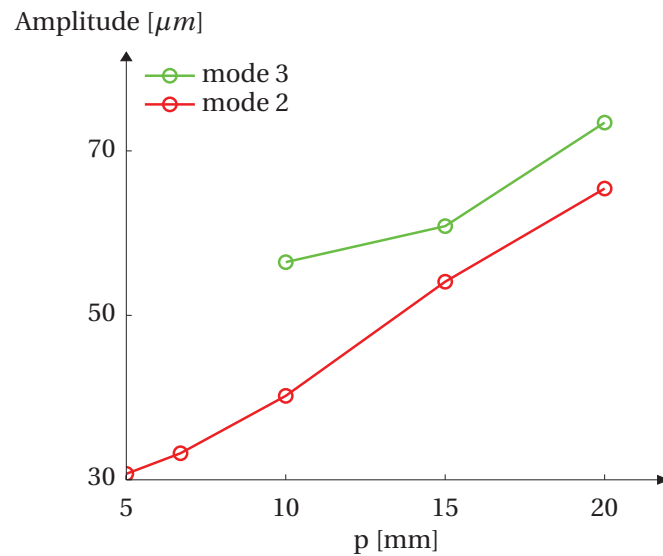
Figure 3.22: Plate displacement with same area

According to this study, we can increase the plate displacement by adjusting the piezoelectric actuator shape and orientation when the surface is kept constant. The longest edge of the piezoelectric actuator should be positioned according to the desired bending mode. One restriction is that the piezoelectric actuator dimension should be smaller than the half wavelength [64].

3.3.3 Piezoelectric actuator's thickness and number of layers

Besides limiting the piezoelectric actuator area, the total thickness of the piezoelectric actuator (equivalent piezoelectric actuator layer numbers in multilayer piezoelectric actuator when the single layer's thickness is fixed) may be reduced to avoid energy dissipation. This is because the actuator capacitance of a multi-layer actuator depends on the actuator area, the actuator thickness and the number of layers (details see A.3). Previously we have investigated the area influence, here we will study how to design the actuator thickness and the number of layers.

First, let's consider the role of the deformation of the piezoelectric actuator in the displacement of the plate. To do that, playing with the piezoelectric coefficient (d_{31}, d_{33}) of the actuator, we are able through a FE analysis to investigate individually the x, y, and z deformation. We will discuss three cases:

- Case 1: considering all the deformation
- Case 2: only x and y deformation
- Case 3: only z deformation

The applied voltage is equivalent to 100 V_{pp} and the damping ratio is 0.0009. Fig. 3.23 gives the plate displacement of the three cases. Case 1 and case 2 have almost the same displacement, respectively 52.56 μm and 53.17 μm. The difference is only 1.16%. However, the case 3 presents very small displacement compared to case 1 and 2. We can thus consider that the plate displacement is created mainly by piezoelectric actuator x, y direction deformation.

This result shows that x, y deformations of piezoelectric actuator determine the plate displacement rather than z deformation. This indicates that thinner piezoelectric actuator (few layers) may be designed for the plate resonator. The advantage is that with smaller capacitance, according to Eq. (2.6) and Eq. (2.7), piezoelectric actuator drive current and power will be smaller. This will definitely decrease the drive cost.

Table 3.9 shows the simulation results of plate displacement when using fewer layer. The piezoelectric actuator thickness changes to be 1 mm, half of the previous one. To obtain the same electric field, the supply voltage is set equivalent to 50 V_{pp}.

The maximum difference of plate displacement between 'piezo of 2 mm' and 'piezo of 1 mm' is 12.38%. This validates that fewer layers of piezoelectric actuator can create the same plate displacement. This is mainly because the piezoelectric actuator x, y deformations keep the same. When we decrease the number of the layer, the piezoelectric actuator's surface on x, y plane is kept constant. Moreover, we keep the electric field to be the same. Therefore, piezoelectric actuator x, y deformation keep the same even if the piezoelectric actuator thickness decreases.

This indicates that the same plate displacement may be obtained by multi-layer piezoelectric actuator which has less layers, thus decreasing the power supply. Indeed, the capacitance
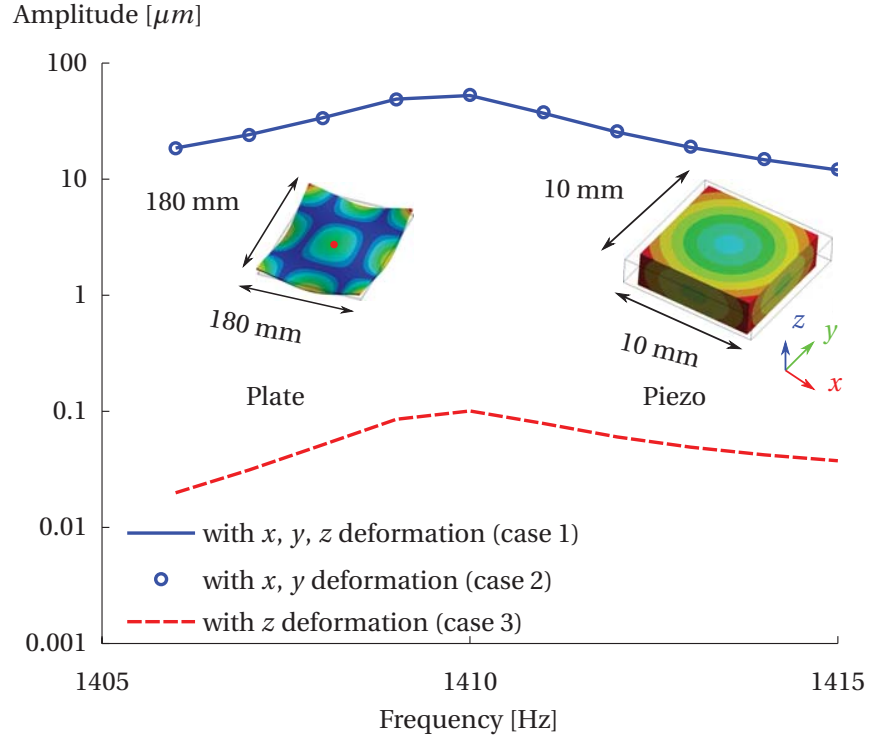
Figure 3.23: Plate's vibrating amplitude according to the piezo deformation

Table 3.9: Maximum plate displacement comparison for the different total thickness of the piezoelectric actuator

ζ	piezo of 2 mm		piezo of 1 mm		Difference
	f	max. A	f	max. A	
	[Hz]	μm	[Hz]	μm	%
0.0018	553	90.45	556	79.25	-12.38
0.0009	1410	55.54	1415	51.85	-6.64
0.0020	2766	20.62	2775	18.48	-10.38

of the piezoelectric actuator C_{piezo} depends on the number of layers n and the thickness of a single ceramic layer d_s (Details in appendix A.3). The piezoelectric actuator drive current and dissipation power are both linearly proportional to the capacitance of the piezoelectric actuator (Eq. (2.6) and Eq. (2.7)) [52]. If we assume that d_s is constant. The total thickness d_t will be proportional to the number of layers ($d_t = n \cdot d_s$). With this premise, the piezoelectric actuator with a thinner total thickness has a smaller capacitance. Therefore, piezoelectric actuator drive current and power dissipation will be smaller and thus decrease the drive cost.

3.4   Plate geometry influence on mode shapes

The mode shapes of a mechanical structure are determined by its geometry, material and boundary conditions. Depending on the boundary condition, plate can have different mode shapes. However, some rules are applicable for all the conditions. The analytical calculation for natural frequencies of simply-supported plate is used as to explain the general rules for all the boundary conditions, because its analytical analysis is easy. The natural frequencies of four edges simply supported plate can be calculated as follows [69]:

$$\omega_{mn} = \pi^2 \left[\left(\frac{m}{L} \right)^2 + \left(\frac{n}{W} \right)^2 \right] \sqrt{\frac{D}{\rho h}} \tag{3.6}$$

where m, n are the number of half wavelength in x, y direction, respectively. L, W are the length and the width of the plate, respectively. $D = \frac{Eh^3}{12(1-v^2)}$ is the flexural rigidity. E is the Young's modulus, v is the Poisson's ratio and w is the transverse displacement.

According to the Eq. (3.6), we obtain: 1, the resonant frequency is proportional to the thickness of the plate (Examples are shown in [56]); 2, if the plate length-to-width ratio ($\frac{L}{W}$) keeps constant, the mode shape will keep the same; 3, if the plate length-to-width ratio changes, the modes on the plate change [54]. These rules are applicable for all the boundary conditions. Therefore, we will study only the length-to-width ratio influence on the plate mode shapes. In the previous section, we have investigate the modes of a square plate. In this section, we will investigate how the relative nodal line positions between modes change when the plate length-to-width ratio changes. Fig. 3.24 illustrates five simulation mode shapes of a plate whose main body has a size of $160(L) \times 120 (W) \times 3 (h) \ mm^3$. The nodal lines (the blue lines) of these modes are parallel to y direction. These five modes are used as mode reference to investigate the mode shape changes with the influence of plate length-to-width ratio. We fix the plate's length to 160 mm and the thickness to 3 mm.

Some mode shapes disappear due to the length-to-width ratio changes. Table 3.10 lists the results for plate from square plate to the length-to-width ratio equals to 2. Some mode shapes disappear. For example, plate design "D3" has all the five mode shapes as that of plate design "D5". plate design "D8" does not have the mode shape of "M3". Not only the existence of the mode shapes changes, but also the nodal line positions. Fig. 3.25 give the illustration of nodal line positions of plate design "D5", "D3", "D8" and "D9". Because the plate is symmetric, only half of the plate is considered. Plate design "D5" and "D3" both have five modes, but the nodal positions are not the same and the relative nodal positions between modes are different in the two plates. For example, the nodal positions (intersection with dashed line) of mode M2 in two plates are not the same. The relative nodal position between mode M1 and M4 of the two plates are different. Plate design "D8" and "D9" do not have all the five modes.

We propose a method to evaluate the relative nodal line positions to represent the nodal line distribution along x direction of a sequence of standing waves. We expect to have a series of waves whose nodes move in one direction continuously. k_i in Eq. (3.7) is proposed to do this

(a) M1 397 Hz   (b) M2 1136 Hz   (c) M3 2195 Hz

(d) M4 3459 Hz   (e) M5 4668 Hz
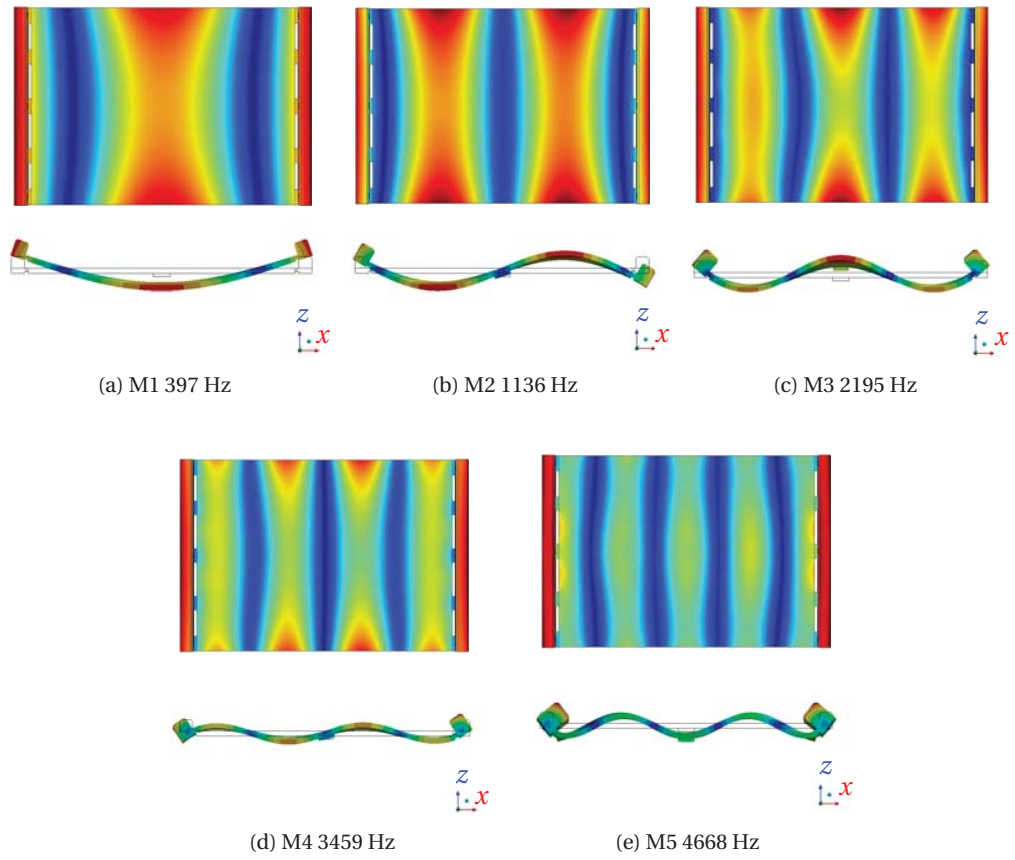
Figure 3.24: Illustration of desired modes

Table 3.10: Modes for different plate

No.	W [mm]	$\frac{L}{W}$	M 1	M 2	M 3	M 4	M 5
D1	160	1.00	—[a]	√[b]	—	—	—
D2	150	1.07	—	√	√	√	—
D3	140	1.14	√	√	√	√	√
D4	130	1.23	√	√	√	—	√
D5	120	1.33	√	√	√	√	√
D6	110	1.45	√	—	√	√	—
D7	100	1.60	√	√	√	√	√
D8	90	1.78	√	√	—	√	√
D9	80	2.00	√	√	—	—	√
D10	70	2.29	√	√	—	√	—
D11	60	2.67	√	√	√	√	√

[a] means the plate does not have the specific mode

[b] means the plate has the specific mode

49

(a) D3 with plate $160 \times 140 \times 3 \; mm^3$

(b) D5 with plate $160 \times 120 \times 3 \; mm^3$

(c) D8 with plate $160 \times 90 \times 3 \; mm^3$

(d) D9 with plate $160 \times 80 \times 3 \; mm^3$
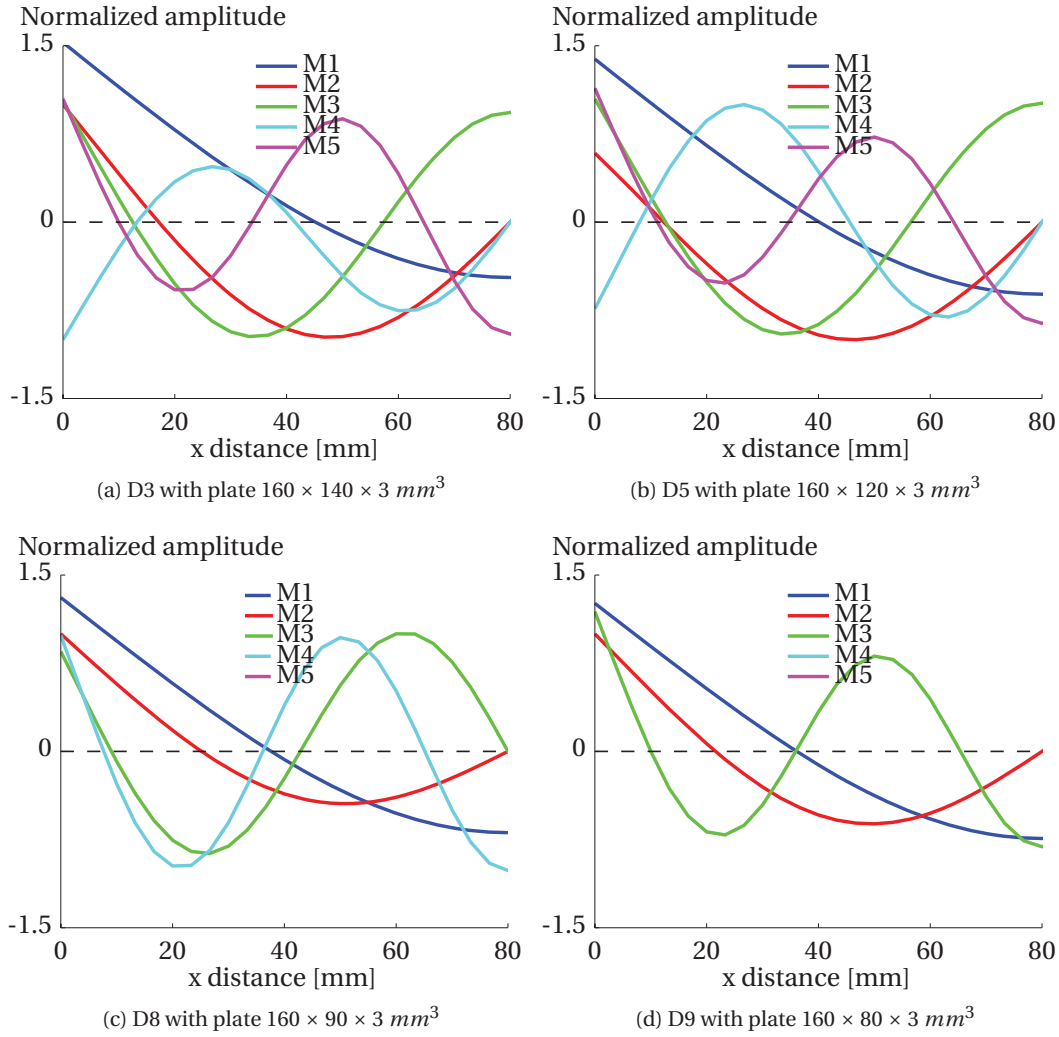
Figure 3.25: Illustration of nodal line position along x direction

analysis. Δx_i is the distance from one node of the first mode to the node of the second mode. λ_i is the wavelength of the second mode (Fig. 3.26). We assume that there is a particle at the node of a standing wave. If there is a second standing wave, k_i for these two modes are smaller than 1, the particle can move from the node of the first mode to the node of the second mode in the defined direction. For example, mode switch from mode A to mode B, the assumed particle can move from the node of mode A to the node of mode B with the direction to right. We can get a desirable series of waves if the following modes satisfy always the relation as the previous two modes.

$$k_i = \frac{\Delta x_i}{\lambda_i/4} \tag{3.7}$$
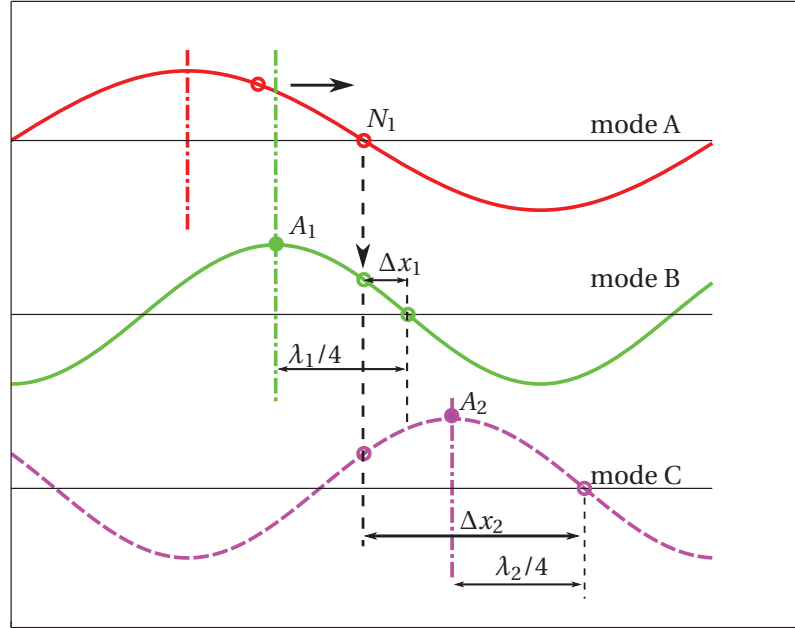
Figure 3.26: Optimization parameters

If $k_i > 1$, in the defined direction, the distance between the two modes are larger than the wavelength of the second mode. For example, mode switch from mode A to mode C, if the defined direction is to right, the assumed particle will not move in the defined direction, but will move to the left (eg. as illustrated in Fig. 3.26). If k_i is equal to 1, the assumed particle is in the anti-node of the second mode. In this case, the assumed particle may move in the same direction that provided by the previous mode or in the reverse direction. It is indeterminate. If k_i is closer to 1, the stability for each two consecutive modes switch is lower.

For the previous plate design, some plates are not able to move the assumed particle to the center. Fig. 3.27 gives an example of a plate that fails to transport the assumed particle to the center of the plate. The plate can only transport the assumed particle from "a" to "s" instead of "b". Whereas, there are plates that are able to move the assumed particle to the center of the plate. Fig. 3.28 gives an example for which the plate is able to transport the assumed particle up to "b" in the correct sequence of mode switch.

For the plate that has a series of standing waves that can move the assumed particle to the center of the plate, k_{max} is used to evaluate the stability of the movement. Table 3.11 lists k_i for all the plate designs that are able to move the assumed particle to the center of the plate. Plate "D3" and "D5" have smaller k_{max} and thus have better transportation stability. Plate "D3" needs four modes to achieve the assumed transportation. Plate "D5" needs five modes to achieve this goal. The plate "D3" is the best in terms of transportation stability and number of modes.
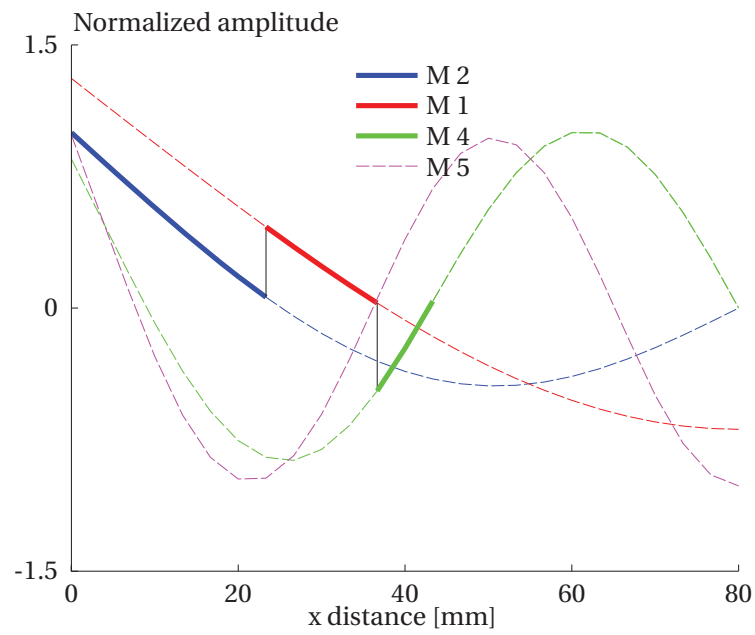
Figure 3.27: Illustration assumed particle with unsuccessful transportation
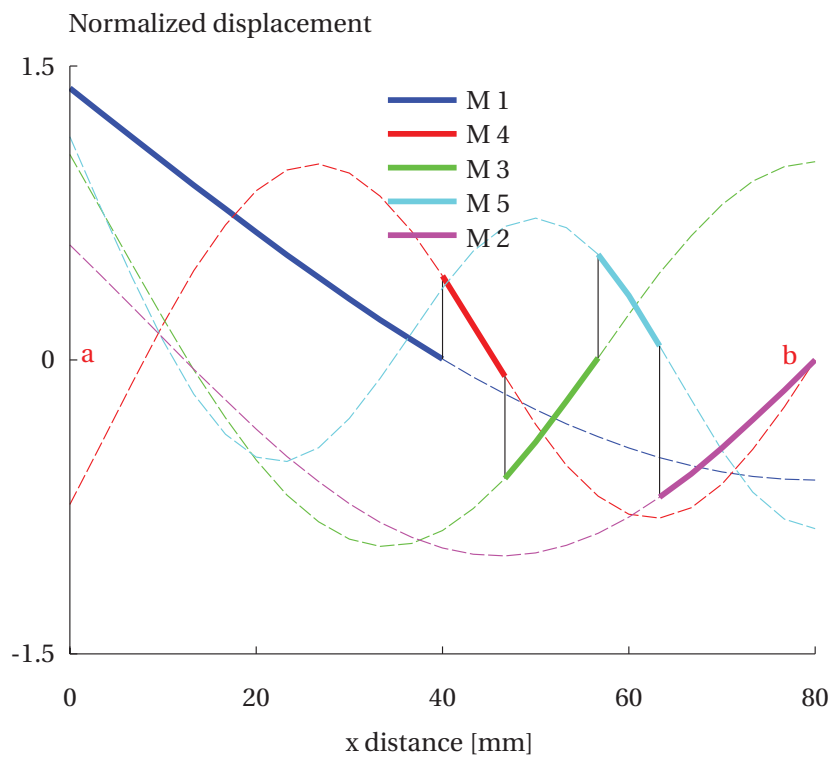
Figure 3.28: Illustration assumed particle with successful transportation

Table 3.11: Plate design evaluation

No.	W	$\frac{L}{W}$	k_1	k_2	k_3	k_4	k_{max}
	[mm]						
D3	140	1.14	0.43	0.50	0.50	—	0.50
D4	130	1.23	0.57	0.50	0.50	—	0.57
D5	120	1.33	0.33	0.43	0.50	0.50	0.50
D7	100	1.60	0.20	0.50	0.75	0.63	0.75
D11	60	2.67	0.57	0.33	0.75	0.44	0.75

3.5 Summary and conclusions

In this chapter, firstly, we give the theories about equation of motion and damping, justify to use free boundary condition and also give the information about piezoelectric actuator. The coherence of the experiments and simulation validates the simulation of FE modal analysis and harmonic response. These simulation allow us obtaining resonant frequencies, mode shapes and vibrating amplitude for the following studies.

With this basic analysis, we have investigated the piezoelectric actuator's dimension and shape influence on plate amplitude. We found that bigger the piezoelectric actuators is, higher the plate amplitude is. We also discover that, for a given surface of the piezoelectric actuator, we can obtain higher amplitude by changing the piezoelectric actuator's shape and orientating the longer length to the direction of bending. The limit is that the larger edge of the piezoelectric actuator should be smaller than the half-wavelength of the mode studied. Moreover, we also found that it is the deformation in x, y direction that determines the plate vibrating amplitude rather than deformation in z direction. This results tell us that we can use thinner multilayer piezoelectric actuator to obtain the same plate displacement meanwhile decreasing the current and power dissipation of the piezoelectric actuator's drive.

We have studied the plate geometry influence on relative nodal line positions between modes. From the simulation results, we found that, the length-to-width ratio of the rectangular plate changes the modes whose nodal lines are parallel to the short edge of the plate. A parameter k_i, which relates the relative distance between the nodal positions of two successive modes and the wavelength of the second mode, was proposed as the first step for plate optimization.

4 The dynamics of a bouncing part with sinusoidally vibrating plate

The parts behaviour under a sinusoidal vibrating plate is a key point to be investigated. The part vertical displacements under different vibrating conditions (vibrating frequency and vibrating amplitude) are investigated. The model is created in Solidworks. We will also choose the widely used method (coefficient of restitution) for the impact between the part and the plate. In this chapter, first, we use the bouncing ball system to validate this impact method by comparing it with the analytical analysis. Then this impact method is chosen to investigate the ball's vertical displacement under few hundreds of hertz to few thousands of hertz, which is much higher than the frequency range in the existing studies. Afterwards, this simulation model is applied to non-point-like part (specifically a cylinder) and the corresponding experiments will be implemented. We will also study the part's horizontal movement from anti-nodes to nodes.

4.1 Part's vertical displacement

4.1.1 Model and validation

We use the widely studied bouncing ball system to validate the impact in Solidworks. The chosen method for impact is the one using coefficient of restitution. Fig. 4.1 depicts the model - a bouncing ball moving freely in the vertical direction on a vibrating plate. It is assumed that the plate is massive compared to the ball and therefore, the motion of the plate is not affected by the impacts of the bouncing ball. The plate vibrates sinusoidally. A, ω and ϕ are the vibrating amplitude, vibrating frequency and initial phase angle. The spring is to balance the gravity force of the plate. Plate main body has a size of $40 \times 40 \times 3 \ mm^3$. The ball diameter is 3 mm. The plate is made of aluminium and the ball is made of steel. The material properties determine the restitution coefficient ($e = 0.2$). The analytical analysis neglects the friction between the ball and the vibrating plate [41]. To validate and compare the Solidworks simulation model, we do not consider this friction, either. In chapter 2, we reviewed the full range of vibrating condition (section 2.3). Here, we will use only the vibration "pattern-one, r = 1" and "pattern-two, r = 1" to validate the numerical simulation in Solidworks.
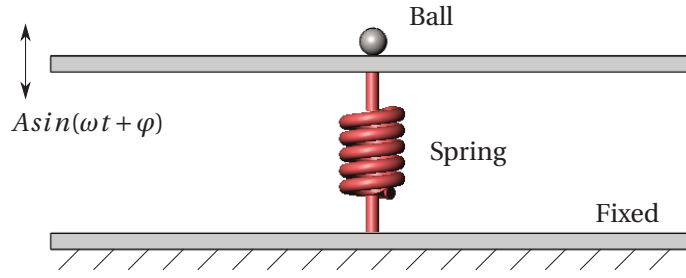
Figure 4.1: Impact validation using bouncing ball system

As presented in section 2.3, in the bouncing ball system, when the plate vibrating condition (vibrating frequency and vibrating amplitude) changes, the ball response is different. If $1 < k < k_{1,1}$, the ball is not able to keep the same bouncing behaviour as that of "pattern-one, r = 1" vibration. When $k_{1,1} < k < k_{2,1}$ ($k_{1,1}$ and $k_{2,1}$ are expressed in equations 2.9 and 2.10), the ball could keep "pattern-one, r = 1" vibration (Fig. 2.13). If $k_{2,1} < k < k_{3,1}$ (k is calculated from Eq. (2.11)), the ball follows "pattern-two, r = 1" vibration ("pattern-two, r = 1" in Fig. 2.13). Here, we fix the vibrating frequency to 50 Hz, which is the typical analysis frequency for the bouncing ball system. By changing the vibrating amplitude, plate relative acceleration k (k is expressed in Eq. (2.8)) is changing, and thus we can obtain the different ball behaviours. Fig. 4.2b gives the simulation results of "pattern-one, r = 1" vibration. Fig. 4.2a gives the simulation results under the critical vibrating amplitude ($A = 211 \ \mu m$) which is not able to provide stable "pattern-one, r = 1" vibration. Fig. 4.2d gives the simulation results of "pattern-two, r = 1" vibration. Fig. 4.2c gives the simulation results under the critical amplitude ($A = 249 \ \mu m$) where the vibration switches from "pattern-one, r = 1" to "pattern-two, r = 1". According to these simulation results, we can calculate the vibration switches boundaries $k_{1,1}$ and $k_{2,1}$ using the vibrating condition in Fig. 4.2a and Fig. 4.2c.

Table 4.1 gives the numerical values for both analytical and simulation results. $k_{1,1}$ and $k_{2,1}$ obtained from the simulation have small difference from the analytical method, less than 2.00% . Therefore, the impact method using restitution coefficient (e) is chosen and will be used in the following analysis.

Table 4.1: Comparison of analytical and simulation results for ball

Variables	Analytical value	Simulation value	Error [%]
$k_{1,1}$	2.094 (A = 208 μm)	2.124 (A = 211 μm)	1.39
$k_{2,1}$	2.544 (A = 253 μm)	2.506 (A = 249 μm)	-1.50

The plate vibrating frequency and amplitude together determine the plate acceleration. The existing researches study the plate acceleration and compare it with gravity acceleration. However, even the vibrating acceleration keeps the same, the combination of vibrating frequency and vibrating amplitude will affect the part's behaviour control. Corresponding vibrating amplitudes for $k_{1,1}$ and $k_{2,1}$ at different vibrating frequency are listed in Table 4.2. We observe

(a) $A = 211\ \mu m$

(b) $A = 220\ \mu m$, Pattern-one, r = 1 vibration

(c) $A = 249\ \mu m$

(d) $A = 260\ \mu m$, Pattern-two, r = 1 vibration
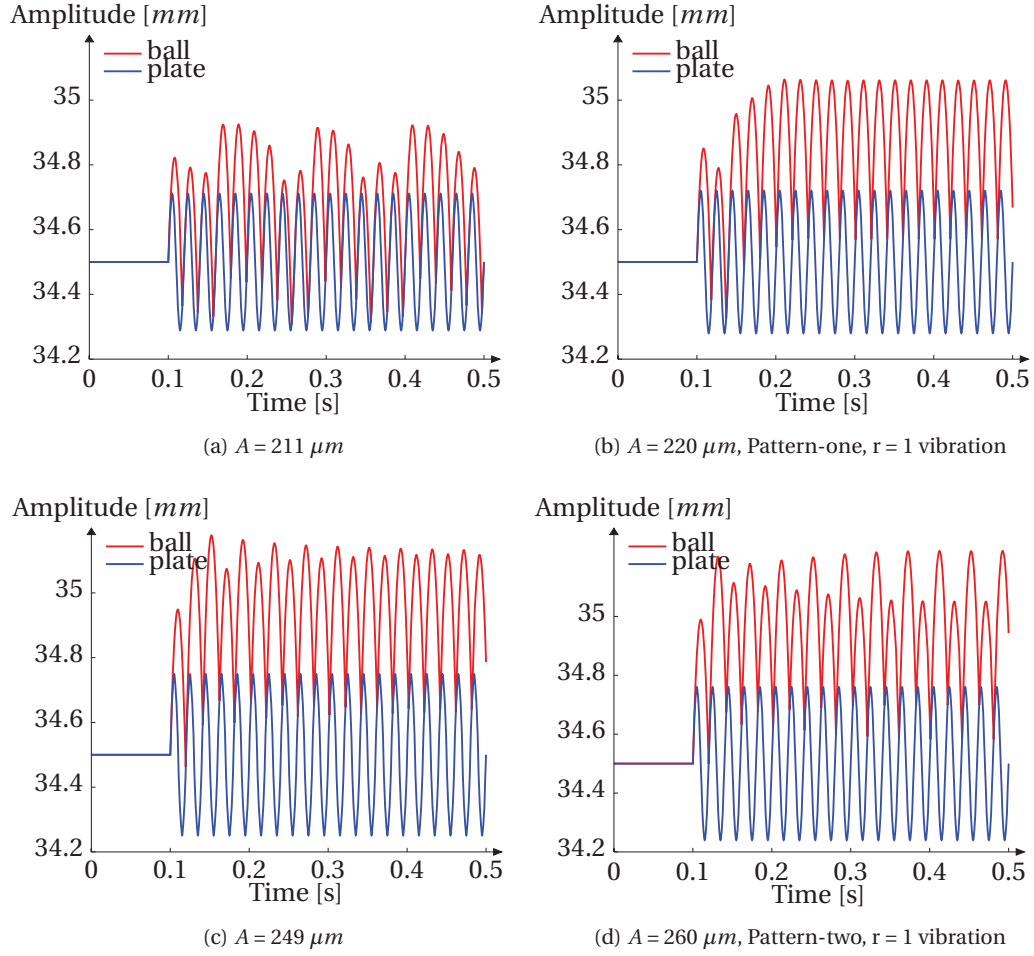
Figure 4.2: Impact model validation using the bouncing ball system under 50 Hz

that for low frequencies (f = 50 Hz, and f = 100 Hz), to keep the "pattern-one, r = 1" vibration, the vibrating amplitude could vary from few micrometers to few tens of micrometers. When the vibrating frequency increases to 500 Hz, to keep the ball to "pattern-one, r = 1" vibration, the vibrating amplitude should keep between 2.08 μm and 2.53 μm, with a vibrating amplitude slot less than one micrometer. This narrow vibrating amplitude range makes it difficult to have period vibration for ball under high frequency vibration.

Table 4.2: Vibrating amplitude range with frequency change for part's periodic vibration

Item	f = 50 Hz	f = 100 Hz	f = 500 Hz	f = 5000 Hz
A for $k_{1,1}$ [μm]	207.96	51.99	2.08	0.021
A for $k_{2,1}$ [μm]	252.62	63.16	2.53	0.024

Mathematical methods used in our analysis

As discussed before, the vibrating frequency of the plate increases, the vibrating amplitude slot for the parts to keep periodic vibration becomes narrow. The vibrating frequency of the structure in our system is generally higher than 500 Hz, and the vibrating amplitude slot will be smaller than 1 μm. This induces the part's vibration chaotic. Due to the chaotic vibration of the parts, we use statistical method to analysis the impacts. If a group of samples follow normal distribution, we can use the mean value (noted as μ) to represent this group of samples and compare with other groups of samples. And the standard error is used as a method to estimate the error of the mean value. We use QQ plot to graphically illustrate whether a group of samples is normal distributed or not. If the QQ plot of a group of data is strongly linear pattern (not necessary proportional), the data follow normal distribution. Moreover, the coefficient of determination (R^2) is used to calculate quantitatively how close it is between a group of data and its QQ plot regressing line. When R^2 is close to 1, we can say that the data follow normal distribution. The value of R^2 defines the percentage of the data that are regressing the straight line.

4.1.2 Ball's vertical displacement

Existing studies have two main features. First, the researches include vibrating of low frequency (less than 100 Hz) [49]. Second, the studies investigate how the plate vibrating condition will affect the ball behaviour, whether it is periodic or chaotic. Under low frequency vibration, if the ball vibrate periodically, the ball's vertical displacement during the impacts can be deduced easily using free flight analysis. However, when the vibrating frequency increases, the amplitude range for periodic vibration becomes small and the vibration becomes chaotic. In this section, we will investigate the parts behaviour under higher frequencies, specifically few hundreds of hertz to few thousands of hertz. These frequencies are discrete because they are determined by the resonant frequencies of the resonant structures. Also because the plate vibration is created by resonance mentioned in the previous chapter, higher the resonant frequency is, smaller the maximum vibrating amplitude is. The investigated target is the vertical displacement. After an impact, the initial vertical velocity v_h, impact interval t_{INTRV} and the maximum vertical displacement h_{max} follow the free flight motion (See Fig. 4.3). They have the relation expressed in equations 4.1 and 4.2. Therefore, when the ball is repeatedly jumping on the vibrating plate, these three parameters are equivalent to study the impacts.

$$h_{max} = \frac{1}{2}\frac{v_h^2}{g} \tag{4.1}$$

$$h_{max} = \frac{1}{8}g(t_{INTRV})^2 \tag{4.2}$$

To constrain the part response in one direction, we have used a cylinder guide, which is called 1D guide in the following (Fig. 4.4). It is made of acrylic. In the simulation, we do not consider the friction between cylinder guide and the part. The restitution coefficient for the 1D guide and ball is determined by their material properties, i.e e = 0.4.
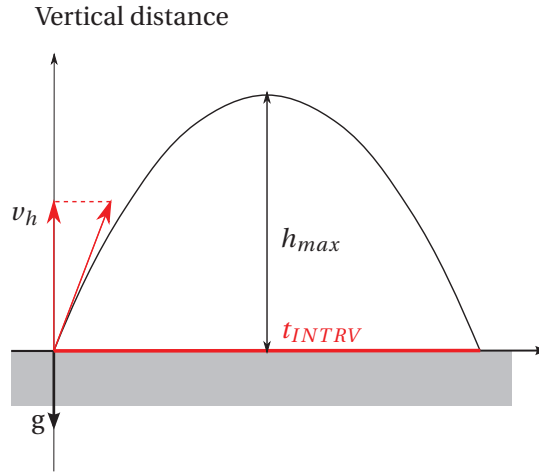
Figure 4.3: The analysis of projectile motion for vertical distance [44]
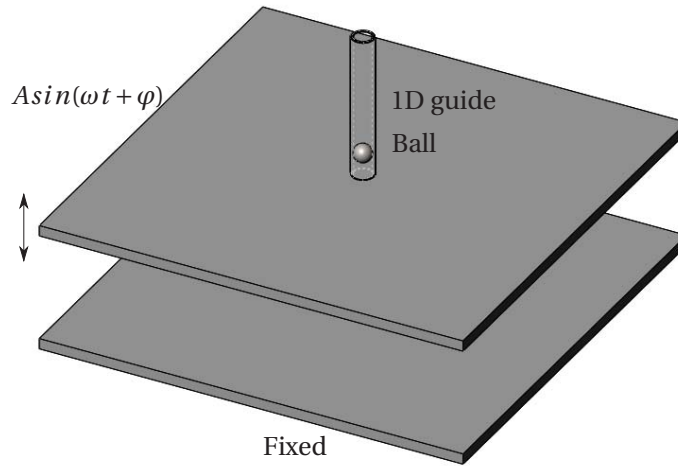
Figure 4.4: Model constrained to 1D vibration

First, the ball under the plate vibration (f = 558 Hz, A = 90 μm) is investigated. This frequency is chosen because it is in the frequency range of high frequency and also it is the resonant frequency of the prototype's first bending mode. The amplitude corresponds to the maximum amplitude obtained in our prototype. When the vibrating frequency is fixed (which are discussed in the previous chapter), vibrating amplitude is the important factor that influences the part impacts. Here we study the ball behaviour under different vibrating amplitude. Fig. 4.5 presents the ball displacement and velocity under repeated impacts. We observe that even if the ball vibration is chaotic, there are still some patterns - the bounces seem to have certain time interval (INTVR). Because the repeated impact process is chaotic, as stated before, we use the statistic method. In simulation, it is easy to obtain directly vertical displacement, initial velocity and impact interval. Here, we choose impact interval t_{INTRV} as the study parameters.
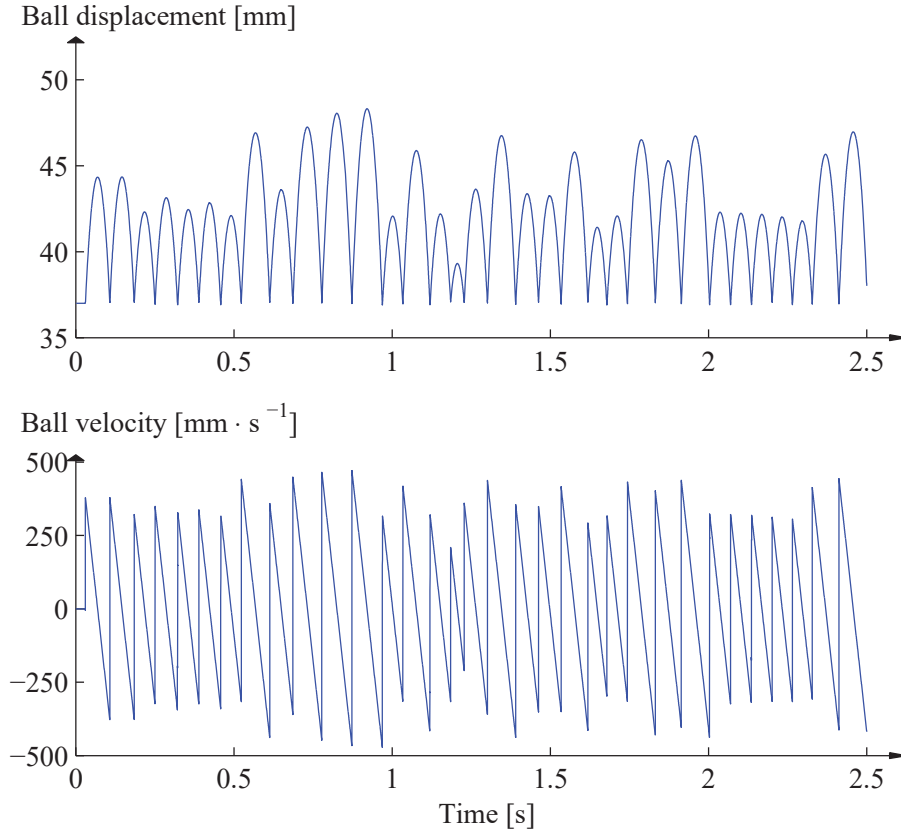
Figure 4.5: Ball behaviour under 558 Hz, 90 μm

Fig. 4.6 gives the bounce interval and analysis under 90 μm vibrating amplitude. Fig. 4.6a gives the bounce interval t_{INTRV} and the mean value μ_{INTRV} ($\mu_{INTVR} = 0.075$ second, red line in Fig. 4.6a). Fig. 4.6b gives the QQ plot. The data are regressing to the straight line. The coefficient of determination R^2 is 0.906. This means 90.6 % of the data are regressing to the straight line. Therefore, we can use the mean interval (μ_{INTVR}) to represent the bounce interval samples and further represent the ball impact behaviour under this

Then, we have investigated the ball behaviour under different vibrating frequencies and vibrating amplitudes. Fig. 4.7 shows three groups of vibrating frequencies, each group has different vibrating amplitude. The data are statistical results. Each data point represents the mean vertical displacement μ_H to represent the part behaviour under certain vibrating condition. The error bar is the range of standard error (SE). For each group of frequency, increasing the vibrating amplitude, ball vertical displacement is higher. To obtain a desired ball vertical displacement, we can use the higher vibrating frequency with smaller vibrating amplitude or lower vibrating frequency with larger vibrating amplitude. For example, to

(a) Bounce interval

(b) QQ plot for normal distribution
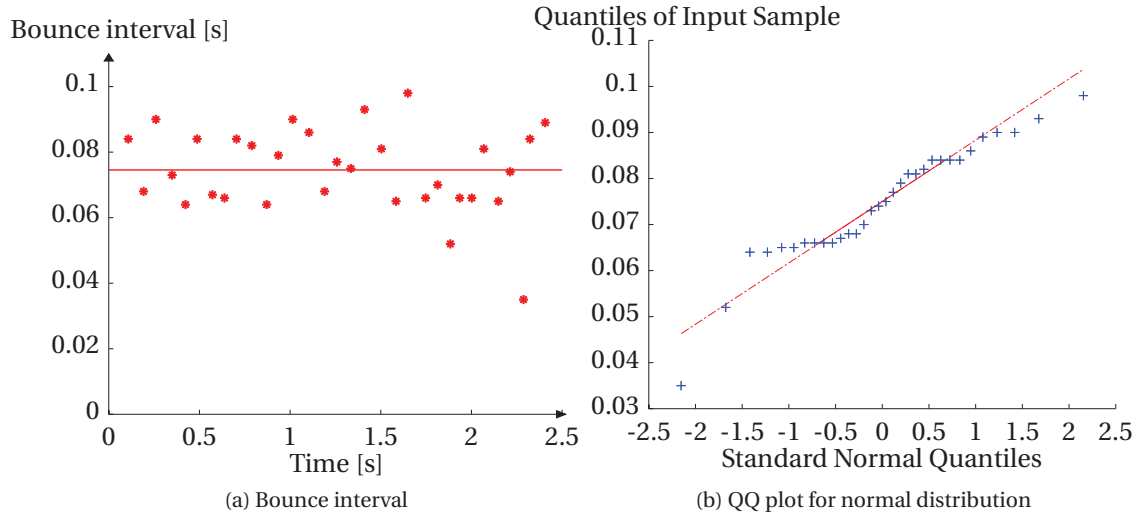
Figure 4.6: Bouncing interval for 90 μm vibrating amplitude

obtain a ball vertical displacement bigger than 4 mm, we can use the frequency-amplitude combination above the dashed black line in Fig. 4.7. Numerical values are listed in Table 4.3. All the coefficients of determination (R^2) are close to 1. This assures that that these intervals are normally distributed.
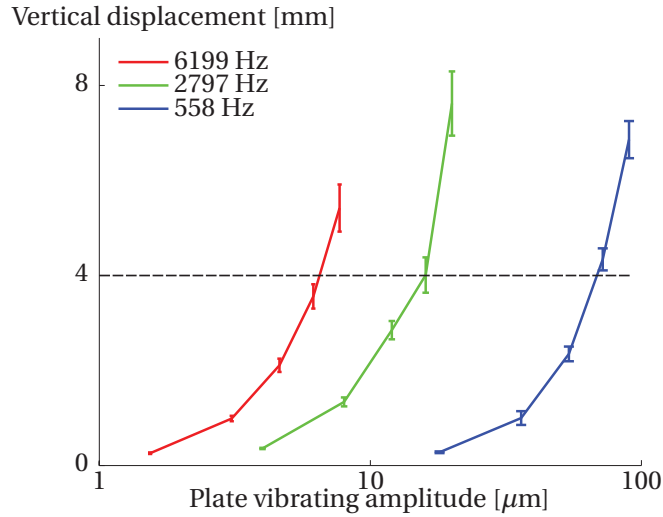
Figure 4.7: Vertical displacement for ball

According to these data, we have proposed the relation between μ_{INTVR}, the vibrating frequency f, the vibrating amplitude A and the restitution coefficient e (Eq. (4.3)). The maximum difference of mean interval between the simulation and prediction is 20.40%. Fig. 4.8 illustrates the simulation mean interval and predict mean interval.

Table 4.3: Ball response under different vibrating conditions

| f | A | μ_{INTVR} | μ_{INTRV} predict | R^2 | μ_H | SE_H | μ_{INTVR} error |
Hz	μm	s	s		mm	mm	%
558	90.0	0.075	0.077	0.935	6.86	0.391	3.26
558	72.0	0.060	0.062	0.907	4.34	0.232	3.87
558	54.0	0.044	0.046	0.915	2.35	0.155	5.83
558	36.0	0.029	0.031	0.868	1.00	0.145	8.40
558	18.0	0.015	0.015	0.953	0.28	0.018	2.36
2797	20.0	0.079	0.086	0.918	7.62	0.676	9.16
2797	16.0	0.057	0.069	0.886	4.01	0.372	20.40
2797	12.0	0.048	0.052	0.941	2.85	0.192	7.16
2797	8.0	0.033	0.034	0.940	1.34	0.094	4.13
2797	4.0	0.017	0.017	0.972	0.36	0.013	0.72
6199	7.70	0.067	0.073	0.930	5.42	0.496	10.38
6199	6.16	0.054	0.059	0.875	3.56	0.256	9.06
6199	4.62	0.042	0.044	0.936	2.11	0.140	6.15
6199	3.08	0.028	0.029	0.949	0.99	0.057	3.39
6199	1.54	0.014	0.015	0.950	0.26	0.016	1.39

$$\mu_{INTRV} = \frac{A \times (2\pi f) \times (1 + e)}{g} \times 2 \qquad (4.3)$$
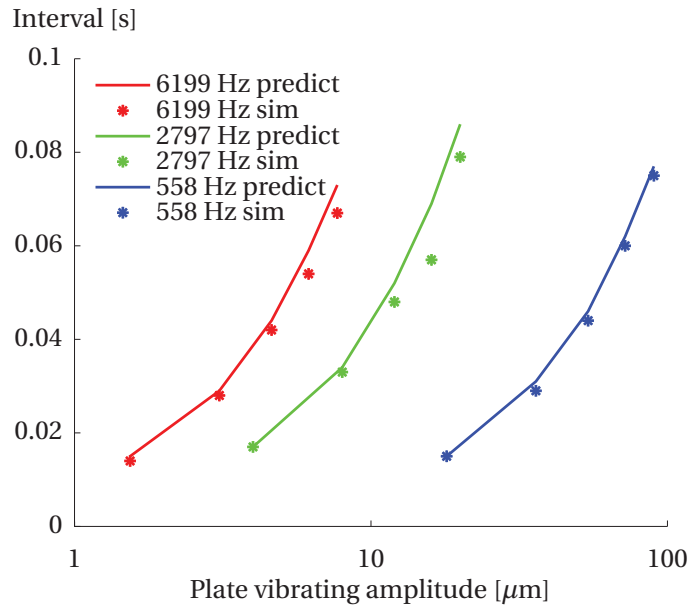
Figure 4.8: Mean interval prediction

4.1.3 Cylinder's vertical displacement and experiments

The above-mentioned research studied the ball in simulation. It is simple due to the point-like feature. We are not able to carry out the experiments because the spherical surface of the ball makes it difficult for the Laser vibrometer to receive the signal. Cylinder part is chosen to be the research object, because it can provide a flat surface so that we can implement the experiments much easier. (The experiments use Doppler Laser Vibrometer (Polytec compact laser vibrometer CLV 1000) to detect the part velocity and thus the cylinder's flat surface allow the CLV 1000 to receive the reflected signals). First, we will give the cylinder impact responses under different vibrating conditions. Afterwards, experiments will be carried out to validate the simulation model.

Fig. 4.9 presents the simulation vertical displacement of cylinder under 558 Hz. Under vibrating amplitude of 90 μm, the cylinder has a much smaller vertical displacement than the ball.
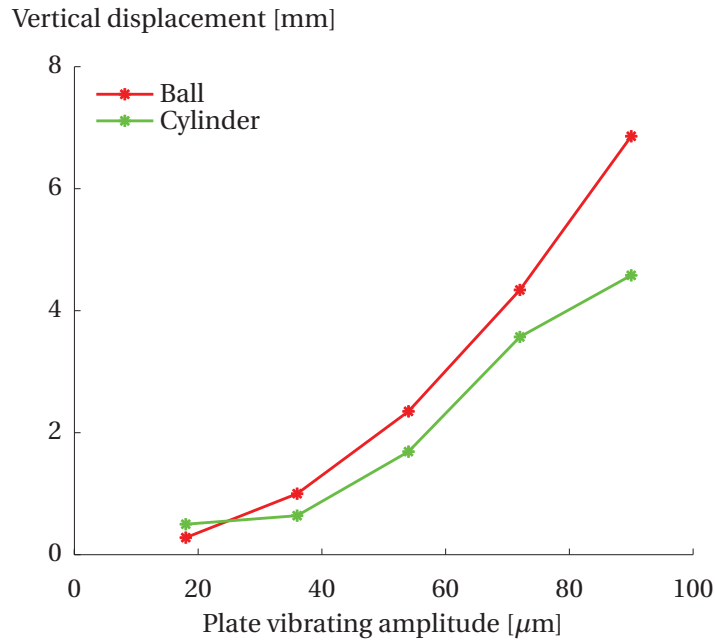
Figure 4.9: Cylinder vertical displacement under 558 Hz

Prototype and experiment

The experiments are implemented with a plate excited by a piezoelectric actuator. The piezoelectric actuator excites the resonance of the plate to obtain desired vibrating amplitude. As said before, the part is a cylinder, which is made of steel and with size of $\Phi\,3\;mm \times 8\;mm$. The velocity is measured with a Doppler Laser Vibrometer (Polytec CLV 1000). The cylinder is chosen, because the CLV needs a flat surface for the laser reflection during the entire impact duration. To constrain the vibration in one dimension, the plastic 1D guide is used (Fig. 4.10).

63

The inner diameter of the 1D guide is 4.60 mm. To decrease the initial horizontal velocity, the experiments are implemented in the center of the anti-node of a resonant mode.
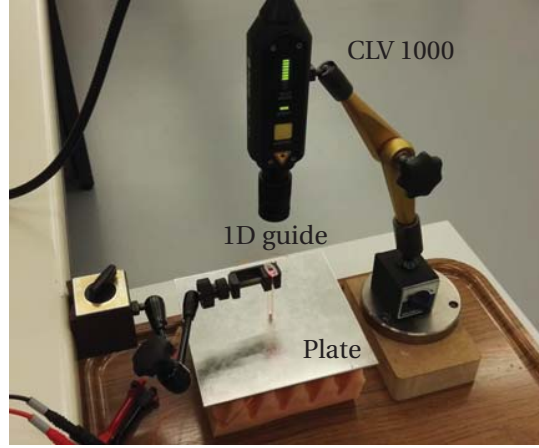
Figure 4.10: Vibration experiment equipment

Fig. 4.11 gives the experimental and simulation cylinder vertical velocity under 558 Hz, 94.48 μm. The sudden changes of velocity represent the impacts. When the vertical velocity has positive value, it has the opposite direction of gravity acceleration. We observe three features. Firstly, at the beginning, the velocity is obviously smaller than later. This is because the plate has transient response and needs time to achieve the final steady state (Fig. 4.12 illustrates the plate velocity transient response from start until steady state).The white signal is the velocity of the position in the center of the plate. From this figure, we can see that the plate needs around 0.4 second to be steady.
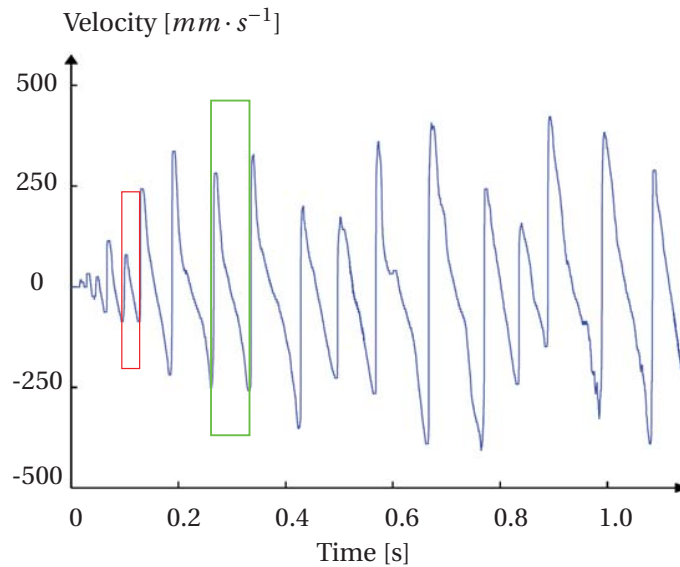
Figure 4.11: Cylinder experimental velocity under 558 Hz, 94.48 μm

Secondly, when the vertical velocity after impact is small, the following velocity curve is more linear (see red rectangular in Fig. 4.11). Whereas when the vertical velocity after impact is larger, the following velocity curve is no longer linear (see green rectangular in Fig. 4.11). The slope is smaller at the latter phase. This is because, even if we put the cylinder initially in the anti-node to decrease the horizontal velocity, there is still a small horizontal velocity. Due to this horizontal velocity, the cylinder may impact with the 1D guide. The impact between cylinder and 1D guide will definitely induce friction and reduce the acceleration. However, the friction is small. This is confirmed by the final vertical velocity under the influence of the friction. For example, the velocity curve in the green rectangular, the maximum negative velocity is -253.90 $mm \cdot s^{-1}$ and the maximum positive vertical velocity is 281.30 $mm \cdot s^{-1}$. The vertical velocity is 9.74 % smaller due to the friction. Thirdly, the impact intervals seem to have a similar pattern to that shown in Fig. 4.5.
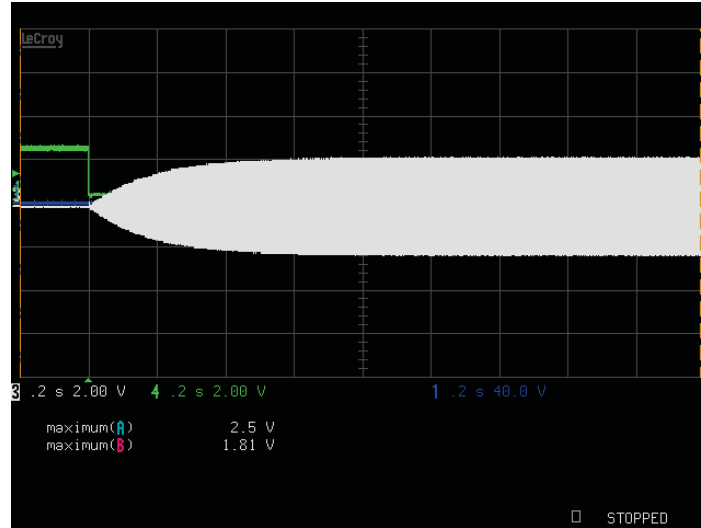
Figure 4.12: Plate transient response to steady state

Fig. 4.13 shows the QQ plot of experimental interval. The data is distributed around the linear line. The coefficient of determination (R^2) is 0.973. This confirms that we can use the mean interval to represent the cylinder impacts under vibration.

As discussed before, we neglect the friction for simplification. The simulation vertical velocity results under 558 Hz, 90 μm are shown in Fig. 4.14. The velocity curves are linear after each impact. In the simulation, there is not transient time due to the simulation condition, the plate has the predefined vibrating amplitude of 90 μm immediately. Thus, the cylinder obtains large vertical velocity immediately after the beginning of the simulation.

Fig. 4.15 gives the vertical velocity under 558 Hz, 18.9 μm. The vertical velocity is much more linear after each impact. This result confirms the previous hypothesis - the large vertical velocity increases the horizontal displacement and thus induces the impact between cylinder and 1D guide. In this figure, we present the data from 0.2 second, because the interval under

Quantiles of Input Sample
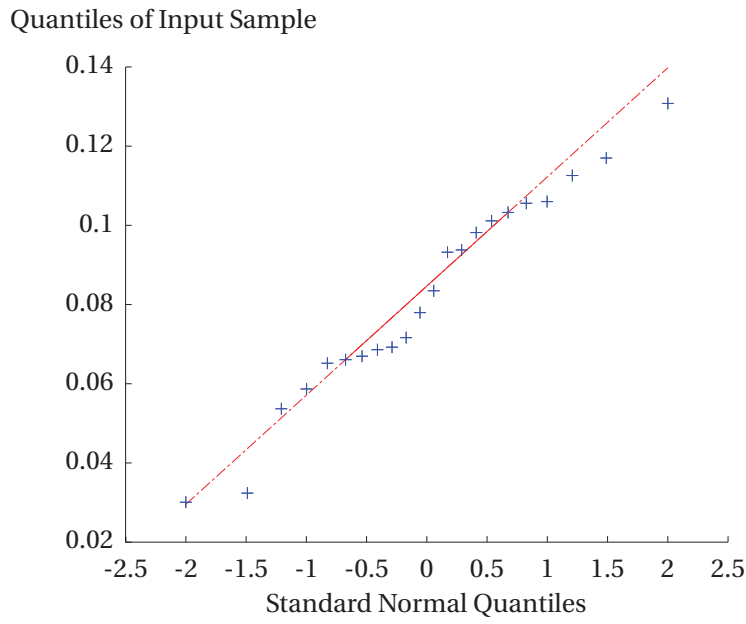
Figure 4.13: QQ plot for cylinder experimental interval under 558 Hz, 94.48 μm

Velocity $[\text{mm} \cdot \text{s}^{-1}]$
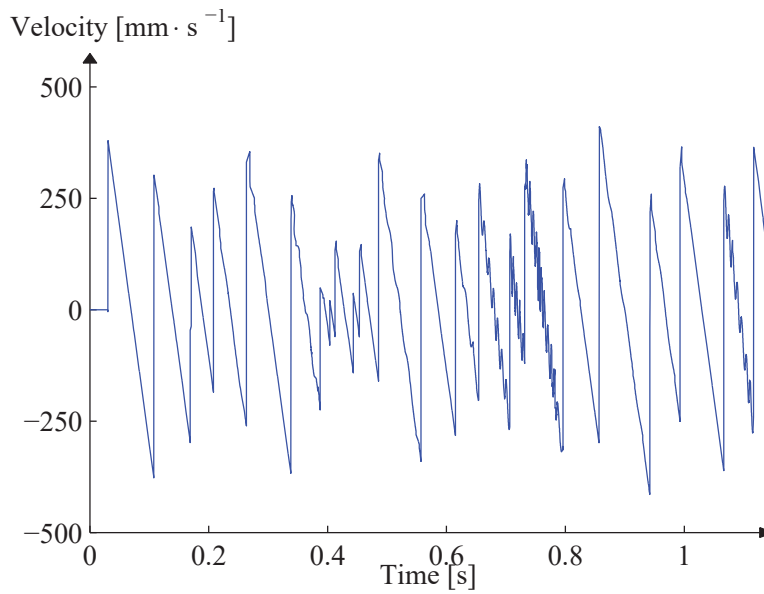
Figure 4.14: Cylinder simulation velocity under 558 Hz, 90 μm

this vibrating condition is smaller. We remove the beginning stage of plate vibration (transient time) to be much clearer to illustrate the results.

Fig. 4.16 gives the experimental and simulation results comparison for three groups of vibrating conditions. The numerical comparison is listed in Table 4.4.
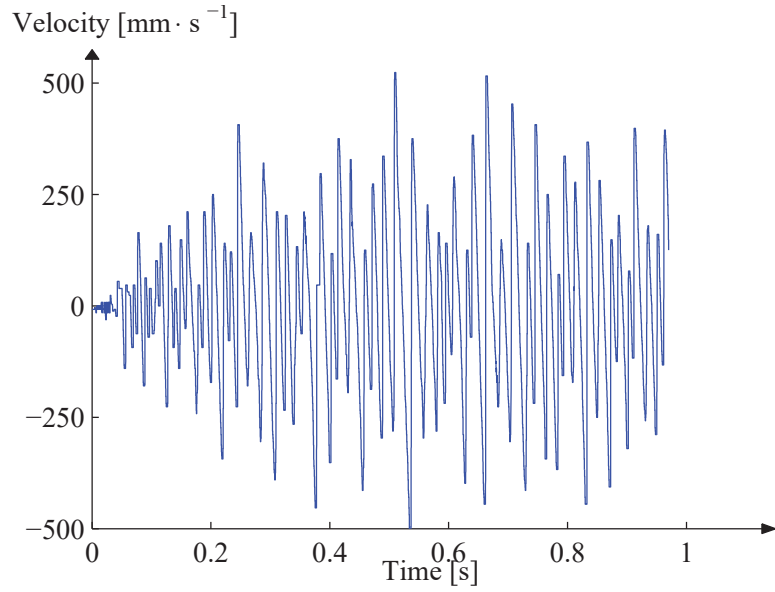
Figure 4.15: Cylinder experimental velocity under 558 Hz, 18.9 μm
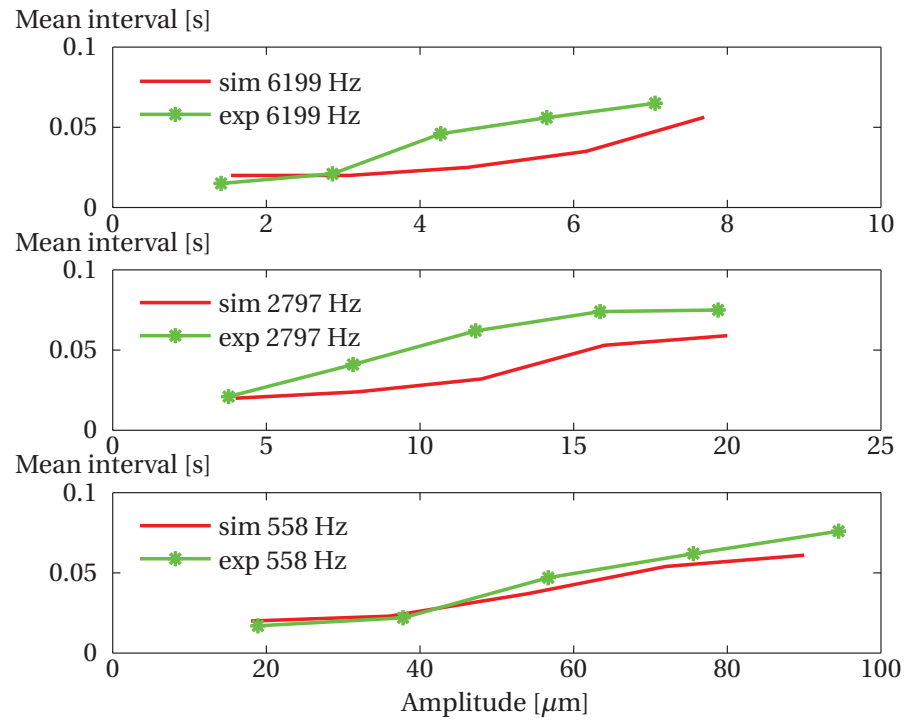
Figure 4.16: Experimental and simulation results comparison

Table 4.4: Experimental and simulation results comparison

f	A	Exp μ_{INTRV}	Sim μ_{INTRV}	error
Hz	μm	s		%
558	90.0	0.076	0.061	-19.47
558	18.0	0.017	0.020	13.79
2797	20.0	0.063	0.075	-16.58
2797	4.0	0.020	0.021	-5.49
6199	7.70	0.056	0.065	-13.46
6199	1.54	0.020	0.015	18.97

4.2 Part's horizontal movement

If the vibrating plate is inclined or the interaction between the part and the vibrating plate provides to horizontal force, the parts may have a horizontal displacement such as researches mentioned in section 2.3. Hongler et al [29] has studied a bouncing ball with a vibrating plate which has a small angle with the horizontal level and its vibration direction has an angle with the plate surface. Their studies refer to vibrating condition with low frequency (few tens of hertz) periodical transportation, we will investigate the parts behaviour under high frequency vibration of a resonant plate. To transport the part from anti-node to node, we should control the vibrating amplitude the part's vertical displacement to be small enough in order to avoid the part jumping randomly on the plate.

4.2.1 Simulation

Model description

3D simulations are carried out through SolidWorks$^{\text{TM}}$. The model includes a plate (Fig. 4.17) whose one edge is fixed and the opposite edge is driven by a sinusoidal vibration. These two edges are used to simulate the nodes and anti-nodes of a resonant plate, respectively. The nut is made of steel, and the plate of aluminium. The dimension of the simulated plate is $40 \times 40 \times 1 \ mm^3$, and the nut is M 2.5.
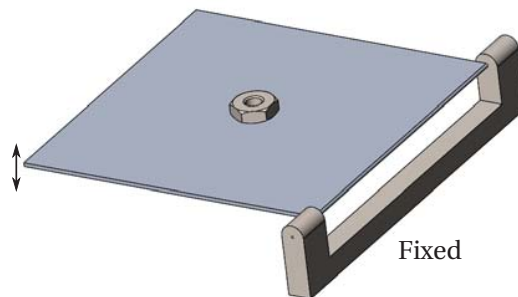
Figure 4.17: Interaction model for nut and plate

Previous studies focus on point-like parts such as ball. For parts with complex geometry, there is no analytical analysis. We will use the comparison between simulation and experimental results to validate the model established in Solidworks. The horizontal movements are influenced by the friction, thus will we include friction in the simulation. In Solidworks, we can model the friction with these parameters: μ_s, μ_k, v_s and v_k. μ_s is the static friction coefficient and μ_k is the dynamic friction coefficient. Supposing there is no relative motion between two objects which are moving together with the velocity v, due to the static friction. v_s is the static friction transition velocity which specifies the velocity at which the static frictional force is overcome and the two objects start having a relative motion. v_k is the dynamic friction transition velocity which specifies the velocity at which dynamic friction becomes constant. Fig. 4.18 illustrates the static and dynamic friction force versus velocity. The corresponding coefficients are assigned automatically, based on the materials we define for the contact objects. They may be set manually if necessary.
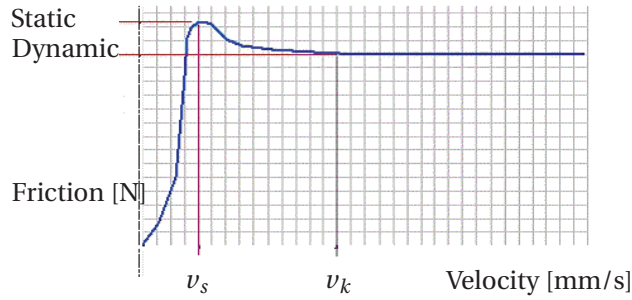
Figure 4.18: Friction in the contact [58]

Moreover, the geometry of nuts are much more complicated than that of ball, it is difficult to converge using the coefficient of restitution to calculate the impact normal force. Therefore, we have used the stiffness k_n to approximate the material stiffness at contact surface between the nut and the plate. Using this method, the normal contact force F_n can be expressed as in Eq. (4.4). x_n is the penetration of one object into the other during the impact (shown in Fig. 4.19). γ is the parameter used to improve numerical convergence. They are assigned automatically based on the materials, also. They may be set manually if necessary, as well.

$$F_n = k_n x_n + \gamma \qquad (4.4)$$
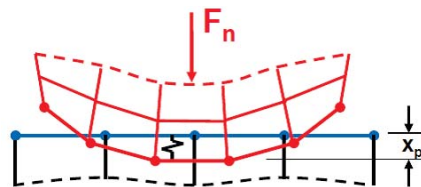
Figure 4.19: Illustration for impact force and penetration [58]

69

Simulation representation

Fig. 4.20 presents the simulation result of the nut under vibration which is equivalent to 4750 Hz, 1.00 μm. According to this figure, we can obtained that the horizontal velocity is 1.65 $mm \cdot s^{-1}$.
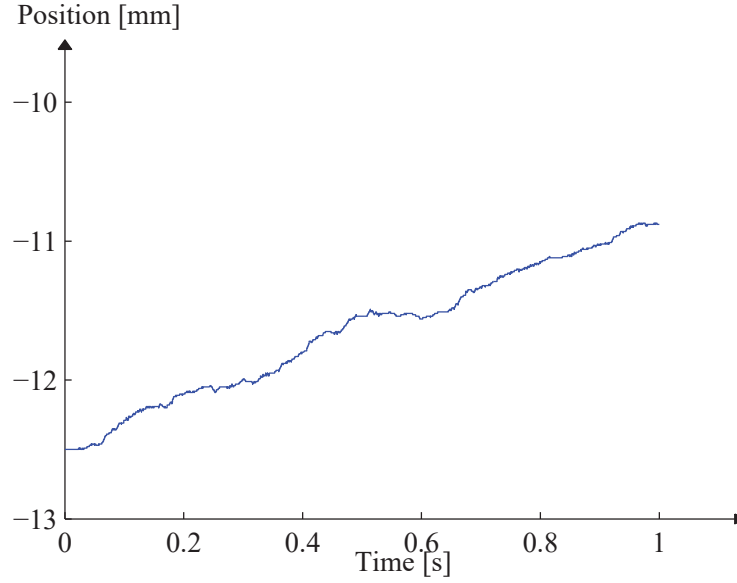
Figure 4.20: Horizontal displacement for nut

4.2.2 Experiments

Experimental setup and procedure

The experimental setup includes a vibrating plate which is driven by one piezoelectric actuator, and the nut. The vibrating plate is a $160 \times 120 \times 3$ mm^3 aluminium plate. The vibrating plate is supported by foam. The vibrating amplitude is measured by a laser vibrometer. To determine the experimental transport rate, high speed camera is used to record the vibration. The high speed camera was set up to 500 frames per second.

Two vibrating conditions have been investigated:

- $f = 4750 Hz$, 1.00 μm amplitude
- $f = 8775 Hz$, 1.11 μm amplitude

Parts are subjected to standing waves created by one piezoelectric actuator and thus move from anti-nodes to nodes.

Results and discussion

Table 4.5 shows experimental and corresponding simulation results under 4750 Hz and 8775

70

Hz. v_H-Exp is the average experimental results for the horizontal transport rate. v_H-Sim is the simulation results for the horizontal transport rate. Experiments have been carried out six times for each conditions. For 4750 Hz, the average transport rate is 1.44 $mm \cdot s^{-1}$, and the standard deviation is 0.27 $mm \cdot s^{-1}$. For 8775 Hz, the average transport rate is 4.17 $mm \cdot s^{-1}$, and the standard deviation is 0.64 $mm \cdot s^{-1}$. There is certain consistency between experimental and simulation results.

Table 4.5: Transport rate comparison

	Frequency	Amplitude	v_H-Exp	v_H-Sim	Difference
	Hz	μm	$mm \cdot s^{-1}$	$mm \cdot s^{-1}$	%
1	4750	1.00	1.44	1.65	14.58
2	8775	1.11	4.17	3.01	27.82

4.3 Summary and conclusions

This chapter has allowed investigating the interaction between a part and a resonant vibrating plate. At the beginning, the numerical simulation is validated by comparing it to the existing analytical bouncing ball system. The resonant frequencies of a plate are discrete. Using the same resonant exciter, resonant frequency and amplitude has the following correlations: higher the resonant frequency is, lower the vibrating amplitude is; lower the resonant frequency is, higher the vibrating amplitude is. Numerical simulations on the ball's vertical displacement has shown that we can obtain a certain displacement by either a high vibrating frequency with low amplitude or a lower frequency with higher amplitude. Experimental and numerical results coherence has validated the numerical simulation. Thus, we can predict the mean interval of the chaotic vibration of the ball according to the vibrating frequency, amplitude and restitution coefficient. The simulation and experiment results of a cylinder have shown the numerical simulation using the coefficient of restitution for the impact can predict the non-point-like object even if there are still some mismatches.

In the second part, we have investigated the nut horizontal movement from anti-nodes to nodes. The established model has considered the amplitude variations from anti-node to node (the amplitude changes linearly to the distance between the impact points to the node). Part's vertical displacement is limited to small value during the horizontal movement in order to avoid the parts' random movement. This has led to a slow part's horizontal movement.

The simulation and experimental results show that it is possible to use 3D simulations to model the complex geometry parts. In particular, it seems possible to use this 3D simulation to predict the vertical displacement and horizontal movement of the parts.

The numerical simulation in this chapter validates only for the impact in which the two objects could be considered rigid. It is no more consistent if the impact is too flexible. Moreover, the studies in this chapter are simplified method to give the first step for part's vibration behaviour

on a resonant plate with higher frequency than the bouncing ball system.

5 Applications

5.1 Introduction

In chapter 3, we have investigated the modes (resonant frequency and mode shape) of a free boundary square plate and how to increase the vibrating amplitude of the resonant mode by piezoelectric actuator design. These studies provides the basis to choose desirable mode shapes and obtain necessary vibrating amplitude that are necessary in this chapter. In chapter 4, we have investigated the parts vertical displacement and impact interval under different vibrating frequency and vibrating amplitude. These studied will be used in this chapter to obtain the desirable part behaviour by controlling the vibrating conditions. In this chapter, we will discuss the feasibility of different applications by integrating the previous studies, considering free boundary square plate. Firstly, we will discuss the standing wave switches strategies to separate parts. This includes choosing the right modes, control the vibrating amplitude and duration. Then, we will make use of a series of standing waves in the right sequence to transport parts. Afterwards, we will investigate the method to create quasi-travelling wave using degenerate modes.

The resonant plate will refer to an industrial tooling plate size with slightly modification. The parts separated in our thesis are confined to simple shape (such as standard mechanical hex nuts). A commercial piezoelectric actuator, which is familiar to our lab, is chosen for the first step (See appendix A.4).

5.2 Standing waves for parts separation

5.2.1 Principle

The modes studied in our system are standing waves. In two dimensions, they have nodal lines and anti-nodal lines patterns. These anti-nodal lines and nodal lines are determined by the resonant structure's properties (size, shapes, material and boundary conditions) and remain stationary in the structure after the structure's properties are chosen. This predicable

feature can be used to design flexible parts feeding system in order to reduce the random vibration in the current feeding system.

A typical 1D standing wave is described in Fig. 5.1. The nodes (the solid red points) are locations where the displacement is always zero. The maximum vibration amplitude position (the solid black point, as shown in Fig. 5.1) is the anti-node. When the parts are not around the nodes (e.g. the green hollow balls positions), they move towards nodes after certain time of vibration. When we extend this principle to 2D standing waves, the parts always come to nodal lines eventually. Thus, by design, we are able to predict the position of the parts on the plate after vibration.
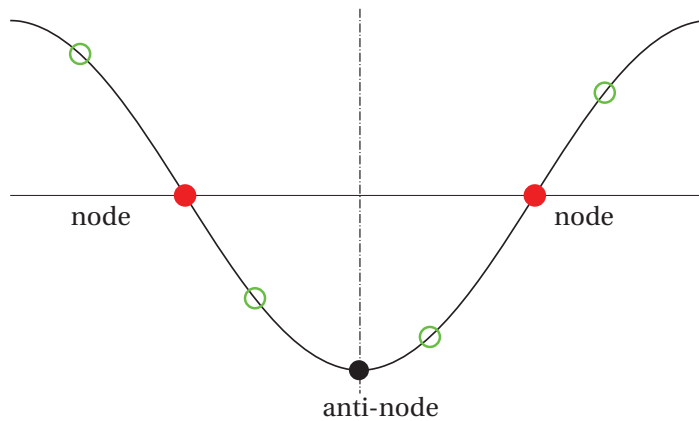
Figure 5.1: 1D standing wave

According to the study in chapter 4, for a specific resonant mode, the part vertical displacement increases with the vibrating amplitude. Thus, it becomes feasible to separate the parts which are tangled with each other. The anti-nodes of the plate have the maximum vibrating amplitude in the vicinity of them. When the plate vibrating amplitude is limited by its design, we can use anti-nodes as the positions for separating. Normally, the initial parts positions are indefinite - they are not always in the positions for which the vibrating amplitude is sufficient to separate tangled parts. One solution is that the parts are pre-positioned where the vibrating amplitude is large enough in the following vibration. We want to have two resonant modes, the anti-nodes of the second resonant mode should match the nodes of the first resonant mode. We will call the first resonant mode "pre-positioning mode" and call the second resonant mode "separating mode". This can be achieved by using a pair of "X mode" (in the plate center whose nodal lines are diagonals of the plate, illustrated as the mode in Fig. 5.2a, named as in [54]) and "Ring mode" (in the plate center whose nodal lines are parallel to the diagonal of the plate but not go through the center of the plate, the nodal lines may encircle the plate center like a ring, illustrated as the mode in Fig. 5.2b).

Fig. 5.2 presents an example of this mode pair for separation. The normalized displacement (red and black curve) is the mode shape profile for each mode along the line which goes

through the center of the plate and is parallel to the plate edges. The normalized displacement (normalized with the maximum displacement along the line as the reference for each mode) is used, as already mentioned in chapter 3 when presenting the mode in Fig. 3.5, because the values of the deformation in simulation have no physical significance. On the two normalized displacement curves of the two resonant modes, there are three points: A0, B1 and B3 (we do not consider the points along the edges of the plate). If we firstly use resonant mode of 2629 Hz as pre-positioning mode, the parts will definitely move to A0 along the red line through the plate center. Then if we switch to the resonant mode of 2778 Hz for separating mode, the position A0 becomes anti-node, the parts are able to be separated due to the large vibrating amplitude. Similarly, because the nodes of resonant mode 2778 Hz are the anti-nodes of 2669 Hz, we can use resonant mode of 2778 Hz as pre-positioning mode, and use resonant mode of 2669 Hz as separating mode.
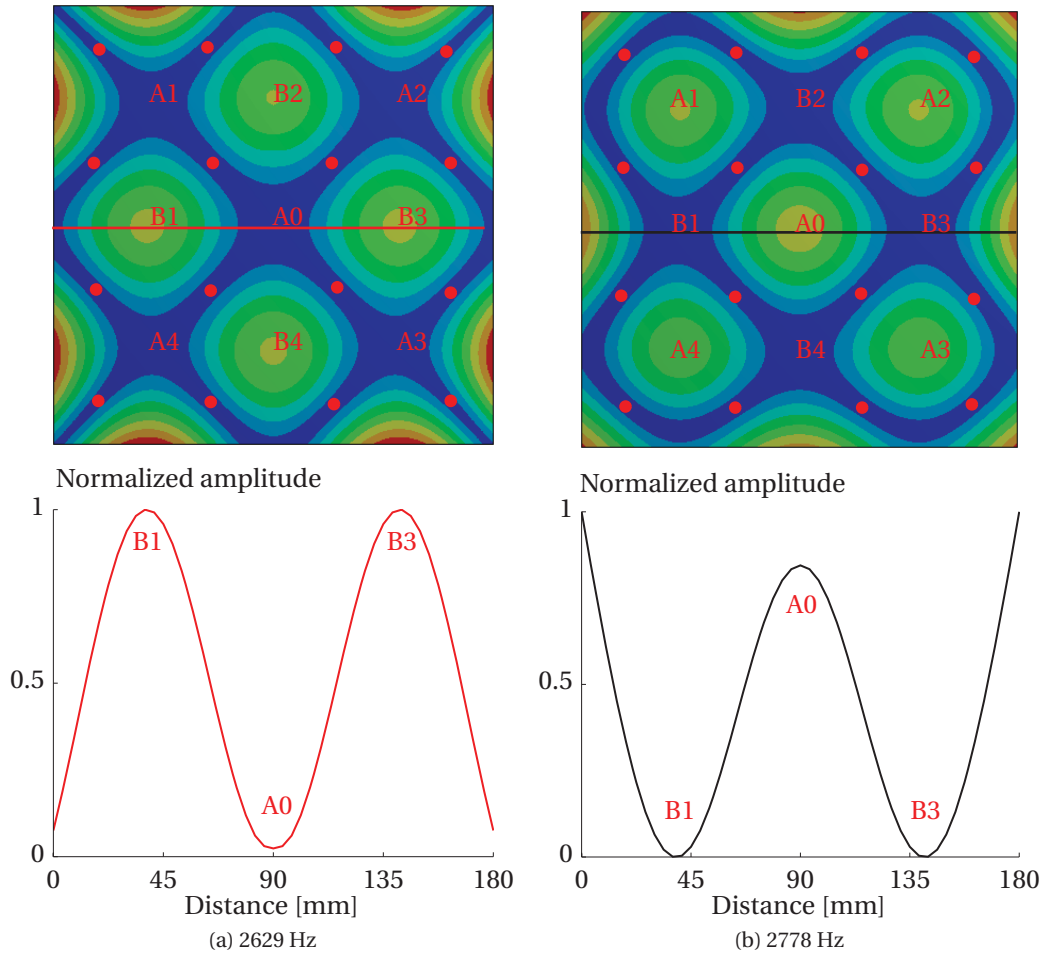
Figure 5.2: Pre-positioning and separating mode choice illustration

5.2.2 Discussion

2D "Dead position"

When we extend this principle to two dimensions, there are also effective points that could be used to separate parts from them, such as point groups of A0 - A4 and B1 - B4. Whereas, there are some particular positions that become "Dead position" (which are nodes in both modes, red points shown in Fig. 5.2). Thus if the parts move to these position, the method using only a pair of modes "X mode" and "Ring mode" fails to separate the parts. However, it is possible to use a third mode to move the parts on these "Dead position" if the vibrating condition of the third mode is sufficient to move the parts. For this specific case, the mode with resonant frequency of 12370 Hz exists which is illustrated in Fig. 5.3. The previous "Dead positions" are close to the anti-nodes of this mode. If the vibrating condition of mode 12370 Hz is able to move the parts on its anti-nodes, parts on these "Dead positions" are able to be separated. Otherwise, this method fails to separate parts which are moved to these positions. This means that the parts are not completely under control.
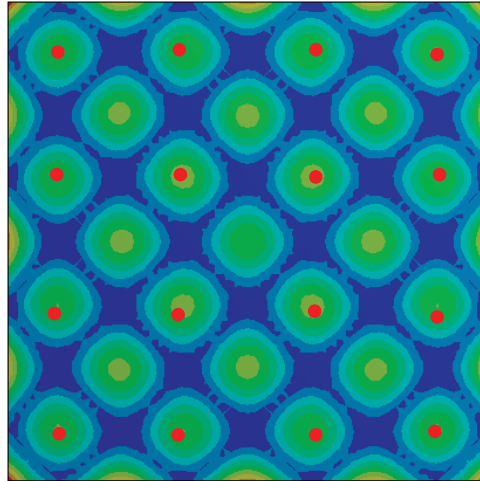
Figure 5.3: Eigenmode of 12370 Hz

Pair modes' characteristics of square plate

The pair modes that are illustrated in Fig. 5.2a only exist for square plate. They have special characteristics and therefore they are suitable for the separation application in terms of efficiency. Normally, for a rectangular plate, along x, or y, the positive half wave and negative half wave alternates, as shown in Fig. 5.4b. However, in square plate, the special modes ("X mode" and "Ring mode") exist. From Fig. 5.2a, we observe that the mode shape along x does not alternate between positive half wave and negative half wave any more. But the positive half wave and negative half wave alternate along line which is parallel to the diagonal, as shown in Fig. 5.4a. These kind of pair modes has the characteristics that the anti-nodes of the one mode is the nodes of the other mode. In this case, after pre-positioning, the parts at anti-nodes has equal possibility to move towards the anti-nodes of the second mode (as illustrated in

Fig. 5.5a). As for the typical modes that exist in rectangular modes, the anti-nodes of the one modes is not exact the nodes of the first mode (as illustrated in Fig. 5.5b). Thus, the parts after pre-positioning are likely to move towards some of the nodes.

(a) 2629 Hz

(b) 2360 Hz
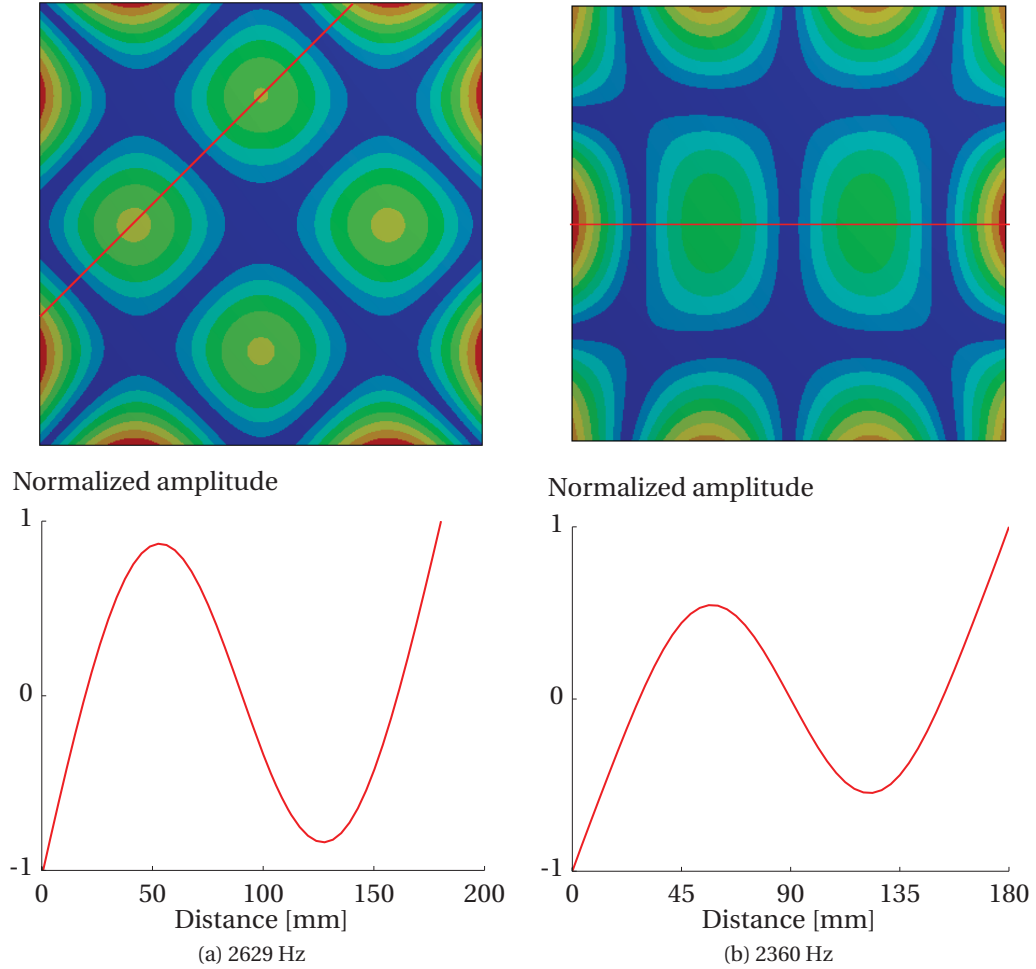
Figure 5.4: Modes comparison

More effective separating positions

As shown in Fig. 5.2, if we use the resonant mode of 2629 Hz as the separating mode and the eigenmode of 2778 Hz as the pre-positioning mode, there are four effective separating positions (B1 - B4), which are the anti-nodes of the separating mode and nodes of the pre-positioning mode. If we want to increase the number of effective separating positions, we can choose the resonant modes which have more number of half waves. Fig. 5.6 presents an example with more effective separating positions for the same plate as before. The wavelength of these two modes are smaller, it is obvious that they are able to separate the parts that have smaller size than that could be separated in previous two modes. The number of half waves is

(a) nodal lines of mode 2629 Hz and 2778 Hz

(b) nodal lines of mode 2359 Hz and 2338 Hz
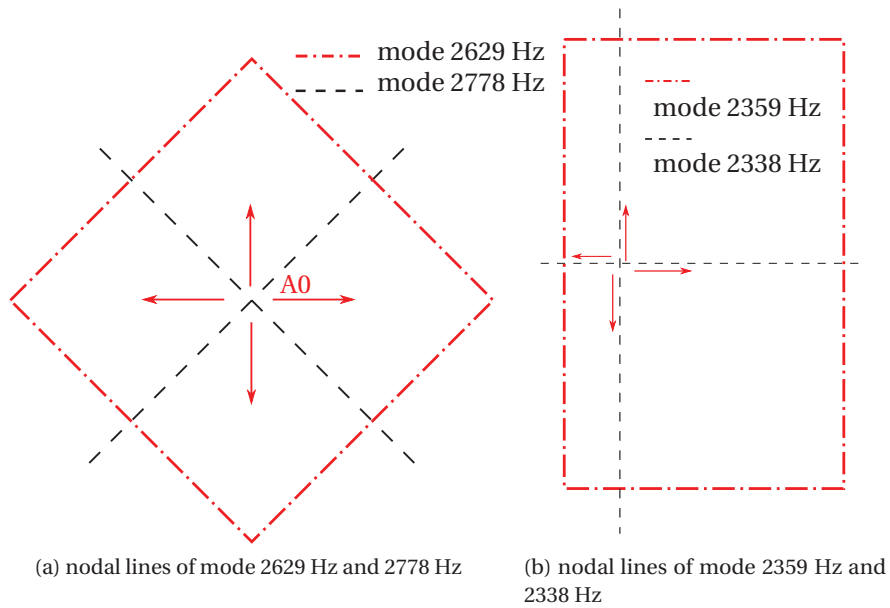
Figure 5.5: Modes for separation comparison

bigger, the resonant frequency is higher. With same piezoelectric actuator voltage excitation, normally the vibrating amplitude at anti-nodes is smaller. However, the study in chapter 4 in Fig. 4.7 shows that it could provide the same parts impact behaviour as that of lower frequency, higher vibrating amplitude. Therefore, these two eigenmodes can be used as pre-positioning mode and separating mode, respectively, in order to have more effective separating positions at one time.

(a) 6585 Hz

(b) 6749 Hz
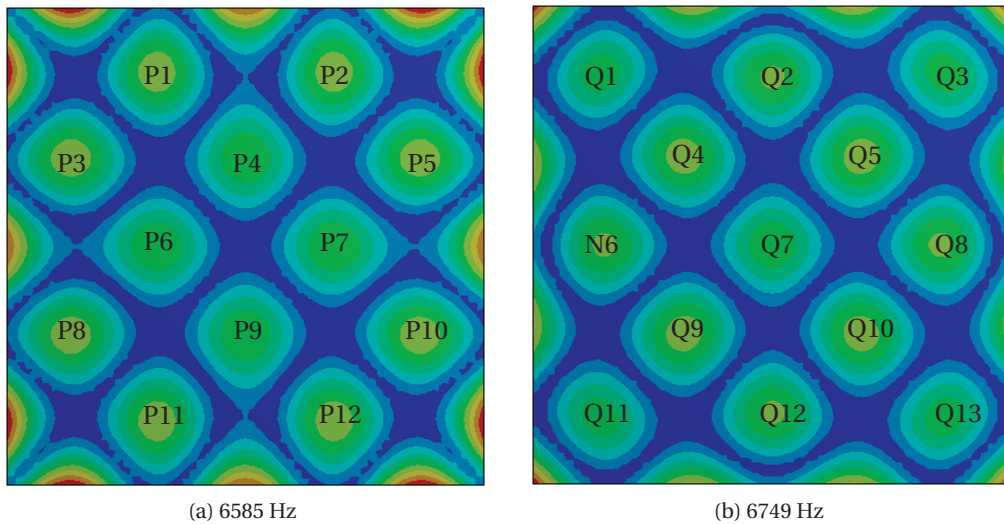
Figure 5.6: Modes with more effective separating points

Separating process control

Taking these factors into accounts, a basic procedure using this idea to separate parts is illustrated in Fig. 5.7. We take the 1D separation along center line in Fig. 5.2 for illustration. f_1 and f_2 are the pre-positioning and separating mode frequency as discussed before. The half dashed red arrows indicate that the initial part positions are indefinite, but they will go definitely to A0 wherever the initial positions of the parts (neglecting the nodes on edges of the plate). The solid black arrows indicate that the parts should be separated away from A0 and stop between A0 and B1 or A0 and B3 in order to avoid gathering of parts at points B1 and B3. The frequencies f_1 and f_2 are chosen according to the principle explained before for pre-positioning and separating mode. In the pre-positioning process, the vibrating amplitude A_1 should be large enough to provide sufficient vibration, and moreover the duration of pre-positioning mode vibration t_1 should provide enough time to allow the parts to arrive in A0. In the separating process, to effectively separate the parts from A0, the vibrating amplitude A_2 should be large enough. To avoid the parts gathering to the nodes of the separation mode (B1 or B3), the vibrating duration t_2 should be short enough. For example, we use the 2797 Hz as the separating mode for ball separation. If the ball could be separated with impact vertical displacement of 4 mm (this vertical displacement depends on the parts material, shape, mass of center and so on), according to the study in chapter 4 for vertical displacement in Fig. 4.7, the plate should provide vibrating amplitude bigger than 16 μm. To avoid the parts gathering again at points B1 and B3, the vibration duration t_2 should be carefully controlled. According to the experiment results, for nut separation, t_2 should be between 100 ms to 300 ms.

Pre-position

f_1, A_1, t_1

B1   A0   B3

Separation

f_2, A_2, t_2
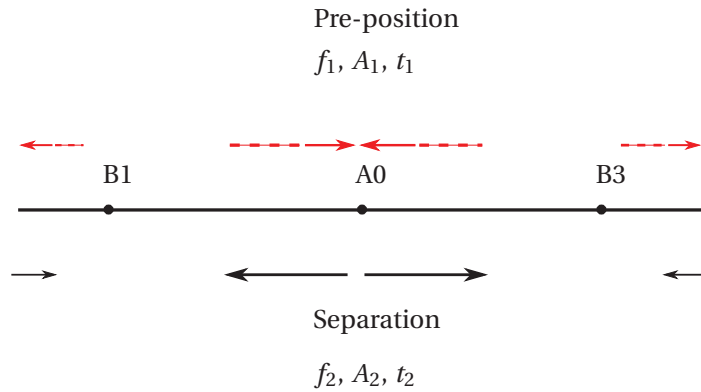
Figure 5.7: Illustration for parts separating process

To effectively separate the parts, there are some general rules that we need to take into account: 1, the parts should be rigid enough, otherwise the vibrating energy which separates the parts will be damped; 2, parts dimension should be at least smaller than a quarter of the wavelength; 3; the vibrating amplitude should be large enough to provide sufficient vertical displacement. Here are the general statements, for specific parts feeding applications, these factors should be adjusted according to the parts shape complexity, parts stiffness, and pair-mode resonant frequency.

5.2.3   Experiments

Experiments with eighty nuts are implemented. Plate main body has a size of $180(L) \times 180\,(W)$ $\times$ 3 (h) mm^3. The nuts are M 2.5 (as shown in Fig. 5.8). The nominal hole D = 2.5 mm, across flat A/F = 5 mm, height H = 2 mm. Fig. 5.9 shows the experimental results. Corresponding operations are listed in Table 5.1. To well spread the parts on the whole plate, the plate firstly starts by vibrating at 558 Hz. Then the mode of 2646 Hz is used to pre-position the parts. According to the experiments results after operation "O2" in Fig. 5.9, all the parts move around the anti-nodal lines. Then the mode of 2797 Hz is used to separate parts around the pre-position positions. Experiments results in red circles after vibrating condition "O3" show that parts are well separated from anti-nodes. The vibrating duration of mode 2797 Hz is short, 100 ms. Therefore, we see that majority of the parts are between anti-nodes and nodes and have not gathered together to the nodes of separating mode yet (parts states in Fig. 5.9 after operation O3). Using pre-positioning mode of 2646 Hz and separating mode of 2797 Hz alternatively, there are "Dead positions", which are the nuts position after operation "O4". This are illustrated as red points in Fig. 5.2. Mode of 12314 Hz can be used to move parts from "Dead positions" and better prepare the parts for next separation. The detail of this separation example is shown in appendix B
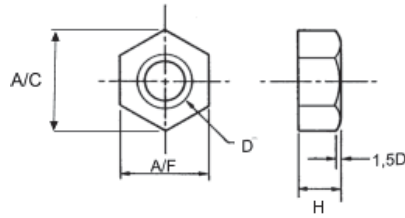
Figure 5.8: Nut

Table 5.1: Separation experiment condition

Operation	frequency [Hz]	Voltage [V]	duration [ms]	goal
O1	558	130	1,500	spread parts
O2	2646	130	2,000	pre-position parts
O3	2797	130	100	separate parts
O4				pick up the separated parts
O5	12314	130	1,000	move parts from "Dead positions"

Ten pre-positioning and separating alternative modes are implemented to check the efficiency of this method. We define that the parts whose the distance between the center is larger than 10 mm are separated and will be picked up by the gripper (Practical clearance is determined by the resolution of the vision system and the clearance needed for the robot gripper). There are 100 nuts to be separated. At the beginning, the parts are spread with mode of 558 Hz. Then
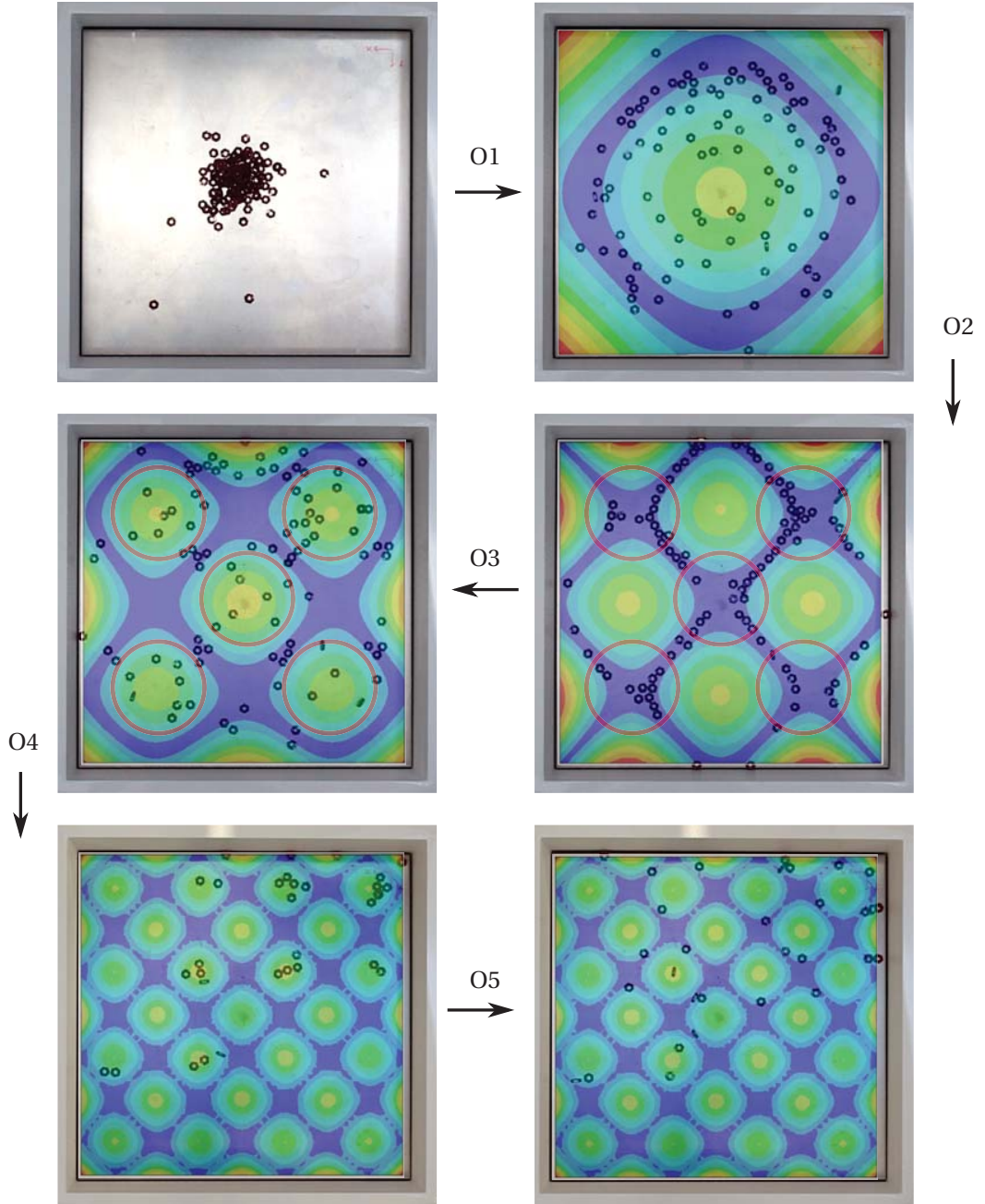
Figure 5.9: Parts separation experiment illustration

the plate vibrates with ten steps. Each step, the plate uses firstly the pre-positioning mode of 2646 Hz for two seconds with 120 V_{pp}. And the plate is switched to separating mode of 2797 Hz for 0.1 seconds with 120 V_{pp}. After one step, the separated parts are picked up with grippers (Here is simulated with manually pick up). The step is repeated for tens times which totally last around thirty seconds considering the mode switch time. Here the mean value of

this total number is 70. The practical throughput of the parts feeder for separation is highly dependent on the speed of the vision system and the robot for picking up the parts [12]. This is out of our researches, and it can be considered in the future for the industrial parts feeder design.

Table 5.2: Separated parts statistic

| Test | Vibration | | | | | | | | | | Total |
No.	1	2	3	4	5	6	7	8	9	10	
1	9	8	15	14	5	3	8	3	4	7	76
2	7	9	7	11	11	3	10	7	6	2	73
3	9	7	17	5	5	4	9	7	6	7	76
4	13	12	15	9	4	7	5	2	4	5	76
5	6	14	6	11	6	7	5	4	7	1	67
6	3	10	11	5	9	6	9	3	2	3	61
7	7	12	6	8	8	5	4	4	5	3	62
8	10	7	8	8	7	7	11	2	3	4	67
9	5	10	10	12	11	10	6	2	1	6	73
10	6	7	7	7	8	10	5	5	5	5	65

This method is less sensitive to the parts changing. The same method could be used for various of parts.

5.3 Standing waves for transportation

Fig. 5.10 illustrates the principle to transport workpieces. It consists in using a series of resonant modes with different node lines. For each resonant mode, the workpiece on the plate surface will go towards the node lines after few vibrations. Combining correctly these modes, the workpiece can be continuously transported along one direction as shown in Fig. 5.10. To achieve these particular features, the plate dimension should be chosen to target the specific resonant modes.

The main body of the experimental plate is $160 \times 120 \times 3\ mm^3$. Fig. 3.24 and Fig. 5.11 illustrate the simulation results of the resonant modes and the relative node lines along "data line" from the edge "m" to the center of the plate "b". Since the plate is symmetric, only transportation on half of the plate is studied. According to the relative node line position, the sequence for the entire transportation is: 397 Hz $\longrightarrow$ 3459 Hz $\longrightarrow$ 2195 Hz $\longrightarrow$ 4668 Hz $\longrightarrow$ 1136 Hz.

Corresponding prototype is manufactured. The piezoelectric actuators are used to create the expected resonant modes. Some foams are underneath the plate to provide free equivalent boundary conditions. Sugar (highlighted in red) is used to demonstrate the modes shape and the node lines ("Chladni figures" [14]). The workpiece used for the transportation experiment is nut "M 2.5".
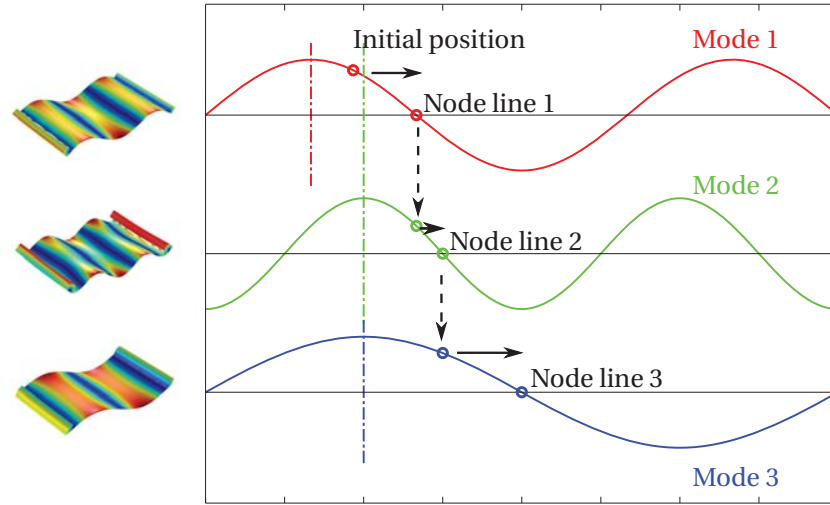
Figure 5.10: Transport principle using combined standing waves
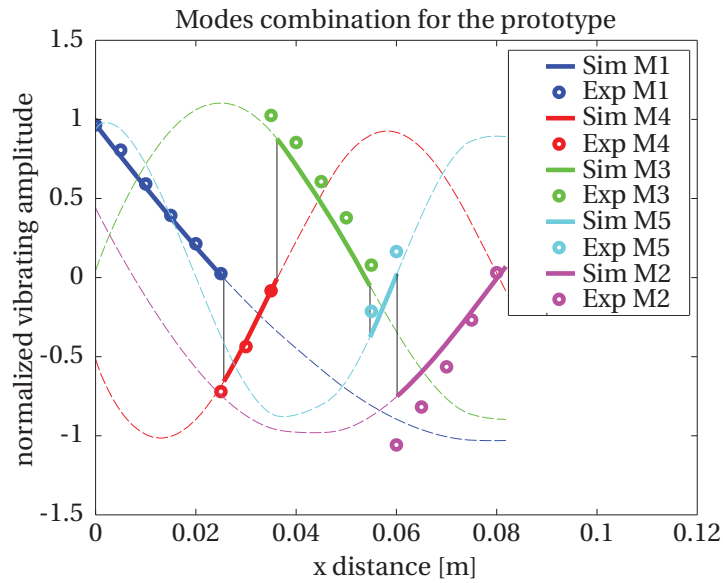
Figure 5.11: Different resonant modes along "data line"

Fig. 5.12 displays the experimental results corresponding to the simulations from Fig. 3.24. Table 5.3 shows the numerical comparison of the resonant frequencies for simulation and experimental results. The maximum difference is 3% and may come from the manufacturing tolerance.

For the workpiece transportation experiment, the sequence is: 402 Hz $\longrightarrow$ 3546 Hz $\longrightarrow$ 2242 Hz $\longrightarrow$ 4756 Hz $\longrightarrow$ 1154 Hz. Fig. 5.11 shows the experimental results of each normalized resonant shape profile (with labels "o"). The experimental and simulation results have certain

(a) M1 402 Hz

(b) M2 1154 Hz

(c) M3 2242 Hz

(d) M4 3546 Hz

(e) M5 4756 Hz
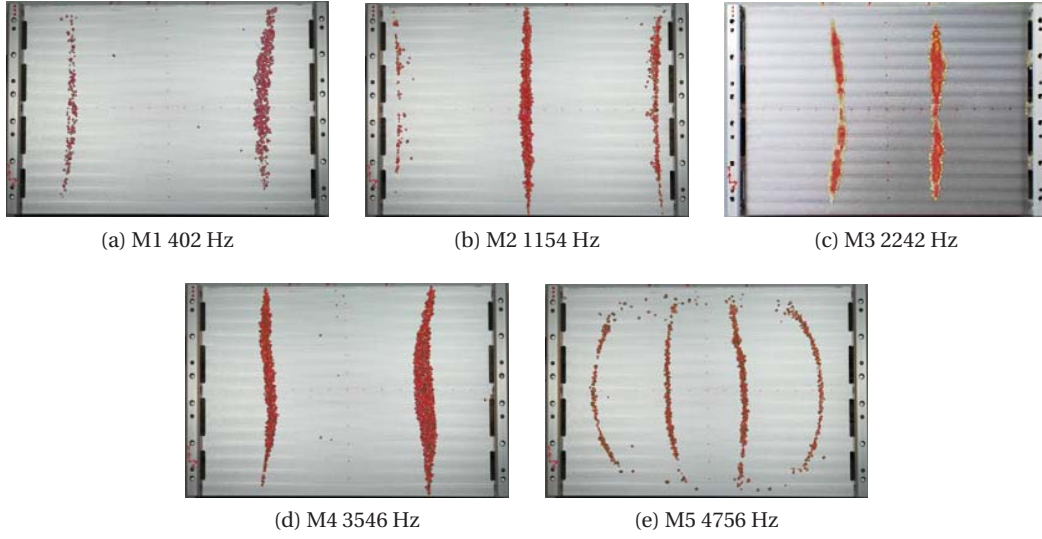
Figure 5.12: Experimental results for different resonant modes

Table 5.3: Resonant frequencies comparison

Mode	Simulation f [Hz]	Experimental f [Hz]	Difference [%]
M 1	397	402	1.26
M 2	1136	1154	1.58
M 3	2195	2242	2.14
M 4	3459	3546	2.52
M 5	4668	4756	1.89

Table 5.4: Workpiece transportation vibrating parameters

Frequency [Hz]	Voltage [V]	Duration [s]	Distance [mm]
402	100	8.0	23.0
3546	100	8.0	8.0
2242	40	5.0	18.0
4756	100	5.0	4.0
1154	60	8.0	22.0

Table 5.5: Stability evaluation for prototype

	Mode switch	Simulation	Experiments	Difference [%]
k_1	M 1 $\longrightarrow$ M 4	0.46	0.36	-21.74
k_2	M 4 $\longrightarrow$ M 3	0.60	0.67	11.67
k_3	M 3 $\longrightarrow$ M 5	0.24	0.19	-20.83
k_4	M 5 $\longrightarrow$ M 2	0.47	0.61	29.79

consistency. The initial position is 5 mm from the edge. Experiment details for each mode are listed in Table 5.4. The total transport time is 34.0 seconds. The total transport distance is 75.0 mm. Piezoelectric actuator drive voltages and mode duration depends on experimental data. The transport speed is slow. Low working voltages (e.g 2242 Hz, 1136 Hz) are used to obtain stable workpiece vibration especially between the modes switches. This can be improved by optimizing the plate geometry dimension to adjust the relative nodal positions as explained. The optimization can help to improve the stability of the vibration so that higher voltage can be used for specific modes and bigger transport speed can be obtained. The experimental and simulation results for the stability evaluation are listed in Table 5.5. The maximum k_i is 0.67, this means the transportation for this prototype is stable.

$k_i < 1$ is the necessary condition for transporting parts in one direction continuously rather than the sufficient condition. Besides this, the parts should not have too much vertical displacement, which will definitely lead to random vibration. Moreover, the range of parameter k_i should be reduced further according to the different geometry parts.

5.4 Standing waves combination for quasi-travelling wave

Mathematically, the basic travelling wave is the one-dimensional sinusoidal wave described by the equation 5.1. A travelling wave could be created by the superposition of two standing waves (in Eq. (5.2)) which have the same amplitudes but differ in phase by $\frac{\pi}{2}$ spatially and temporally. In circular plate or a ring, due to the circular symmetry, resonant modes with identical resonant frequency but different spatial patterns (called degenerate modes) exist . By superimposing these degenerate modes, travelling wave can be obtained [26]. In rectangular plate, modes with same resonant frequency can be obtained by choosing specific plate length/width ratio [42]. In square plate, due to the symmetry of the plate edges, modes with same resonant frequency are obtained directly. Manceau et. al [43] have investigated it using degenerate modes in clamped square plate. Here we will focus on using degenerate modes of a completely free square plate to create travelling wave.

$$u(x, t) = A sin(kx - \omega t) \tag{5.1}$$
$$= A sin(kx)cos(\omega t) - A cos(kx)sin(\omega t) \tag{5.2}$$

5.4.1 Simulations

Using the same method as in [43], Fig. 5.13 presents a pair of degenerate modes (mode (0, 3) and mode (3, 0)) and its principle (Fig. 5.14) to create the travelling wave. First, the resonant frequencies of mode with different spatial patterns are identical. In Fig. 5.13, the nodal lines are not ideally parallel to the plate edges because of the coupling between bending motions in two directions. The red squares are the activated piezoelectric actuators underneath the plate. Piezoelectric actuator in spatial pattern 2 is activated with $\frac{\pi}{2}$ temporally delay compared to the one in spatial pattern 1. Correspondingly in Fig. 5.14, the dash-dot black lines (⋯) and

solid red lines are the nodal lines and anti-nodal lines of resonant mode for spatial pattern 1. The dotted black lines ($\cdots$) and solid green lines are the nodal lines and anti-nodal lines of resonant mode for spatial pattern 2. Under these two excitations, the maximum amplitude of the propagating wave trace is the dark blue dashed line. The dark blue star symbols indicate the results with phase increment of $\frac{\pi}{6}$. The wave propagating direction is counter clockwise (CCW). We observe also there are nine vortexes in the quasi-travelling wave (the node intersections of the two modes). These vortexes will always have small vibrating amplitude. Fig. 5.15 present the key moments of the plate surface displacement. The red points in each moment is the maximum displacement inside the plate. They are corresponding to the blue stars. When the piezoelectric actuator in spatial pattern 2 is activated with $\frac{\pi}{2}$ temporally leading compared to the piezoelectric actuator in spatial pattern 1, the wave propagating direction will be clockwise (CW).

(a) 1382 Hz spatial pattern 1   (b) 1382 Hz spatial pattern 2
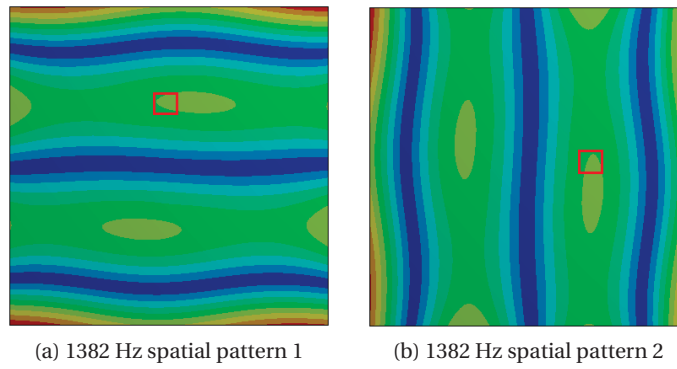
Figure 5.13: Degenerate modes 1382 Hz
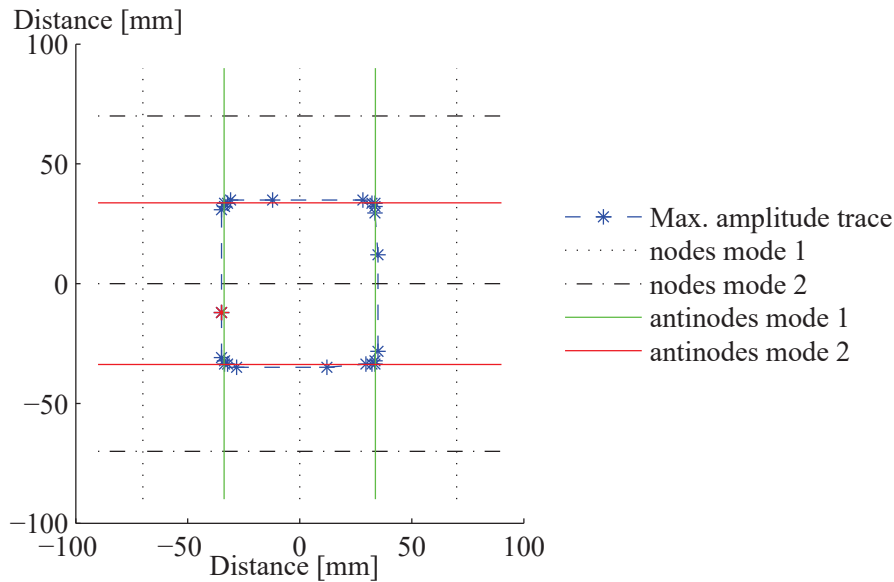
Figure 5.14: Quasi-travelling wave using mode (0, 3) and mode (3, 0)
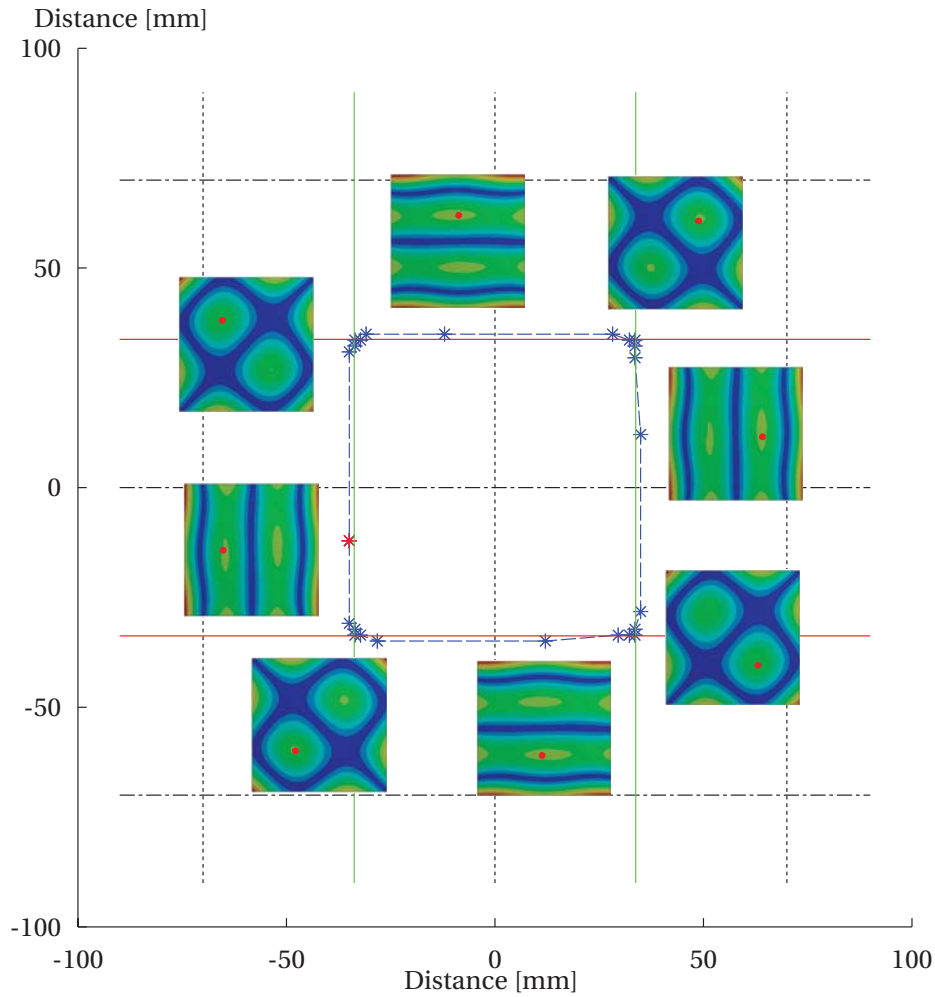
Figure 5.15: Quasi-travelling wave illustration

Fig. 5.16 and Fig. 5.17 provide the amplitude and phase feature of the quasi-travelling wave. According to the Eq. (5.1), the typical travelling wave has two features: constant propagating amplitude A and linear phase change along wave propagation direction. In Fig. 5.16, the propagating amplitude is not constant but vary around a constant value. In Fig. 5.17, the phase changes along the propagating trace even it is not exactly linear. Thus, we call this propagating wave as quasi-travelling wave.

The quasi-travelling wave trace is rectangular rather than a round circle according to the study from Manceau et al.. Moreover, due to the free boundaries, the plate modes are definitely different from that of the clamped plate. Thus for the same geometry of plate, this free boundary quasi-travelling wave provide different wave propagating trace from that of fixed

boundaries.
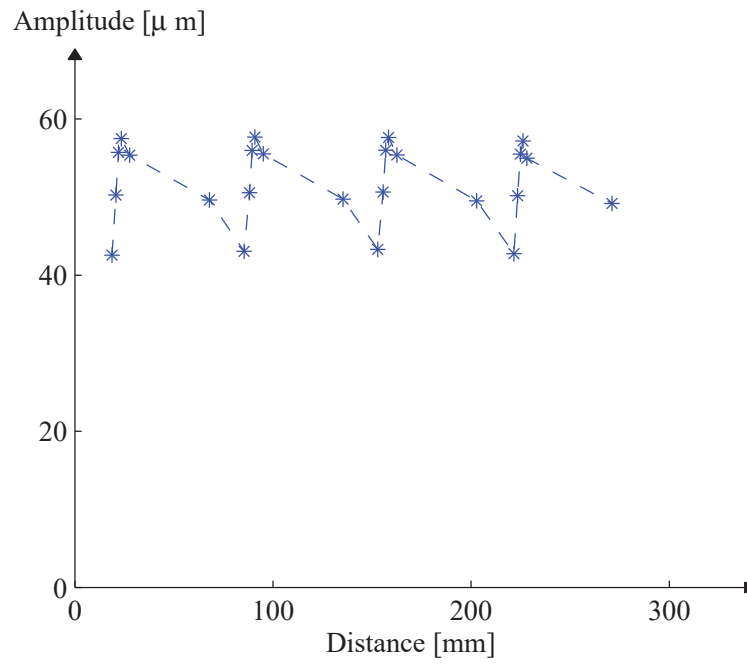
Figure 5.16: Quasi-travelling wave amplitude along wave propagation for 1382 Hz
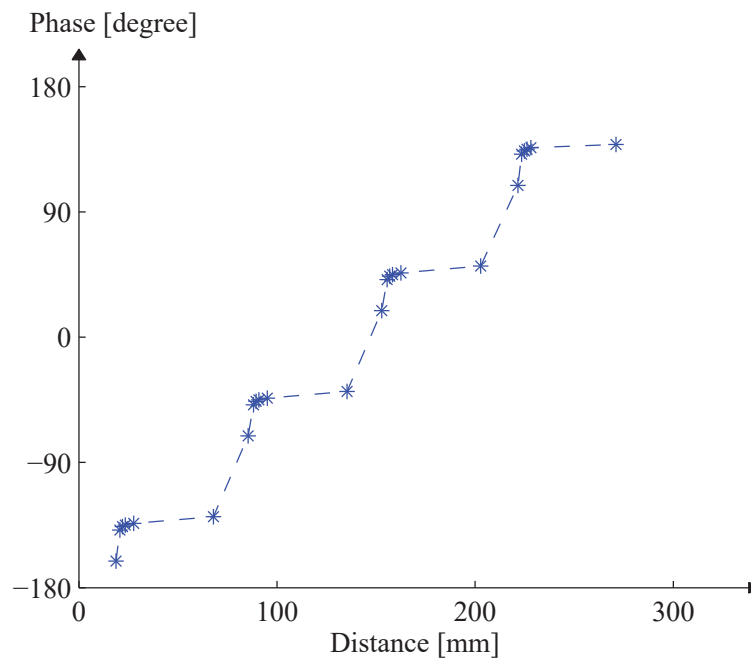
Figure 5.17: Quasi-travelling wave phase along wave propagation for 1382 Hz

Using previous degenerated modes (mode (0, 3) and mode (3, 0)), the quasi-travelling wave has one trace. If we combine the degenerate modes that have more number of half waves, we

expect to obtain more quasi-travelling waves. Fig. 5.18 and Fig. 5.19 give the degenerate modes (mode (0, 5) and mode (5, 0)) and its corresponding quasi-travelling waves. In Fig. 5.18, the nodal lines are not parallel to the plate edges due to the coupling between bending motion in x, y directions. In Fig. 5.19, the nodal lines and anti-nodal lines are represented with lines that are parallel to the plate edges to simplify the analysis. Different from the unique quasi-travelling created from mode (0, 3) and mode (3, 0), this quasi-travelling wave has nine quasi-travelling trace(red and black dashed trace in Fig. 5.19). They have both clock wise direction and counter clockwise directions at the same time. These quasi-travelling waves are the simulation results. They deviate from the simplified anti-nodes. However, we observe that there is only few of difference. And the quasi-travelling waves generally follow the anti-nodal lines. Therefore, we can approximately predict the quasi-travelling waves according to the degenerate modes in study.

(a) 4472 Hz spatial pattern 1   (b) 4472 Hz spatial pattern 2
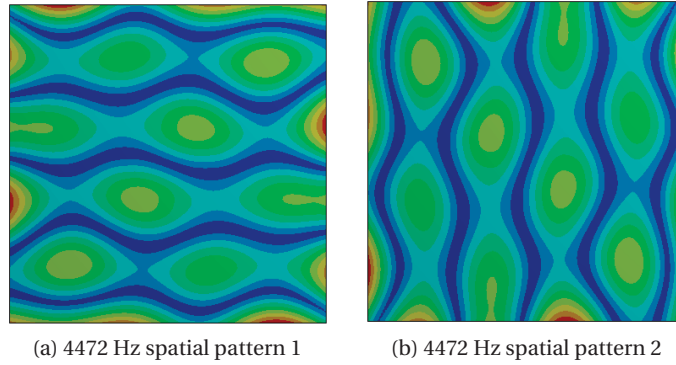
Figure 5.18: Degenerate modes 4472 Hz
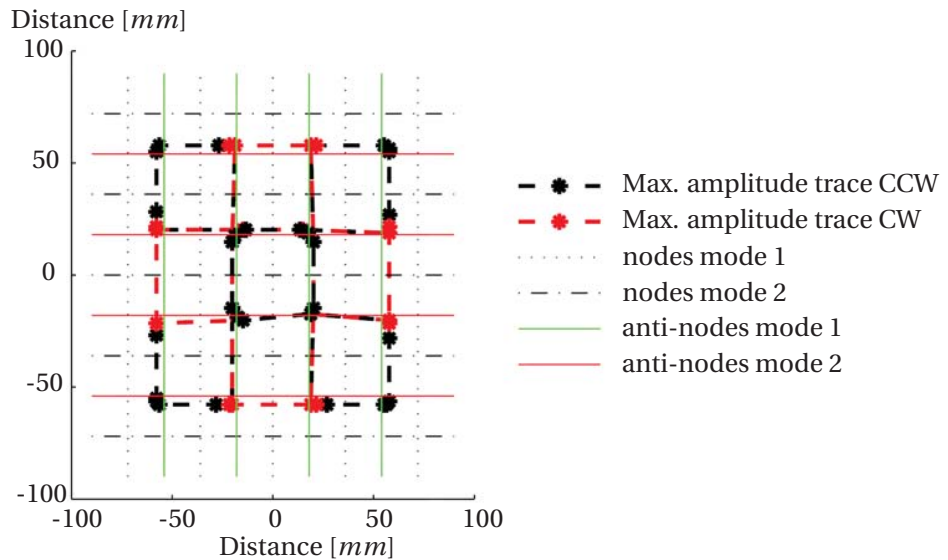
Figure 5.19: Quasi-travelling wave using mode (0, 5) and mode (5, 0)

5.4.2 Experiments

Experiments using a square aluminium plate with two piezoelectric actuators are performed. The plate size is of $180 \times 180 \times 3$ mm^3. The piezoelectric actuators are glued underneath the plate at the positions P1 (0 mm, 33.75 mm, -3 mm) and P2 (33.75 mm, 0 mm, -3 mm). The resonant frequencies for the two modes shown in Fig. 5.13a and Fig. 5.13b are 1,398 Hz and 1,407 Hz. The frequency difference between the two modes may come from the manufacture tolerance. Fig. 5.20 shows the experimental mode shape when exciting the corresponding piezoelectric actuator separately.

(a) Mode shape 1 with 1402 Hz   (b) Mode shape 2 with 1402 Hz
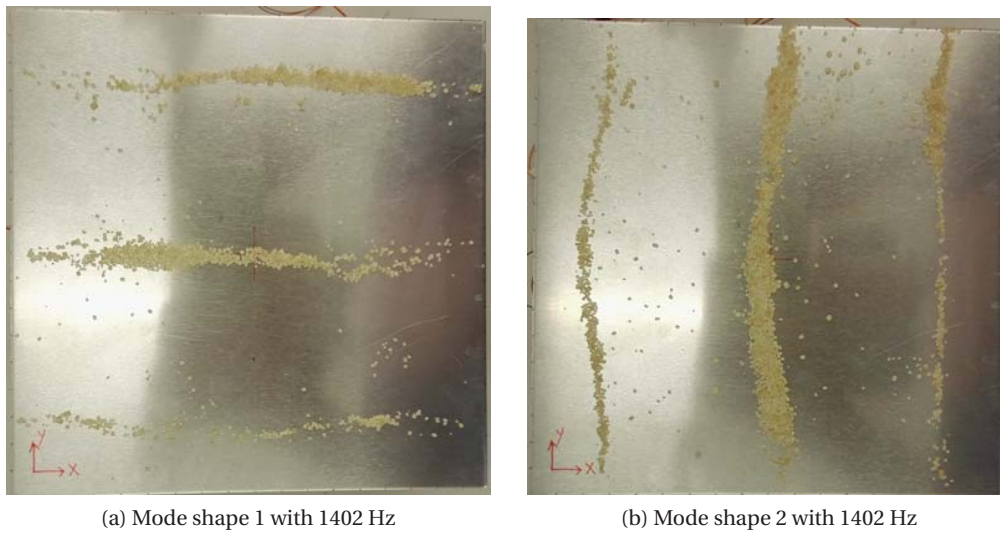
Figure 5.20: Experimental degenerated modes

Previous results validate that the degenerate modes exist. To create quasi-standing wave in the square plate, we will use the frequency of 1,402 Hz, which works for both resonant modes and provide same amplitudes for the equivalent positions. Fig. 5.21 shows the sugar position after vibration when the piezoelectric actuator at position P2 is activated with $\frac{\pi}{2}$ temporally delay compared to piezoelectric actuators at position P1. Compared to Fig. 5.14, the positions of sugar are the nine vortexes.

For a standing wave, the phase shift between all the position on the plate and an exciting actuator voltage should be constant, roughly 90 degrees. If the quasi-travelling exist, the phase shift between the points along the quasi-travelling wave and a fixed actuated voltage should change for one period. The phase difference between the plate displacement and the voltage of the piezoelectric actuator at position P2 along the predict quasi-travelling wave (red square in Fig. 5.21) in counter clockwise direction are shown in Fig. 5.22b. The amplitude variation along quasi-travelling wave is shown in Fig. 5.22a.
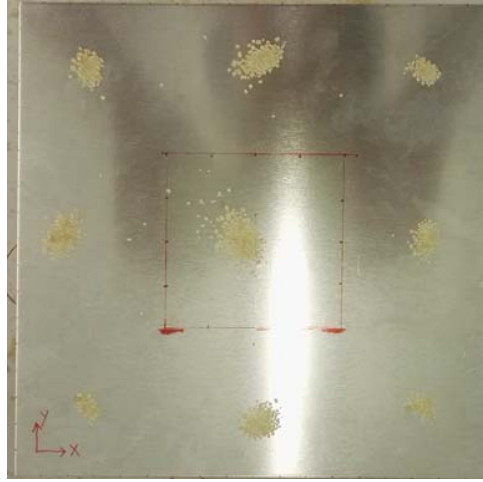
Figure 5.21: Quasi-travelling wave with vortexes
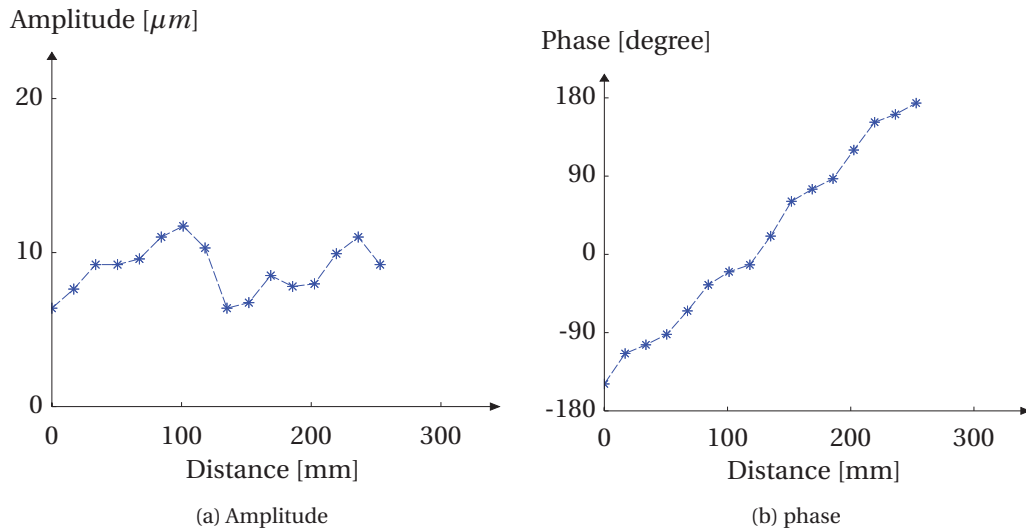
(a) Amplitude

(b) phase

Figure 5.22: Amplitude and phase variation along quasi-travelling wave in CCW direction

5.5 Summary and conclusions

In this chapter, we have applied the aforementioned researches to three applications. Firstly, for part separation, two desirable standing waves in a square plate have been used to separate parts. The two modes should satisfy the following condition: the anti-nodes of the first mode are the nodes of the second mode and the nodes of the first mode are the anti-nodes of the second mode. Moreover, the time duration and the vibrating amplitude of the plate's two standing waves have been well controlled to achieve the separation more efficiently with reduced random vibrations. Secondly, a series of standing waves in a rectangular plate has been obtained to transport the parts from one end of the plate to the center of the plate.

Experiments have been carried out to validate this approach. Thirdly, degenerated modes in the square plate have been used to create quasi-travelling wave. This has been validated in simulation and experiments.

Publication related to this chapter:

- D. Shi, Y. Civet and Y. Perriard. "Design and optimization of piezoelectric actuated plate Eigenmodes for workpiece transportation", *IEEE/ASME International Conference on Advanced Intelligent Mechatronic (AIM 2015)*, Busan, Korea, July 7-11, 2015.

6 Conclusions

First, we have investigated the resonant modes of a square plate and a rectangular plate. Among these mode shapes, we have chosen the suitable modes for two objectives. The first objective was to separate parts. It has been done with special pairs of mode of a square plate. These kinds of pair of modes have the following features: the anti-nodes of the first resonant mode are the nodes of the second resonant mode; and the nodes of the first resonant mode are the anti-nodes of the second resonant mode. The second objective was to transport parts. We have investigated the length-to-width ratio of a rectangular plate influence on the relative nodes positions and obtained a plate with a series of standing waves which could be used in the right sequence in order to transport a part in one direction continuously.

We have investigated the piezoelectric actuator influence on the plate amplitude. With bigger piezoelectric actuators (length smaller than half wavelength), we have obtained higher amplitude. For a given surface, the studies have shown that we could obtain higher amplitude by changing the piezoelectric actuator's shape and orientating the longer length to the direction of bending mode. This research helped us to obtain the desirable amplitude with the given piezoelectric actuator's drive constraints.

We have used numerical simulations to investigate the parts vertical displacement under different vibrating frequency and amplitude. According to the studies, we have found that we can obtain a certain vertical displacement of a part by combing of either high vibrating frequency and low amplitude or a lower vibrating frequency and higher amplitude.

With regards to the parts horizontal movement, we have limited the part's vertical displacement to avoid random part vibration by controlling the plate amplitude and thus obtained stable horizontal movement. Using the above-mentioned series of standing waves in the right sequence, the plate could transport the part in one direction continuously.

Experiments on parts separation and parts transportation have been performed. This includes the resonance analysis and mechanical interactions. Parts separation experiments do not only validate the feasibility but also demonstrate the promising improvement for industrial

applications. Parts transport experiments also validate the feasibility of the strategy. However, the efficiency and stability needs to be improved in the future.

The limitation of the part-plate interaction is that our numerical simulation is valid only for the impact that are considered as rigid (for example impact between metal and acrylic). It is no more consistent if the impact is too flexible (such as impact with the rubber), because the damping is not considered in our model.

6.1 Original contributions

The contributions drawn for academic and industrial point of view are presented in the following.

6.1.1 Academic contributions

- *Piezoelectric actuator's dimension and shape influence on the vibrating plate amplitude*

  Few researches focused on the plate vibrating amplitude increment. In this thesis, piezoelectric actuators' dimension and orientation influence on the plate vibrating amplitude has been investigated. According to our researches, we discovered that bigger the piezoelectric actuator is, larger the vibrating amplitude is as long as the piezoelectric actuators' maximum length is smaller than half wavelength. Moreover, we have found that for a piezoelectric actuator with a given surface, shape modifications could increase the vibrating amplitude. Limiting the piezoelectric actuators' shape to rectangular, the large edge of the piezoelectric actuator should be orientated consistency with the bending modes. The limit of the large edge is the length of the half-wavelength.

- *Plate geometry influence on relative nodal line position between modes*

  We have studied the plate geometry influence on relative nodal line positions between modes. From the simulation results, we found that, the length-to-width ratio of the rectangular plate changes the modes whose nodal lines are parallel to the short edge of the plate. A parameter k_i (refer to section 5.3), which relates the relative distance between the nodal positions of two successive modes and the wavelength of the second mode, was proposed as the first step for plate optimization.

- *Part's vertical displacement under a vibrating plate*

  For the first time, parts' vertical displacement under a resonant vibrating plate has been underlined for researches. The resonant frequencies of a plate are discrete. Using the same resonant exciter, resonant frequency and amplitude of the plate has the following correlations: higher the resonant frequency of the plate is, lower the vibrating amplitude is; lower the resonant frequency, higher the vibrating amplitude. Numerical simulations on the part's vertical displacement show that we can obtain a certain vertical displacement of the part by either high vibrating frequency and low amplitude of the plate or a

lower frequency and higher amplitude of the plate (refer to 4.1). This was validated with experimental results.

- *Part's horizontal movement from anti-nodes to nodes*

The horizontal movement considered in this thesis refers to the movement from anti-node to node. We have implemented numerical simulations to study the horizontal movement. The amplitude from anti-node to node changes. Our numerical simulation considered this amplitude changes. To avoid random parts vibration during the horizontal movement, we have limited the plate vibrating amplitude. Even if this strategy led to slow velocity, it has allowed us to move the parts from anti-node to node stably.

6.1.2   Industrial contributions

- *Standing waves used for tooling plate separation*

For the first time, standing waves using with a specific sequence (first pre-position parts standing wave and then separation standing wave) for parts separation have been proposed. The desirable standing waves of a square plate were chosen. With the research of increasing the plate vibrating amplitude, corresponding separation experiments were carried out and demonstrate the separation feasibility for simple parts, such as nuts.

- *Standing waves used for transport conveyor in flexible parts feeder*

For the first time, a series of standing waves with optimized relative nodal line position for parts transportation was put forward. We have studied the plate geometry influence on the relative nodal position and provide the necessary condition for transport parts in one direction continuously. A prototype was manufactured and used to validate this idea.

6.2   Outlook

Considering the already done work, suggested work for academic and industrial perspectives are the following:

6.2.1   Academic outlook

- *Piezoelectric actuator dimension and shape design guidance for general plate amplitude increment*

In this thesis, we have investigated the piezoelectric actuator dimension and shape influences on amplitude of a square plate for two kinds of modes: 1, the modes that have the same number of half wavelength in x, y directions and 2, the modes that are parallel to one edge of the plate. It will be interesting to investigate the influence on general rectangular plate and other kinds of modes (such as modes that do not have the

same number of half wavelength in x, y directions) and give the piezoelectric actuator guidance for general plate amplitude increment.

- *Parts interaction with more complex profile of the resonant mode*

  In this thesis, with regard to part-plate interaction affected by plate amplitude, we have considered the amplitude changes from anti-nodes to nodes. In our numerical simulation, we have simplified the plate to rigid vibration and simulated the amplitude change from anti-node to nodes using a linear variation. Actually, when the plate resonates, the plate bends. It will be interesting to consider the bending rather than the simplified linear variation from anti-node to node for interaction study.

- *System's chaotic vibration*

  The part's behaviour according to the vibrating plate studied in this thesis is chaotic. We have used the normal distribution statistical method to investigate the chaotic vibration of one part. Actually, in the entire system, there are multiple parts and also the vibrating system. It will make sense to investigate the energy state of the entire system by another statistical measure - entropy, which describe the system as a whole.

6.2.2 Industrial outlook

- *Modifications for industrial part feeder application*

  After the feasibility validation of this novel approach with simple parts shapes and simple vibrating tooling plate, more researches can be implemented for designing a single tooling plate for a series of parts with similar dimension and shapes. Moreover, the surface of the tooling plate could be expected to be modified (such as with holes) to orientate the complicated parts.

- *Noise improvement*

  The present working frequency is exactly audible frequency, which leads to undesirable noise. This could be solved by either adding sound insulation room for the system or increasing the working frequency beyond the audible frequency.

A Piezoelectric actuators

A.1 Simulation and experiment DC offset influence

The piezoelectric actuator in this document is supplied by a sinusoidal signal with DC offset (half of the peak-to-peak voltage). For simulation, we can use harmonic analysis with pre-stress static analysis to simulate this. This appendix presents the harmonic analysis is sufficient to model the pre-stressed static analysis.

Fig. A.1 presents simulation results of the plate displacement with or without DC offset. Without DC offset, the maximum amplitude is 53.99 μm. With DC offset, the maximum amplitude is 54.06 μm. The difference is 0.11%. The difference is small. Therefore, we can use the harmonic analysis without DC offset to continue the other studies for the sake of implementation simplicity.
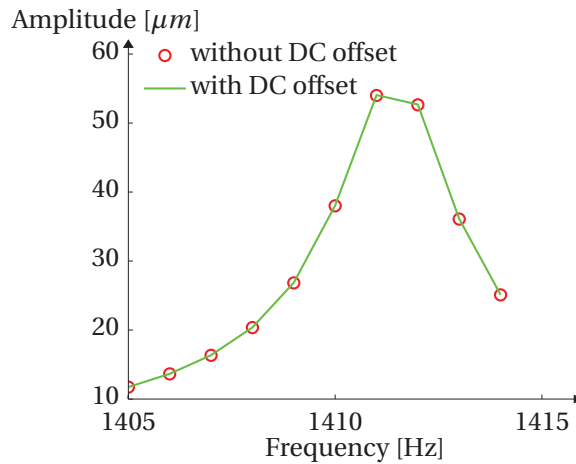
Figure A.1: Simulation plot displacement comparison

A.2 Piezoelectric actuator parameter transformation

In Ansys, the coupled equations are in the stress/electric field form (Theory reference for Mechanical APDL and mechanical application in [1]):

$$\{T\} = \left[c^E \right] \{S\} + [e] \{E\} \tag{A.1}$$

$$\{D\} = [e]^T \{S\} + \left[\epsilon^S \right] \{E\} \tag{A.2}$$

where

$\{T\}$ = stress vector (six components xy, yz, xz)

$\{S\}$ = strain vector (six components x, y, z, xy, yz, xz)

$\{D\}$ = electric displacement vector (three components x, y, z)

$\{E\}$ = electric field vector (three components x, y, z)

$\left[c^E \right]$ = stiffness matrix at constant electric filed

$[e]$ = piezoelectric matrix relating stress/electric field

$\left[e^t \right]$ = piezoelectric matrix relating stress/electric field (transposed)

$\left[\epsilon^S \right]$ = dielectric matrix evaluated at constant stress

To use the manufacture provided data in Ansys, the strain/electric-field form matrices need to be transformed to stress/electric-field form. The transformation relations are:

$$\left[c^E \right] = \left[s^E \right]^{-1} \tag{A.3}$$

$$[e] = \left[s^E \right]^{-1} [d] \tag{A.4}$$

$$\left[\epsilon^S \right] = \left[\epsilon^T \right] - \left[d^t \right] \left[s^E \right]^{-1} [d] \tag{A.5}$$

The left part of Eq. (A.3), Eq. (A.4) and Eq. (A.5) are the Ansys input. The right part of these three equations are the manufacture-supplied data. Moreover, the vector element sequence in $\{T\}$ and $\{S\}$ are different between the supplier and ANSYS.

A.3   Multi-layer piezoelectric actuator capacitance

When operating below the resonant frequency, a piezoelectric behaves as a capacitor. The capacitance of the actuator depends on the area, the thickness of the ceramic and material properties. When the actuator is multilayer, electrically connecting in parallel, the capacitance also depends on the number of layers.

The capacitances of a multi-layer actuator can be estimated by:

$$C_{piezo} = n \cdot \epsilon_{33}^T \cdot S \cdot d_s^{-1} \tag{A.6}$$

where
n = the number of layers = $\frac{I_0}{d_s}$
ϵ_{33}^T = the dielectric constant $[As/Vm]$
S = electrode surface area of a single layer $[m^2]$
d_s = distance between the individual electrodes (layer-thickness) [m]
I_0 = actuator length

A.4   Noliac piezo ceramic parameters

PIEZO CERAMICS

Piezo ceramics specifications

Properties	Symbol & unit	NCE40	NCE41	NCE46[*]	NCE51	NCE53	NCE55	NCE56	NCE57[*]	NCE59[*]	NCE80
DIELECTRIC PROPERTIES (tolerances +/- 10%)											
Relative Dielectric Constant	$\frac{\varepsilon^T_{33}}{\varepsilon_0}$	1250	1350	1300	1850	1600	5000	2900	1800	2900	1050
Dielectric Loss Factor	$tg\delta$ [10^{-4}]	25	40	30	190	130	220	140	170	190	20
Dielectric Loss Factor at 400V/mm	$tg\delta$ [10^{-4}]	140	200								100
ELECTROMECHANICAL PROPERTIES (tolerances +/- 5%)											
Coupling Factors**	k_p	0.58	0.57	0.57	0.65	0.56	0.62	0.64	0.59	0.64	0.55
	k_{31}	0.34	0.33	0.33	0.37	0.32	0.39	0.37	0.33	0.37	0.30
	k_{33}	0.70	0.68	0.68	0.72	0.65	0.72	0.74	0.70	0.75	0.68
	k_t	0.50	0.50	0.47	0.51	0.47	0.50	0.50	0.47	0.52	0.48
Piezoelectric Charge Constants	$-d_{31}$ [10^{-12} C/N]	140	130	130	195	150	260	250	170	240	100
	d_{33} [10^{-12} C/N]	320	310	290	460	360	670	580	425	575	240
Piezoelectric Voltage Constants	$-g_{31}$ [10^{-3} Vm/N]	11	11	11	13	9	9	9	11	10	11
	g_{33} [10^{-3} Vm/N]	27	25	28	27	23	19	20	27	23	27
Frequency Constants	N^E_p [m/s]	2160	2280	2230	1940	2180	1970	2000	2010	1970	2270
	N^D_t [m/s]	1980	2000	2040	2010	2040	1990	2030	1950	1960	2050
	N^E_1 [m/s]	1470	1600	1500	1400			1530	1400	1410	1610
	N^D_3 [m/s]	1340	1500	1800	1390			1400	1500	1500	1500
PHYSICAL PROPERTIES (tolerances +/- 5%)											
Mechanical Quality Factor	Q_m	700	1400	>1000	80	80	70	80	80	90	1000
Density	ρ [10^3 kg/m^3]	7.75	7.90	7.70	7.80	7.60	8.00	7.65	7.70	7.45	7.80
Elastic Compliances	s^E_{11} [10^{-12} m^2/N]	13	13	13	16	16	17	18	17	17	11
	s^E_{33} [10^{-12} m^2/N]	17	16	20	19	18	21	20	23	23	14
Curie Temperature	T_c [°C]	325	290	330	340	340	170	250	350	235	305

*) For multilayer components only.

**) Measured in accordance with standard EN 50324.

The values listed above are for reference purposes only and cannot be applied unconditionally to other shapes and dimensions. Values vary depending on the components' actual shape, surface finish, shaping process and post-processing.

B Parts separation experimental details

In the thesis, for parts separation, we use two standing waves alternatively. In this appendix, we use also the third standing wave for the "Dead positions" once to improve the separation. In total, there are 99 nuts are put in the center of the plate at the beginning. Afterwards, the plate performs the operations successively in Table B.1. The nuts are M 2.5. The clearance for the distance between the center of the two nuts is 8 *mm*.

Table B.1: Nuts separation experiments

Separation	Frequency [Hz]	Voltage [V]	Time [s]	Parts separated
1	558	120	1.5	
	2650	120	2.0	
	2797	120	0.1	13
2	2650	120	2.0	
	2797	120	0.1	10
3	2650	120	2.0	
	2797	120	0.1	9
4	2650	120	2.0	
	2797	120	0.1	3
5	2650	120	2.0	
	2797	120	0.1	5
6	2650	120	2.0	
	2797	120	0.1	10
7	2650	120	2.0	
	2797	120	0.1	7
8	2650	120	2.0	
	2797	120	0.1	7
9	2650	120	2.0	
	2797	120	0.1	4
10	12314	120	1.0	
	2650	120	2.0	
	2797	120	0.1	13

Appendix B. Parts separation experimental details

This experiments is slightly different from the experiments in 5.2. In operation 10, before using the two standing waves of 2650 Hz and 2797 Hz, we use the standing wave with resonant frequency of 12314 Hz, which is used to move the nuts from the "Dead positions". We can clearly see that with the help of third mode, the parts that can be separated are more afterwards like shown in operation 10.

Bibliography

[1] *Theory reference for the mechanical APDL and mechanical applications*, ansys12.0 edition, 2009.

[2] V. Adams and A. Askenazi. *Building better products with finite element analysis*. Cengage Learning, 1999.

[3] M. Akama. Elliptic vibratory part-feeding device, Aug. 27 1991. US Patent 5,042,643.

[4] Ansys. Ansys workbench (version 15.0). http://www.ansys.com/, 15.0.

[5] R. Barboni, A. Mannini, E. Fantini, and P. Gaudenzi. Optimal placement of pzt actuators for the control of beam dynamics. *Smart Materials and Structures*, 9(1):110, 2000.

[6] K.-F. Böhringer, V. Bhatt, and K. Y. Goldberg. Sensorless manipulation using transverse vibrations of a plate. In *Robotics and Automation, 1995. Proceedings., 1995 IEEE International Conference on*, volume 2, pages 1989–1996. IEEE, 1995.

[7] G. Boothroyd et al. *Assembly automation and product design*, volume 536. Cambridge Univ Press, 2005.

[8] F. Buchi, I. Nesnas, and B. R. Carlisle. Impulse-based, flexible parts feeder, May 2 2000. US Patent 6,056,108.

[9] T. G. Carne, D. T. Griffith, and M. E. Casias. Support condtions for experimental modal analysis. *Sound and Vibration*, 41(6):10–16, 2007.

[10] F. Casset, J. Danel, C. Chappaz, Y. Civet, M. Amberg, M. Gorisse, C. Dieppedale, G. Le Rhun, S. Basrour, and P. Renaux. Low voltage actuated plate for haptic applications with pzt thin-film. In *Solid-State Sensors, Actuators and Microsystems, 2013 Transducers & Eurosensors XXVII: The 17th International Conference on*, pages 2733–2736. IEEE, 2013.

[11] F. Casset, J. Danel, P. Renaux, C. Chappaz, G. Le Rhun, C. Dieppedale, M. Gorisse, S. Basrour, S. Fanget, and P. Ancey. Characterization and post simulation of thin-film pzt actuated plates for haptic applications. In *Thermal, mechanical and multi-physics simulation and experiments in microelectronics and microsystems (eurosime), 2014 15th international conference on*, pages 1–4. IEEE, 2014.

Bibliography

[12] G. C. Causey, R. D. Quinn, N. A. Barendt, D. M. Sargent, and W. S. Newman. Design of a flexible parts feeding system. In *Robotics and Automation, 1997. Proceedings., 1997 IEEE International Conference on*, volume 2, pages 1235–1240. IEEE, 1997.

[13] G. C. Causey, R. D. Quinn, and M. S. Branicky. Testing and analysis of a flexible feeding system. In *Robotics and Automation, 1999. Proceedings. 1999 IEEE International Conference on*, volume 4, pages 2564–2571. IEEE, 1999.

[14] Chladni. Chladni figure. https://en.wikipedia.org/wiki/Ernst_Chladni#Chladni_figures, 1787. last modified on 27 October 2015.

[15] S. Choi and D. Lee. Modal analysis and control of a bowl parts feeder activated by piezoceramic actuators. *Journal of Sound and Vibration*, 275(1):452–458, 2004.

[16] A. S. Cordero. *Analyzing the parts behavior in a vibratory bowl feeder to predict the Dynamic Probability Profile.* PhD thesis, UNIVERSITY OF PUERTO RICO MAYAGUEZ, 2004.

[17] E. Dimitriadis, C. Fuller, and C. Rogers. Piezoelectric actuators for distributed vibration excitation of thin plates. *Journal of Vibration and Acoustics*, 113(1):100–107, 1991.

[18] W. Duan, S. T. Quek, and Q. Wang. A novel ring type ultrasonic motor with multiple wavenumbers: design, fabrication and characterization. *Smart Materials and Structures*, 18(12):125025, 2009.

[19] D. J. Ewins. *Modal testing: theory and practice*, volume 6. Research studies press Letchworth, 1995.

[20] Z.-F. Fu and J. He. *Modal analysis.* Butterworth-Heinemann, 2001.

[21] C. Gertsch and O. Ryser. Parts feed device, July 29 2003. US Patent 6,598,730.

[22] K. Ghosh and R. C. Batra. Shape control of plates using piezoceramic elements. In *Symposium on Active Materials and Smart Structures: Society of Engineering Science 31st Annual Meeting*, pages 107–121. International Society for Optics and Photonics, 1995.

[23] J. H. Ginsberg. *Mechanical and structural vibrations: theory and applications.* Wiley New York, 2001.

[24] K. Goldberg, B. V. Mirtich, Y. Zhuang, J. Craig, B. R. Carlisle, and J. Canny. Part pose statistics: Estimators and experiments. *Robotics and Automation, IEEE Transactions on*, 15(5):849–857, 1999.

[25] I. Han and Y. Lee. Chaotic dynamics of repeated impacts in vibratory bowl feeders. *Journal of sound and vibration*, 249(3):529–541, 2002.

[26] M. Hermann and W. Schinköthe. Piezoelectric travelling wave motors generating direct linear motion. In *Conference Proceedings, S*, volume 200, page 203, 1999.

104

[27] C. Hernandez, Y. Bernard, and A. Razek. Ultrasonic traveling wave micropump for liquid, May 23 2011. US Patent App. 13/701,859.

[28] P. J. Holmes. The dynamics of repeated impacts with a sinusoidally vibrating table. *Journal of Sound and Vibration*, 84(2):173–189, 1982.

[29] M.-O. Hongler, P. Cartier, and P. Flury. Numerical study of a model of vibro-transporter. *Physics Letters A*, 135(2):106–112, 1989.

[30] M.-O. Hongler and J. Figour. Periodic versus chaotic dynamics in vibratory feeders. *Helvetica Physica Acta*, 62(1):68–81, 1988.

[31] T. Iijima, M. Wada, Y. Nakagawa, and H. Itoh. Ultrasonic motor using flexural standing wave. *Japanese Journal of Applied Physics*, 26(S1):191, 1987.

[32] I. Karjalainen, D. Gudmundsson, and K. Goldberg. Optimizing robotic part feeder throughput with queueing theory. *Assembly Automation*, 27(2):134–140, 2007.

[33] R. B. Kelley, J. R. Birk, H. A. Martins, and R. Tella. A robot system which acquires cylindrical workpieces from bins. *Systems, Man and Cybernetics, IEEE Transactions on*, 12(2):204–213, 1982.

[34] Z. Kusculuoglu, B. Fallahi, and T. Royston. Finite element model of a beam with a piezoceramic patch actuator. *Journal of Sound and Vibration*, 276(1):27–44, 2004.

[35] G. Kuwabara and K. Kono. Restitution coefficient in a collision between two spheres. *Japanese journal of applied physics*, 26(8R):1230, 1987.

[36] K.-M. Lee and R. Blenis. Design concept and prototype development of a flexible integrated vision system. *Journal of robotic systems*, 11(5):387–398, 1994.

[37] S. Lee, B. Ngoi, L. Lim, and S. Lye. Determining the probabilities of natural resting aspects of parts from their geometries. *Assembly Automation*, 17(2):137–142, 1997.

[38] A. W. Leissa. Vibration of plates. Technical report, DTIC Document, 1969.

[39] G. Lim. On the conveying velocity of a vibratory feeder. *Computers & structures*, 62(1):197–203, 1997.

[40] X. Liu, Y. Civet, and Y. Perriard. Quality factor and vibration amplitude estimation of a piezoelectric-actuated system using impedance measurements. *Proceedings of the 18th International Conference on Electrical Machines and Systems (ICEMS)*, 2015.

[41] A. C. Luo and R. P. Han. The dynamics of a bouncing ball with a sinusoidally vibrating table revisited. *Nonlinear Dynamics*, 10(1):1–18, 1996.

[42] J. Manceau and F. Bastien. Linear motor using a quasi-travelling wave in a rectangular plate. *Ultrasonics*, 34(2):257–260, 1996.

Bibliography

[43] J.-F. Manceau, S. Biwersi, and F. Bastien. On the generation and identification of traveling waves in non-circular structures-application to innovative piezoelectric motors. *Smart materials and structures*, 7(3):337, 1998.

[44] Mechanics. Classical mechanics. https://en.wikipedia.org/wiki/Classical_mechanics, 2016.

[45] A. Meitzler, H. Tiersten, A. Warner, D. Berlincourt, G. Couqin, and F. Welsh III. Ieee standard on piezoelectricity, 1988.

[46] B. Mirtich, Y. Zhuang, K. Goldberg, J. Craig, R. Zanutta, B. Carlisle, and J. Canny. Estimating pose statistics for robotic part feeders. In *Robotics and Automation, 1996. Proceedings., 1996 IEEE International Conference on*, volume 2, pages 1140–1146. IEEE, 1996.

[47] Noliac. Actuators for quasi-static applications. http://www.noliac.com/, NCE46.

[48] K. Ooe and A. Doi. Vibration-type particle separation device with piezoceramic vibrator. In *Smart Materials, Nano-and Micro-Smart Systems*, pages 72700P–72700P. International Society for Optics and Photonics, 2008.

[49] M. Parameswaran and S. Ganapathy. Vibratory conveying analysis and design: a review. *Mechanism and Machine Theory*, 14(2):89–97, 1979.

[50] M. Pastor, M. Binda, and T. Harčarik. Modal assurance criterion. *Procedia Engineering*, 48:543–548, 2012.

[51] S. Perroud, T. Hafner, and Y. Mussard. System for supplying components, Oct. 8 2013. US Patent 8,550,233.

[52] PI. Piezoelectrics in positioning. Technical report, 2008.

[53] G. Rosati, M. Faccio, A. Carli, and A. Rossi. Convenience analysis and validation of a fully flexible assembly system. In *Emerging Technologies & Factory Automation (ETFA), 2011 IEEE 16th Conference on*, pages 1–8. IEEE, 2011.

[54] T. Rossing and N. H. Fletcher. *Principles of vibration and sound*. Springer Science & Business Media, 2012.

[55] E. Setter and I. Bucher. Flexural vibration patterning using an array of actuators. *Journal of Sound and Vibration*, 330(6):1121–1140, 2011.

[56] D. Shi, Y. Civet, and Y. Perriard. Design and optimization of piezoelectric actuated plate eigenmodes for workpiece transportation. In *Advanced Intelligent Mechatronics (AIM), 2015 IEEE International Conference on*, pages 1265–1270. IEEE, 2015.

[57] C. E. Smith and N. P. Papanikolopoulos. Vision-guided robotic grasping: Issues and experiments. In *Robotics and Automation, 1996. Proceedings., 1996 IEEE International Conference on*, volume 4, pages 3203–3208. IEEE, 1996.

[58] Solidworks. Solidworks 2013 edition motion study. http://www.solidworks.com/, 2013.

[59] N. Tufillaro and A. Albano. Chaotic dynamics of a bouncing ball. *Am. J. Phys*, 54(10):939–944, 1986.

[60] N. Tufillaro, T. Mello, Y. Choi, and A. Albano. Period doubling boundaries of a bouncing ball. *Journal de Physique*, 47(9):1477–1482, 1986.

[61] K. Uchino. *Piezoelectric actuators and ultrasonic motors*, volume 1. Springer Science & Business Media, 1997.

[62] K. Uchino. *Entrepreneurship for engineers*. CRC Press, 2009.

[63] K. Uchino and S. Takahashi. Multilayer ceramic actuators. *Current Opinion in Solid State and Materials Science*, 1(5):698–705, 1996.

[64] S. Vidoli and F. Dell'Isola. Vibration control in plates by uniformly distributed pzt actuators interconnected via electric networks. *European Journal of Mechanics-A/Solids*, 20(3):435–456, 2001.

[65] J. V. Vilán, A. S. Robleda, P. G. Nieto, and C. C. Placer. Approximation to the dynamics of transported parts in a vibratory bowl feeder. *Mechanism and Machine Theory*, 44(12):2217–2235, 2009.

[66] J.-M. Vorstenbosch, F. Bourgeois, S. Koelemeijer Chollet, and M. Tichem. First results on vibration feeding of small parts in the presence of adhesive forces. *Assembly Automation*, 24(2):177–183, 2004.

[67] G. Winkler. Analysing the hopping conveyor. *International Journal of Mechanical Sciences*, 21(11):651–658, 1979.

[68] S. Yagi. Method and apparatus for controlling piezoelectric vibration, June 1999. US Patent 5,910,698.

[69] C. Zhao. *Ultrasonic motors: technologies and applications*. Springer Science & Business Media, 2011.

Curriculum Vitae

Dan SHI

Born on Dec. 09, 1986

Chinese

dan.shi@alumni.epfl.ch

Educations

2012 - 2016	PhD student at Integrated Actuators Laboratory (LAI) in Microengineering, School of engineering in École Polytechnique Fédérale de Lausanne (EPFL, Swiss Federal Institute of Technology in Lausanne), Switzerland
2009 - 2012	Master of Science in Electric Machines and Electric Apparatus in Zhejiang University, China
2005 - 2009	Bachelor of Science in Electrical Engineering and Automation in Zhejiang University, China

Publications

1. **D. Shi**, Y. Civet and Y. Perriard. "Influence of piezoelectric actuator geometry on resonant vibrating amplitude", *IEEE/ASME International Conference on Advanced Intelligent Mechatronic (AIM 2016)*, Banff, Canada, July 12-15, 2016. Full paper accepted.

2. **D. Shi**, Y. Civet and Y. Perriard. Design and optimization of piezoelectric actuated plate Eigenmodes for workpiece transportation, *IEEE/ASME International Conference on Advanced Intelligent Mechatronic (AIM 2015)*, Busan, Korea, July 7-11, 2015.

3. **D. Shi**, Y. Civet and Y. Perriard. Modelling and design of complex geometry parts vibratory conveying. *The 17th International Conference on Electric Machine and Systems (ICEMS2014)*, Hangzhou, China, October 22-25, 2014.

4. X.Liu, **D. Shi**, Y. Civet and Y. Perriard. Modelling and optimal design of a ring-type structure for the generation of a travelling wave, *The 16th International Conference on*

Electric Machine and Systems (ICEMS2013), Busan, Korea, 2013.

5. **D. Shi**, C. Auvigne, R, Besuchet, C. Winter and Y. Civet and Y. Perriard. Optimal design of inductive coupled power transfer with applications to electric cars. *The 16th International Conference on Electric Machine and Systems (ICEMS2013)*, Busan, Korea, 2013.